universität wien

MASTERARBEIT / MASTER'S THESIS

Titel der Masterarbeit / Title of the Master's Thesis

"Investigation on the impact of alkyl substituent variation of tridentate naphthoquinone based organoruthenium(II) anticancer agents to their aqueous stability and redox properties."

verfasst von / submitted by

Alexander Rosner BSc

angestrebter akademischer Grad / in partial fulfilment of the requirements for the degree of

Master of Science (MSc)

Wien, 2021 / Vienna 2021

Studienkennzahl lt. Studienblasse / degree programme code as it appears on the student record sheet:	A 066 862
Studienrichtung lt. Studienblatt / degree programme as it appears on the student record sheet:	Chemie
Betreut von / Supervisor:	o. Univ.-Prof. Dr. Dr. Bernhard Keppler
Mitbetreut von / Co-Supervisor:	DI Dr. Wolfgang Kandioller

ACKNOWLEDGEMENTS

Not only scientific background and laboratory work are foundation of this work, but essentially the individuals who made all of it possible. I therefore would like to thank the following people:

o. Univ.-Prof. Dr. Dr. Bernhard Keppler for the opportunity to participate in his research group at the department of Inorganic Chemistry.

Special thanks to DI Dr. Wolfgang Kandioller for support and advice for this work. Many thanks for the positive influence on my academic development since my bachelor thesis.

Special thanks to my colleagues and former colleagues of lab 6: Sophia, Heiko, Valentin, Max and Babsi. Thank you for the very friendly working atmosphere, advice and constructive after-work discussions.

The NMR team and all operators for measuring my samples.

Dipl.-Ing. (FH) Alexander Prado-Roller and Natalie Gajic for analyzing my crystals.

Mag. Theiner and the team of the microanalytical laboratory for measuring the elemental analysis of my samples.

Mag. Veronika Knoll and Mag. Elfriede Limberger for administrative support.

Special thanks to my parents Hildegard and Manfred and my whole family for emotionally and financially supporting my study. Without you, even first steps on academic ground would not have been possible.

Special thanks to my very closest: Christoph, Sophie, Hannah, Julian and Philipp. No matter the point we got to know us – thank you for support and honest friendship throughout all these years.

I would like to thank all my friends for their company and support.

Also thank you to all members of the group at the department of Inorganic Chemistry.

ABSTRACT

Research on transition metal based anticancer agents has led to novel and interesting approaches. Ruthenium-based agents have shown suitable properties and high structural diversity, with two representatives under current investigation in clinical trials (BOLD-100, TLD1433). Organometallic ruthenium(II) complexes exhibit high toxicity towards cancer tissue both *in vitro* and *in vivo*. Activation *via* aquation is the common mechanism of initiating cytotoxic activity. Therefore, balancing leaving group- and ligand design is critical for these metallodrugs, in order to prevent adverse effects (*e.g.* premature activation), and fine tune pharmacokinetic properties. Recently, an *in situ* generated *N,O,O*-tridentate ligand motif has been investigated in previous works. This novel class of metal arene complexes features a bioactive naphthoquinone ligand and a pyrazole moiety, which react *in situ* to this tridentate architecture. Impressive cytotoxic properties have been examined to correlate to complex stability, whereas unexpectedly high selectivity towards certain cancer cell lines was observed. Electron donating substituents on the naphthoquinone moiety have been shown to increase stability and cytotoxicity, exemplary for derivatives featuring methyl and ethyl groups. Starting from these, a ligand variation was conducted in course of this master thesis, with choice of longer and branched alkyl chains. Initially, ligands and complexes were synthesized and characterized *via* NMR spectroscopy and elemental analysis. In regard to different synthetic methods, moderate to good yields were obtained for ligands. Complexes were obtained in good yields. Theoretically, higher stability should be achieved by introduction of different alkyl substituents, whereas solubility would be expected to decrease. Stability was measured *via* UV/Vis and influence on redox properties was examined from preliminary cyclic voltammetry experiments. Overall, higher stability was observed for longer and branched alkyl derivatives, whereas solubility decreased, accordingly. Unsurprisingly, redox properties were not influenced by the choice of different alkyl substituents. However, complex mechanisms of redox chemistry were observed at harsh conditions, highly differing from the free ligands'. Cascades of reductive processes likely involve formation of ruthenium(I) species or reduction of the complexes' carbonyl. Presumably, these processes are not applicable in biological medium, as high potentials are mandatory.

ZUSAMMENFASSUNG

Übergangsmetallbasierte Komplexe sind seit vielen Jahren Thema der medizinischen Chemie. Platinbasierte Verbindungen finden seit Jahrzehnten klinische Anwendung, weisen aber deutliche Nachteile auf. Neuartige Metallkomplexe auf Rutheniumbasis zeigen interessante Differenzen in ihrer Wirkungsweise, was sie zu vielversprechenden Kandidaten auszeichnet. Die Nachteile etablierter Verbindungen (z. B. geringe Selektivität, Resistenzen) könnten so überwunden werden. Zwei rutheniumbasierte Komplexe befinden sich derzeit in klinischen Phasen: BOLD-100 und TLD1433. Organometallische Rutheniumverbindungen sind ein weiterer vielversprechender Ansatz. „Piano stool" Komplexe weisen ein stabilisierendes Aren auf, während weitere Liganden für eine Feinabstimmung der Eigenschaften variiert werden können. Vor kurzem wurde gezeigt, dass bei der Reaktion eines Organoruthenium-Dimers mit einem bioaktiven Naphthochinon und Pyrazol ein neuartiges dreizähniges Ligandenmotiv, koordiniert an das Metallzentrum, *in situ* gebildet wurde. Diese organometallischen Komplexe zeigten eine hohe Stabilität in wässrigem Medium, aber überraschenderweise auch beeindruckend hohe zytotoxische Wirkung. Außerdem wurde Selektivität für bestimmte Krebszelllinien beobachtet. Interessanterweise wurde bei Verwendung alkylsubstituierter Naphthochinone eine höhere Stabilität festgestellt, was durch den induktiven Effekt der Alkylgruppen erklärt werden kann. Intakter Transport in die Krebszelle spielt bei der klinischen Anwendung und der Vermeidung toxischer Nebeneffekte eine große Rolle und im Rahmen dieser Masterarbeit wurde deswegen der Einfluss verschiedener Alkylsubstituenten auf die Stabilität und das Redoxverhalten der entsprechenden Rutheniumkomplexe überprüft. Die Synthese von alkylierten Naphthochinonen und deren Komplexe, sowie Charakterisierung mittels NMR und Elementaranalysen stand am Beginn der praktischen Arbeit. Die Liganden wurden in moderaten bis sehr guten Ausbeuten isoliert, je nach verwendeter Synthesemethode. Die Komplexe wurden in guten Ausbeuten in hoher Reinheit erhalten. Die Stabilitätsmessungen wurden *via* UV/Vis durchgeführt und zeigten einen Trend zu höherer Stabilität in Korrelation mit längeren und verzweigteren Alkylsubstituenten. Zyklovoltammetrie diente zur Aufklärung der Redoxprozesse. Durch Variation der Alkylsubstituenten wurden erwartungsgemäß keine unterschiedlichen elektrochemischen Mechanismen beobachtet. Für alle Komplexe fanden Kaskaden reduktiver Prozesse statt, jedoch erst bei sehr harschen Bedingungen. Dies unterschied sich stark von der literaturbekannten Redoxchemie der freien Liganden, was eine sehr unterschiedliche biologische Wirkungsweise indiziert. Jedenfalls sind diese elektrochemischen Prozesse der Komplexe nicht im (krebs-)zellulären Medium zu erwarten.

INHALT

1 INTRODUCTION

1.1 CANCER

Cancer is a collective term for malignant diseases, which arise from anomalies in organisms on both cellular and molecular level. Realignment of healthy cells' biological characteristics can be entailed by aggressive interaction with surrounding tissue and other compartments of the body. Severe forms of cancer are life threatening and therefore major object of examination. Research on origins, but also distinction from healthy cells in terms of metabolism and (micro-)environment, has led to a better understanding of cancer throughout the last decades.[1] The next chapters provide an overview about the current status of incidences and mortality worldwide, cancer biology and therapeutic approaches.

1.1.1 Worldwide incidences and mortality

Various forms of cancer afflict people worldwide, to emerge from converging factors like a country's demography, standard of living or other epidemiological parameters. In the past, the non-communicable disease has always been a factor for premature death, but had been surmounted by other, mostly infectious diseases. Progress in medical research led to improved treatability of those, going along with higher life expectancy.[2] Today, cancer has become the first or second highest cause of premature death in most countries worldwide, besides or after cardiovascular diseases.[3] For 2020, 19 million incidences were estimated in total, whereas ten million cases ended deadly worldwide.[4] Every tenth woman and one eighth of men are likely to be affected by some form of malignant disease throughout their life.[3] Differing between affected parts of the body, sex and age is important, as origins are multifactorial.[1]

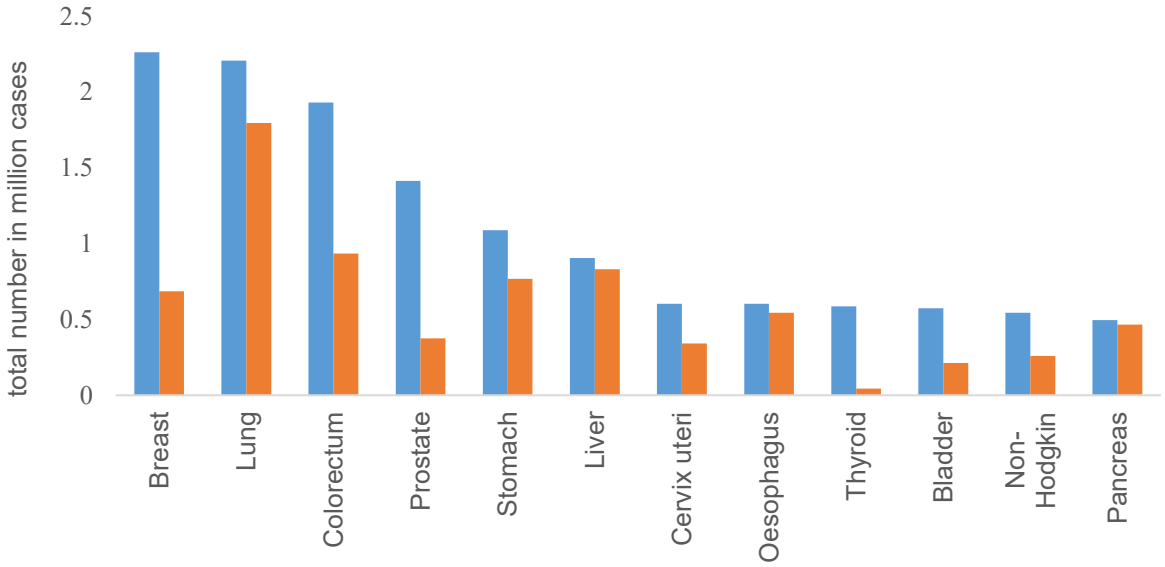

Figure 1: Cancer incidences (blue) and mortality (orange) by cancer site. Estimated numbers worldwide 2020, all sexes.[4]

Breast cancer is both the predominantly diagnosed and deadliest form of cancer to women, having even surpassed the total number of lung cancer incidences in 2020 (Figure **1**).[4] Multifactorial influence on the hormonal balance by contraceptives or later age pregnancies were shown to add up to conventional risk factors and genetic predisposition. In higher income countries, the mortality rates have declined over the past years, presumably being result of early diagnoses, resulting from better accessible screenings.[3] Contrarily, lower income areas like Latin America, or Asia have shown an increasing number of deaths, arising from breast cancer.[5] Nevertheless, a big gap between total numbers of deaths to incidences indicates overall good treatability (Figure **1**). Lung cancer is the second most commonly diagnosed form of malignant diseases.[4] Proven to be promoted by tobacco smoking, it goes along with the overall highest mortality rate.[6] Male lung cancer incidents have shown decreasing numbers over the past years due to a recently decreasing amount of male smokers. As a consequence of different smoking behavior due to social declination, women have generally started smoking later than men.[7] Resulting from this, incidence rates have now shifted, to show an increase for women alongside an overall high number of female smokers.[3] But as long term anti-smoking campaigns show impact, numbers are expected to drop within upcoming years.[6] This indicates precaution to be an effective strategy for prevention of malignant diseases. Cleary, this does not work for all forms of cancer, but particularly anti-smoking campaigns can have a positive effect on future incidences of lung cancer.[8] Colorectal cancer is the third most frequently diagnosed form of cancer in both sexes (Figure **1**). Colorectal cancer statistics demonstrate the importance of early detection or precaution measures in cancer prevention. Early examination and corresponding surgical intervention have shown positive effects on the older population's incidence rate in higher income countries. Contrarily, the younger population of those countries has shown an increasing number of incidences, a trend being linked to poor diet, deficient exercise and unhealthy lifestyle in general.[3,8] Prostate cancer is the second highest form of cancer diagnosed for men, after lung cancer.[5] An estimation of 1.4 million incidences for 2020 is opposed by an overall relatively low mortality rate of 375 000 deaths in total (Figure **1**). For prostate cancer, genetic disposition seems to play a major role, alongside classical factors like lifestyle or diet. Early-stage detection has proven to be effective aside from improved treatability throughout the last years. Therefore, mortality rates are declining, whereas numbers of newly diagnosed cases increase with greater awareness for testing.[3,9] Stomach cancer was the most commonly diagnosed form of cancer in the 1960s, but has been passed by others since then.[3] Still, patients have to face a high mortality rate. An estimated number of about 0.7 million deaths oppose about 1.1 million newly diagnosed cases in 2020 (Figure **1**). In addition to classical factors like lifestyle and diet, a high contribution is associated to infection with *Heliobacter pylori*.[3,10] Often causing no symptoms, a fraction of the infected suffer from inflammatory diseases and a variety of cancers. Aside from therapeutic approaches, studies suggest broadly applied screenings and early targeting to be a more effective strategy in order to decrease future incidences.[5] Another malignant disease linked to infection is liver cancer. Alongside alcohol abuse and other factors, Hepatitis B and Hepatitis C are strongly associated with development of hepatocellular cancer, a form of liver cancer represent about 90% of diagnosed cases.[11,12] In 2020, an estimated amount of 905 000 incidences opposed

a total number of 768 thousand deaths (Figure **1**). Overall, numbers of worldwide cancer incidences and deaths are both expected to increase drastically within the upcoming years. Changes in demography and exposure to risk factors alongside higher life expectancy are believed to entail these developments. For 2030, worldwide cancer deaths are expected to reach 13 million, whereas incidences will rise up to exceed over 10 million cases, according to WHO data.[13]

1.1.2 Biology of cancer

Genetic alterations are the origins of malignant diseases. Nutrition, air- and environmental pollution, radiation, genetic predisposition, alcohol and tobacco consumption, chemical carcinogens and viral agents are some of the converging factors to initiate cancer on a molecular level.[3] Induced chromosomal aberration and critical changes on DNA structure or composition, entail grave changes in cellular metabolism.[14] Proto-oncogenes, parts of the genome holding a critical role in cell differentiation and growth, show activation to induce oncogenic activity.[1] Deregulated levels of biomolecules deriving from these oncogenes (*e.g.* RAS, *c*-MYC) are driving forces of uncontrolled growth and proliferation.[15,16] Supportingly, growth suppressive mechanisms tend to be disabled. Overall, these mechanisms cumulate to high complexity and ultimately result in grave changes of cellular behaviour.[14,17,18] Protective mechanisms go along with strong support of growth and proliferation, in order to sustain biological immortality and progression.[19] These realignments are central characteristic of malignant cells. Hanahan & Weinberg attempted to break down these attributes of malignancy into six “Hallmarks of Cancer” in 2000 and 2011 (Figure **2**).[19,20]

Figure 2: The hallmarks of cancer. Adapted from “Hallmarks of cancer: the next generation” by Hanahan and Weinberg.[19]

SUSTAINING PROLIFERATIVE SIGNALING

Healthy cells’ growth is usually initiated by a signaling network involving recognition of external growth factors *via* cell wall receptors.[21] Internally, subsequent cascades of post translational modifications to

biomolecules (*e.g.* phosphorylation cascades) act as modes of both signal transduction and amplification to reach and activate compartments responsible for growth initiation.[22] Exemplary, receptor tyrosine kinases like EGFR (external growth factor receptor) are linked to pathways involving mediators historically named after their discovery in cancer research like Ras (rat sarcoma).[23–25] Balancing levels of the respective proteins and enzymes, respectively their interaction, is critical for healthy cells. Deregulation of these levels is a central characteristic of malignant cells, resulting in excessive promotion of cell growth and proliferation. Mutations have been observed to initiate these irregularities in critical pathways, to entail malignant cellular behavior.[26]

Evading growth suppressors

Tumor suppressing proteins play a critical role in healthy cells. Initiation of repair mechanisms, cell senescence, which is a form of silencing mechanism against unhindered proliferation, cell cycle arrest or self-induced cell death (apoptosis) can be results of tumor suppressing mechanisms.[19,27] Rb and p53 proteins act decisive in suppressive networks to keep a gate to tumorigenesis.[19] Cell cycle progression to the S phase, which involves DNA replication, is controlled by Rb.[28,29] Therefore, transcriptional events are affected by its suppressive function.[30] p53 has a variety of modalities, including initiation of apoptotic signaling, DNA repair, but also inhibitory effects like interaction with mRNA and other effectors. G2/M cell cycle arrest and cell senescence, a state of abandoned cell division, can also be determined. Modulation by stability enhancement or decrement, but also cellular localization is critical for p53 activity.[31–33] In healthy cells, ubiquitination, phosphorylation and acetylation balance promotion of stable p53 or its proteasomal degradation.[34] Problematically, aberrations of Rb and p53 pathways are central characteristic of malignant cells. Mutations in p53 can lead to loss of the tumor suppressive function, deregulation of non-mutated p53 or initiation of oncogenic activity.[35]

Activating invasion and metastasis

Invasion of surrounding tissue is one of the main aspects of malignant cells' destructive nature.[1] Increased cell motility has been addressed as one of the key factors of the diverse modes of single cell or multiple cell invasion. Factors responsible for intercellular adhesion like the epithelial-mesenchymal transition gene (EMT gene) can be weakened, to initiate invasion of surrounding compartments.[36,37] Thus being able to corrupt extracellular tissue is favored by rewired metabolic pathways (*e.g.* glycolysis, nutrient-, fatty acid metabolism), converging in altered cell movement and realignment for cell survival parameters.[38] The extracellular matrix (EMT) of primary tumors plays a major role on the interaction with surrounding compartments. Selective output of metabolites and enzymes not only features degradation of nearby tissue, but also has been affiliated to preventive measures against senescence, apoptosis, and interaction with therapeutic drugs, *e.g.* due to collagen barriers.[39] Body dispersion of malignant cells *via* entrance to the blood stream or lymphatic vessels results from overcoming endothelial surroundings. Metabolic realignments secure cellular survival during transition.[40] Extravasation and localization are influenced by vessel permeability and result in preferred colonialization at certain sites of the body. Additionally depending

on cell line specific characteristics, metastases localize in lymph nodes, liver, bone and other sites and are ought to overcome hostile conditions.[41]

Enabling replicative immortality

Healthy cells' replication is regulated. A number of replicative cycles is usually followed by termination *via* senescence or cell death, in order to limit uncontrolled propagation.[19] These processes are mainly triggered by the shortening of telomere structures on the genome with proceeding number of replication. Telomerase, the enzyme responsible for telomere elongation, shows little activity in healthy cells. In contrast, it is overexpressed in most malignant cells, initiated by genomic aberrations.[19,42,43] This reverse transcriptase is therefore associated with forced telomere elongation and prohibition of biological limitations like senescence and apoptosis. Therefore, a turnover to replicative immortality of malignant cells is central characteristic and problematically leads to uncontrolled proliferation of cancer tissue.[44]

Inducing Angiogenesis

Rewiring cellular surroundings is an important step during cellular growth, division and invasion of cancer. Malignant cells aspire to expedite influx of nutrients and oxygen from extracellular compartments, as well as efflux of dispenses.[19] Therefore, tumor cells strive for buildup of vascular transportation networks *via* angiogenesis. Healthy cells carefully balance promotion and suppression of these processes, whereas malignant cells feature deregulated promotion to outperform inhibitory effects.[45] Exemplary, signaling proteins like the class of vascular endothelial growth factors (VEGF), but also cytokines or oncogenes like c-myc have been associated with the new formation of blood vessels during angiogenesis.[46] In addition, promotion of chronic inflammation on the cancer site leads to recruitment of lymphocytes. These, usually being involved in healing processes, excrete pro-angiogenic factors to support assembling vascular structures.[47–49] Recruitment of endothelial cells for vasculogenesis, the differentiation process to blood vessels, and buildup of branches for existing vascular facilities align angiogenesis as a strong support for cancer cell viability.[45,46,50]

Resisting cell death

Apoptosis is natural for healthy cells. Several pathways of the self-induced cell death are either triggered by cell death receptors or stimulated release of cytochrome c from mitochondria.[51] Caspases then activate cascades of apoptotic pathways, ultimately resulting in the execution of cell death.[52] Apoptosis goes along with cell fragmentation and efficient digestion, but no inflammation or adverse reaction towards surrounding tissue, in contrast to necrosis.[51,53] Circumvention and downregulation of apoptotic initiators like receptors or decisive factors like the protein p53 are contradictive ways against apoptosis by malignant cells. Deregulation of usually carefully balanced pro- and anti-apoptotic proteins, as well as poor expression of caspases add up to avoidance of self-induced cell death in cancer.[54]

1.2 CANCER THERAPY

Progress in therapeutic approaches has always been linked to the medical comprehension of cancer and scientific research in medicine. The beginning of oncology can be dated back to the 1700s.[55] Over the following centuries, termination of outmoded methods and improved treatment conditions was a result of a better understanding of malignant diseases.[55,56] Nowadays, cancer removal *via* surgical intervention is one of the most commonly applied methods for solid tumors. Being the second oldest method for treatment of malignant tissue, radiotherapeutic approaches date back to the pioneer research on the effects of X-rays on matter by Roentgen, Becquerel and Curie.[57,58] Today, radiation therapy is a commonly applied method for treatment of cancer.[59] External beam radiation or internal treatment (*e.g.* radioactive iodine, radiometal based therapeutics like ^{90}Y or ^{177}Lu DOTATATE complexes) are commonly used in combination with other therapeutic methods.[60,61] Immunotherapy bases on modulative effects on the immune system *via* the use of endogenous defense mechanisms against malignant cells. This can involve inhibition of deregulation checkpoints for T-cells, autologous T-cells and prohibiting approaches for anticancer vaccination. Nevertheless, it is associated with toxic adverse effects.[62,63] Targeted therapy is an approach to use biological and chemical differences of malignant cells to healthy cells, to inhibit proliferation with high selectivity. It is often based on targeting critical metabolic pathways *via* small molecules (*e.g.* tyrosine kinase inhibitors for EGFR pathways), hormone therapy or monoclonal antibodies. A high number of targeting drugs are already in clinical use, but drug resistance and adverse effects are still problematic.[64–66] Chemotherapy is a conventionally used treatment for many cancer sites. It is an approach to use medication with cytotoxic or cytostatic properties to counter the aggressive characteristics of malignant cells described in chapter **1.1.2**. Many therapeutic agents aim for suppression of DNA replication *via* direct binding or interaction with replicative factors. Overall, a broad spectrum of chemotherapeutics has been developed to date. Adverse effects due to low selectivity, as well as drug resistances are main problems. Currently used agents, as well as cornerstones in drug development are discussed hereinafter.[67–70]

1.2.1 Platinum(II) based chemotherapy

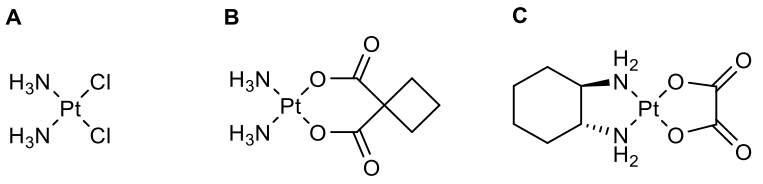

Figure 3: The Platinum(II) based drugs cisplatin (**A**), carboplatin (**B**) and oxaliplatin (**C**).

Platinum(II) drugs have dominated chemotherapy for decades. The most prominent representatives are cisplatin, carboplatin and oxaliplatin (Figure **3**). After approval by the food and drug administration (FDA) in 1978, cisplatin became one of the most established chemotherapeutics, showing versatile impact on a variety of malignant diseases like testicular-, cervical-, ovarian-, lung cancer and others.[71,72] Cisplatin is administered intravenously and undergoes aquation after cellular uptake. *Via* binding to the *N7* of guanine, the platinum core primarily forms 1,2-intrastrand links between DNA bases, but also other adducts like DNA

interstrand links as a mode of cytotoxic activity.[73,74] Carboplatin shows a similar activity profile as cisplatin, to primarily interact with DNA. It is used for treatment of ovarian cancer.[75] Aquation parameters differ from cisplatin, due to the bidentate cyclobutanedicarboxylato ligand as a leaving group. Higher stability of the complex leads to reduced activity, but also reduction in adverse effects.[76,77] Oxaliplatin consists of a diaminocyclohexane ligand and an oxalato leaving group. The drug's antiproliferative activity is also based on DNA interaction similar to cisplatin and commonly used for treatment of colorectal cancer.[78] Overall, despite showing antiproliferative activity, platinum drugs entail severe side effects due to low selectivity over healthy cells. Nephrotoxicity is a general characteristic of platinum drugs, but essentially the main side effect of cisplatin. Ototoxicity, neurotoxicity, cardiotoxicity, liver damage and other severe side effects are associated with platinum drugs in general. Dose limiting toxicity and poor treatment conditions for patients are therefore a main problem of platinum-based chemotherapy.[77] Another problematic issue is drug resistance. Malignant tissue can acquire resistance to chemotherapeutic agents. Therefore, cancer treatment with platinum drugs has its limitations.[79] In order to overcome these problems, research in novel anticancer agents has led to interesting, new approaches in chemotherapy.

1.2.2 Non-platinum based therapeutics

Throughout the last decades, alternatives to platinum-based therapeutics have been object of pharmaceutical research. Novel metal based compounds feature ruthenium, osmium, rhodium, iridium, gold, gallium, cobalt and others in various oxidation states.[80–82] Hence, these variations entail changes in modes of action, activation, stability, redox potential and other factors of cytotoxic behavior. Reduced risk of toxic side effects, stability and solubility in biological medium are important factors for clinical application.[83]

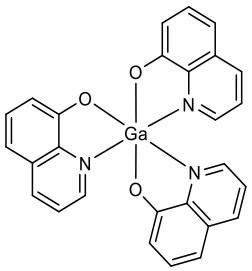

Figure 4: The gallium(III) drug candidate KP46.

KP46 (tris(8-quinolinolato)gallium(III)) is a gallium(III) based orally administrable anticancer drug (Figure **4**). It has already been investigated in an phase I clinical trial.[84] Not primarily interacting with DNA, perturbation of DNA replication is a mode of cytotoxic action, *via* inhibition of the ribonucleotide reductase (RNR).[84,85] The enzyme, containing a redox active iron species at the active site, holds a critical role in DNA synthesis. Being deregulated in malignant cells, the enzyme is a common target in cancer therapy.[86] Due to the chemical similarity of gallium(III) to iron(III), KP46 affects not only the metal center in the RNR, but has also been linked to interaction with other iron dependent cellular compartments (*e.g.* mitochondria).[87]

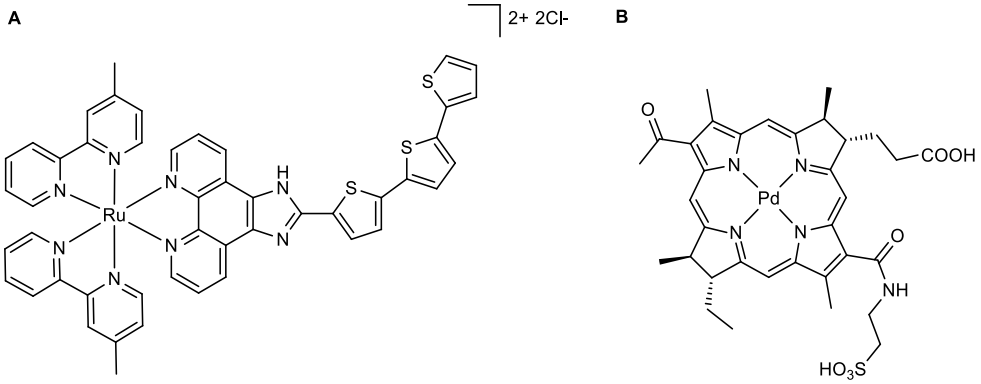

Figure 5: The photosensitizers TLD1433 (**A**) and TOOKAD (**B**).

TLD1433 (Figure **5**) is a ruthenium(II) photosensitizer with an upcoming phase II clinical study for treatment of bladder cancer.[88,89] Based on the photodynamic production of singlet oxygen, the complex was designed featuring bipyridine and phenanthroline ligands with a chromophoric α-terthienyl moiety and a positive charge, with two chloride counter ions. Application in combination with surgical intervention is necessary, in order to gain access *via* green light photon sources.[90,91] Clinical trials have been promising, showing efficacy with moderate adverse effects at therapeutic doses.[91] Padeliporfin (Figure **5**), also called TOOKAD, is a neutral palladium(II) photosensitizer featuring a porphyrin chelate ligand. The metallodrug is currently investigated in multiple studies, namely an upcoming phase III study on urothelial carcinoma in kidney or ureter and an active IIb clinical trial on prostate cancer.[92,93]

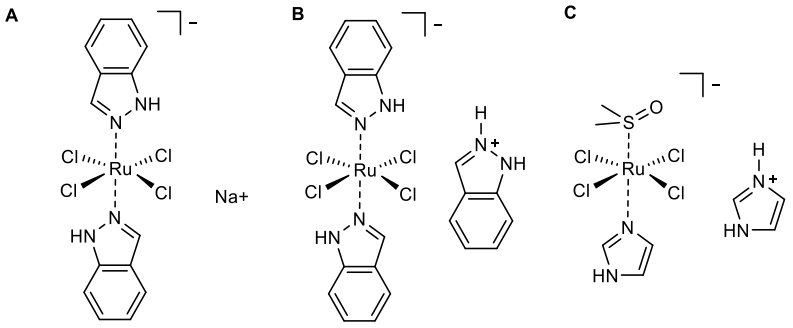

Figure 6: The ruthenium(III) based drugs BOLD-100 (**A**), KP1019 (**B**) and NAMI-A (**C**).

KP1019, having high structural similarity to BOLD-100, has shown promising results *in vivo*. Oxidative stress and interaction with biomolecules are modes of cytotoxic impact. Also DNA binding shows contribution to the antiproliferative activity.[94] No dose limiting adverse effects could be observed in clinical trials. Moreover, stabilization of tumor progression could be achieved.[95] Only differing in the counter ion being indazolium, the ruthenium(III) complex shows poorer solubility than the sodium salt BOLD-100 (Figure **6**). Therefore a high infusion volume was necessary for clinical studies and turned out to be a limiting factor in application.[95–97] BOLD-100 (formerly NKP-1339 and IT-139), currently being tested in clinical phase 1b trial, has shown promising results both *in vivo* and in clinical trials.[98,99] Consisting of two *trans* indazole ligands and four chlorido ligands, the positively charged compound features sodium as a counter

ion (Figure **6**). Reduction to a ruthenium(II) species and subsequent hydrolysis based activation *via* chlorido ligand exchange is a proposed mode of activation for this ruthenium(III) complex.[96] Notably, changes in redox potentials go along with higher reactivity towards molecular targets for the reduced ruthenium(II) species.[100] Interaction with both proteins in serum (albumin, transferrin) and cellular compartments have been shown to be responsible for drug transport and cytotoxic activity. Binding to human serum albumin (HSA) allows accumulation of BOLD-100 in the tumor tissue.[99] Inhibition of GRP78, a protein associated to tumor progression and drug resistance, is one of the suggested modes of action for BOLD-100. The antiapoptotic properties of GRP78 are critical for cancer cell viability.[101,99] Stress induction on biomolecules in the endoplasmic reticulum (ER) adds up to the modes of antitumor activity.[99] In May 2021, the FDA granted BOLD-100 an orphan drug status for treatment of gastric cancer.[102] NAMI-A, a third ruthenium(III) species having entered clinical trials, shows impact on metastases.[103,104] Featuring four chlorido ligands and imidazole and a dimethyl sulfoxide (DMSO) ligand coordinate to the metal center in *trans* position (Figure **6**).[105] Changes in ligand composition and geometry usually take influence on redox potential and kinetics and therefore impacts reactivity towards molecular targets. Hydrolysis parameters differ from BOLD-100 and KP1019, as both chlorido ligands and DMSO tend to exchange.[106] The solution chemistry of NAMI-A therefore entails different behavior *in vivo*, namely antimetastatic properties and moderate cytotoxic activity.[107,108] Despite overall promising *in vivo* data, modest tolerance was observed in a phase I/II study. Lack of efficacy and an overall unsatisfying toxicity profile resulted in termination of clinical investigations.[103,109]

1.2.3 Organometallic therapeutics

Research in transition metal-based therapeutics has ultimately led to the development of organometallic anticancer agents. Featuring stable metal-carbon bonds, representatives of this compound class have yet proven to possess promising attributes towards the field of therapeutic agents. Versatile character of organometallics featuring metallocenes, metal arenes, but also carbon monoxide derivatives or carbene ligands, has given access to a broad spectrum of innovative anti-cancer agents.[110]

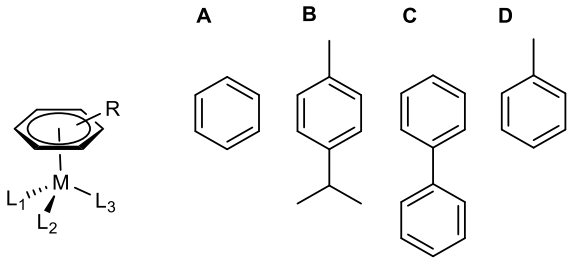

Figure 7: Piano stool complexes; L_n = ligands, R = arene substituent; arene ligands: benzene (**A**), *para*-cymene (**B**), biphenyl (**C**), toluene (**D**).

Ruthenium(II) piano stool complexes have been under investigation for years. This class of anticancer metallodrugs is named after its piano stool looking shape, featuring a stabilizing *fac* coordinated arene as a seat, and arbitrary ligands as the stool's legs (Figure **7**). This composition offers manifold opportunities

for ligand arrangement, *via* mono-, bi- and tridentate scaffolds.[111,203] Thus, ligand kinetics and redox properties are affected, to ultimately result in changes of biological behavior.[112] Arene ligand variation can influence cellular uptake due to its hydrophobic nature, but also affects target interaction (*e.g.* DNA intercalation properties of biphenyl, pictured in Figure **7**), solubility in aqueous systems and complex stability.[113]

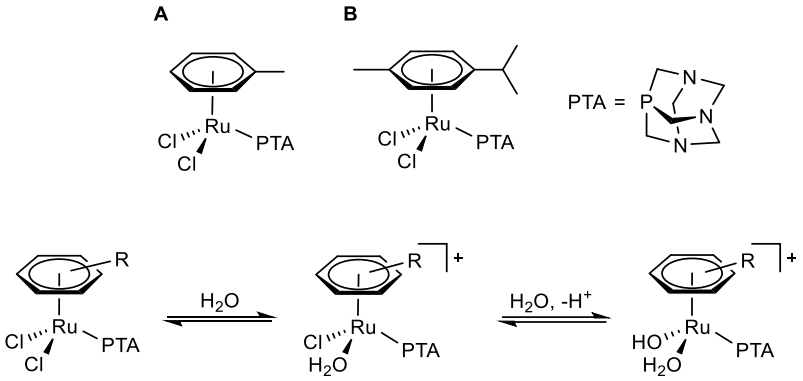

Figure 8: RAPTA-T (**A**), RAPTA-C (**B**); Aquation of RAPTA compounds in aqueous media.[114]

Ruthenium(II) piano stool complexes of the RAPTA (ruthenium arene PTA) class consist of a PTA ligand, two labile chlorido ligands and are distinguished by their arenes. RAPTA-C features a *p*-cymene arene, whereas toluene is applied in RAPTA-T.[115] The eponymous ligand for RAPTA complexes is 1,3,5-triaza-7-phosphaadamantane (PTA), contributing to solubility and biological properties. In aqueous medium, RAPTA compounds show aquation of one or both chlorido ligands, yielding cationic species along the way of target interaction (Figure **8**). Low cytotoxicity towards malignant cells *in vitro*, but good selectivity for metastasis cell lines and high activity *in vivo* were observed.[116] Its mode of action, at first being assumed to base on DNA interaction, is now associated with protein binding. A number of possible targets have been identified, involving extracellular growth factors, cell cycle modulating proteins, histones and ribosomal architecture.[117,118] Interestingly, RAPTA-C was observed to prevent disaggregation from primary tumors at the initiative process of newly formed metastases.[119] RAPTA-C is contemplated for combinational application with targeted therapeutic agents like erlotinib (EGFR inhibitor), due to promising results.[115]

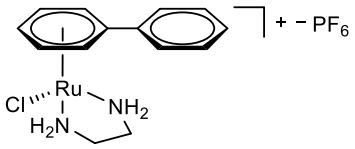

Figure 9: The Piano stool complex RM175.

RM175 is a positively charged piano stool complex, which consists of a bidentate ethylene diamine ligand, a chlorido leaving group, biphenyl arene (Figure **9**) and hexafluorophosphate as counter ion.[120,121] DNA interaction *via* binding to the N7 of guanine was observed similar to the mode of action for cisplatin. Along the way to DNA base binding, interaction with biomolecules such as the cysteine containing peptide

glutathione (GSH) was found. Interaction with biomolecules is a commonly associated event for ruthenium(II) agents, due to its affinity to sulfur and nitrogen donors.[122,123] As a result of cytotoxic action, induced cell cycle arrest in G_2/M and apoptosis was observed.[120,124] Overall, RM175 and RAPTA-C demonstrate the versatile nature and powerful impact of ligand design on organometallics, resulting in grave differences in terms of molecular targets and mechanisms of antiproliferative activity.[119]

1.2.4 Bioactive ligands

Conjugation of bioactive molecules to transition metal complexes is a promising approach in drug development. The unbound ligands' properties are utilized for certain interactions with molecular targets. Binding to specific enzymes, targeted release towards tumor tissue or site-directed transport are possible features of these modulations. Increase of bioavailability and decrease of adverse effects are central objectives.[125] Drugs featuring more than one mode of action (multi-targeted activity) are associated with certain advantages: Interaction *via* diverse modes of action facilitates to target metabolic pathways of cancer in various ways. Circumvention of drug resistances is another feature of multi-targeted drugs, to overcome a major problem in chemotherapy. This also holds the option for redesign of well-studied bioactive agents with adverse effects. Herein, selected examples will be discussed, ultimately highlighting the compound class of interest for this work – ruthenium(II) based half sandwich complexes.[126–128]

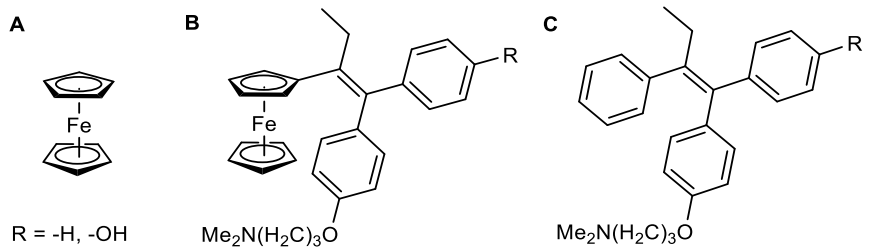

Figure 10: Ferrocene (**A**), (hydroxy-)ferrocifen (**B**, R= OH, H), (hydroxy-)tamoxifen (**C**, R= OH, H).

Ferrocene, being one of the most prominent metalorganics, has engaged research on metallocene-based drugs after being developed in 1950. The lipophilic complex was observed to accumulate in animals in 1969.[129] Production of reactive oxygen species (ROS) leading to damage of DNA and cellular compartments has been linked to cytotoxic activity, thus triggering research on ferrocene bearing metallodrugs.[130,131] Ferrocenyl conjugation to peptides or biologically active molecules (*e.g.* retinoids, testosterone, naphthoquinones) has delivered interesting approaches for both anticancer and antiviral therapeutics.[132,133] Tamoxifen, a common therapeutic against hormone dependent breast cancer, has been used as pharmacophore for a variety of ferrocenyl bearing derivatives. These approaches resulted in the development of ferrocifen and its metabolite hydroxyferrocifen (Figure **10**). Both act *via* interaction with estrogen receptors in breast cancer, but have proven to be active against tamoxifen resistant cell lines.[129] This compound class has been brought up as an early approach for interaction with molecular targets *via* installment of a well-understood, biologically active moiety.[134]

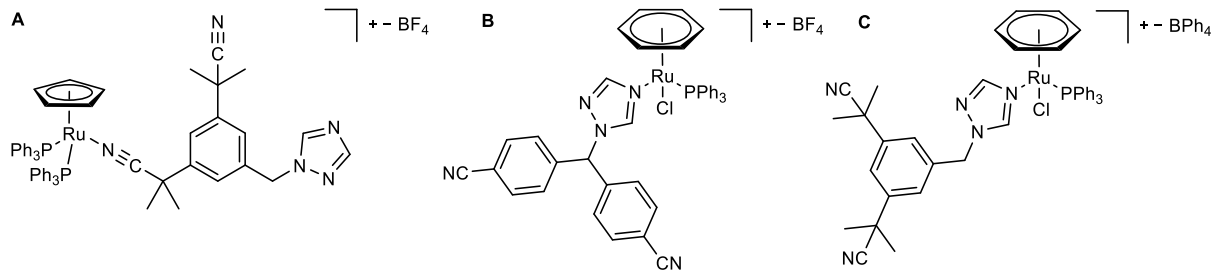

Figure 11: Anastrozole (**A**, **C**) and letrozole (**B**) featuring ruthenium(II) piano stool complexes.[135,136]

Aromatase inhibitors (AIs) act *via* suppression of deregulated estrogen production. Uncontrolled estrogen activity on the ER entails metabolic changes of significance for breast cancer, such as proliferation and angiogenesis. In contrast to tamoxifen, anastrozole or letrozole do not base on interaction with ER, but downregulate estrogen levels *via* binding to cytochrome P450 on the enzyme aromatase.[137–140] Novel approaches to overcome characteristic drug resistance mechanisms, address the use of AIs as pharmacophore for bioactive ruthenium(II) piano stool complexes (Figure **11**). These considerations also accommodate problems in drugs design. An anastrozole featuring ruthenium cyclopentadienyl complex **A** (Figure **11**) has shown high toxicity on breast cancer cell lines, with IC_{50} values in the nanomolar range. Unfortunately, low selectivity over healthy cells, even in comparison to cisplatin, have demonstrated the complexity of targeted drug design. Enzyme docking simulations for compound **A** with aromatase have shown interference of certain amino acids with other moieties of the metallodrug than anastrozole. The cytotoxic impact therefore is linked to other modes of action than enzyme inhibition, with unfortunate results for selectivity.[135] Another work described a letrozole based ruthenium(II) complex (Figure **11**) involving a possible multi-target effect, to add up ligand activity for inhibition *via* cytochrome P450 and the known anticancer activity of piano stool frameworks. Comparative studies with letrozole being replaced with a chlorido ligand showed increased activity, but as ligand variation on this scale entails grave changes on drug characteristics, these results must be considered with caution. However, a multipath activity for cell death by autophagy, triggered by **B** was presumed to involve synergistic effects.[136] A third anastrozole featuring ruthenium(II) complex (**C**) has shown promising results. Favored binding to aromatase and a low *in vivo* adverse toxicity were observed.[141] Overall, these observations for **A**, **B**, **C** make out interesting approaches for ruthenium(II) based anticancer agents with bioactive ligands. Multipath activity towards molecular targets in malignant cells is an approach for circumvention of drug resistance pathways.[142]

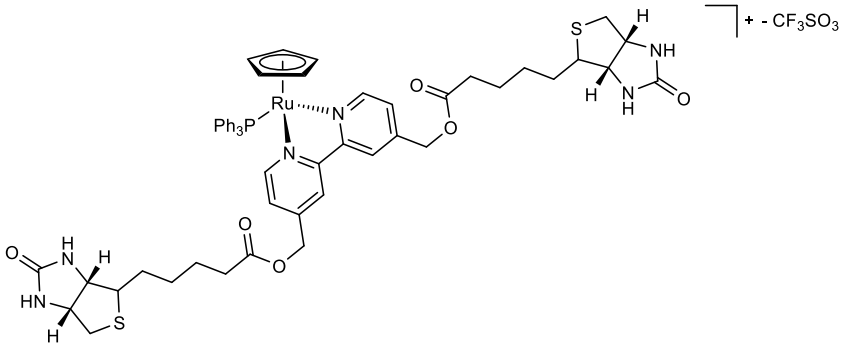

Figure 12: PGP inhibiting ruthenium(II) complex.

Plasma membrane glycoprotein (PGP) is an ATP driven pump, which is associated with drug resistance. Efflux of various drugs (*e.g.* doxorubicin) decreases efficiency of therapy and is therefore a major problem in cancer treatment.[143] These transporters are commonly overexpressed in cancer cells. Drug application in combination with PGP inhibitors is a common approach, alongside use of therapeutics with low sensitivity towards export *via* these transporters.[144] Drug conjugation to biotin has been observed to feature improved drug uptake by cancer cells. Recognition and preferred uptake by malignant cells *via* overexpressed sodium gradient transporters leads to more selective drug delivery and reduced adverse effects towards healthy tissue.[145] Adding up to this positive effect, efflux *via* PGP seems to be hindered. A biotinylated ruthenium(II) complex (Figure **12**) has shown inhibitory potential on PGP, whereas the unfunctionalized complex served as a substrate, to be exported. Different binding towards the transport protein due to the biotin linker were identified as reason for selective inhibition and minor adverse effects *in vivo*.[146]

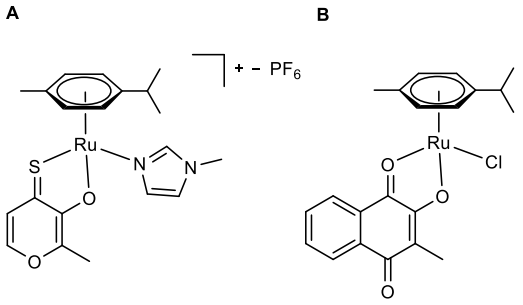

Figure 13: Organometallic topoisomerase inhibitors thiomaltol (**A**) and KP2048 (**B**).[147,148]

Small molecule conjugation to ruthenium(II) piano stool frameworks has spawned a broad field of research on novel substances with diverse modes of anticancer potential. Thiomaltol-, thiopyridone-, flavone- or naphthoquinone-based metallodrugs have been observed to insert distinct activity towards biological targets (*e.g.* inhibition of topoisomerase).[147–149] Importance of rational ligand design has been demonstrated manifold. Thiomaltol based metallodrugs (Figure **14**, **A**) were observed to show higher stability in aqueous solution with leaving group variation from chlorido to 1-methylimidazole. Thus, higher delivery of intact metallodrug to tumor tissue was presumed to be entailed, which is evidence on importance of drug stability for treatment.[147] KP2048 (Figure **14**, **B**), featuring a phthiocol bidentate and a chlorido leaving group, has

been examined *in vivo* on mice. The drug showed distinct activity on tumor tissue, aside from severe side effects on multiple parts of the body. Too high reactivity towards inadvertently reached organs was presumably caused by preliminary activation after administration. However, activity on malignant tissue demonstrated the anticancer potential of naphthoquinone based piano stool complexes.[148] Therefore, adverse reactivity must be diminished, possibly by redesign of ligand architecture or incorporation of a targeting moiety. First approaches involved coupling to polymers, to result in high stability and promising *in vivo* results, whereas adverse effects towards healthy sites were diminished.[148]

1.2.5 The anticancer activity of naphthoquinones

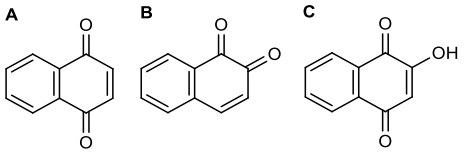

Figure 14: 1,4-Naphthoquinone (**A**), 1,2-naphthoquinone (**B**), 2-hydroxy-1,4-naphthoquinone or lawsone (**C**).

Naphthoquinones are a versatile class of organic molecules, showing anticancer, anti-inflammatory, antiallergic, antiplatelet and other properties of interest for pharmacological use.[150,151] A broad spectrum of quinone and naphthoquinone derivatives have been investigated for therapeutic application, with important representatives originating from nature (plants, microorganisms, fungi).[152] Due to their cytotoxic activity, naphthoquinone and anthraquinone derivates have gained interest as agents in chemotherapy. The mechanisms of biological and cytotoxic activity are diverse but have been extensively studied and were summarized in a review by Pereyra *et. al.* in 2019 (Figure **15**). Hereinafter, these processes will be discussed and depicted on examples.

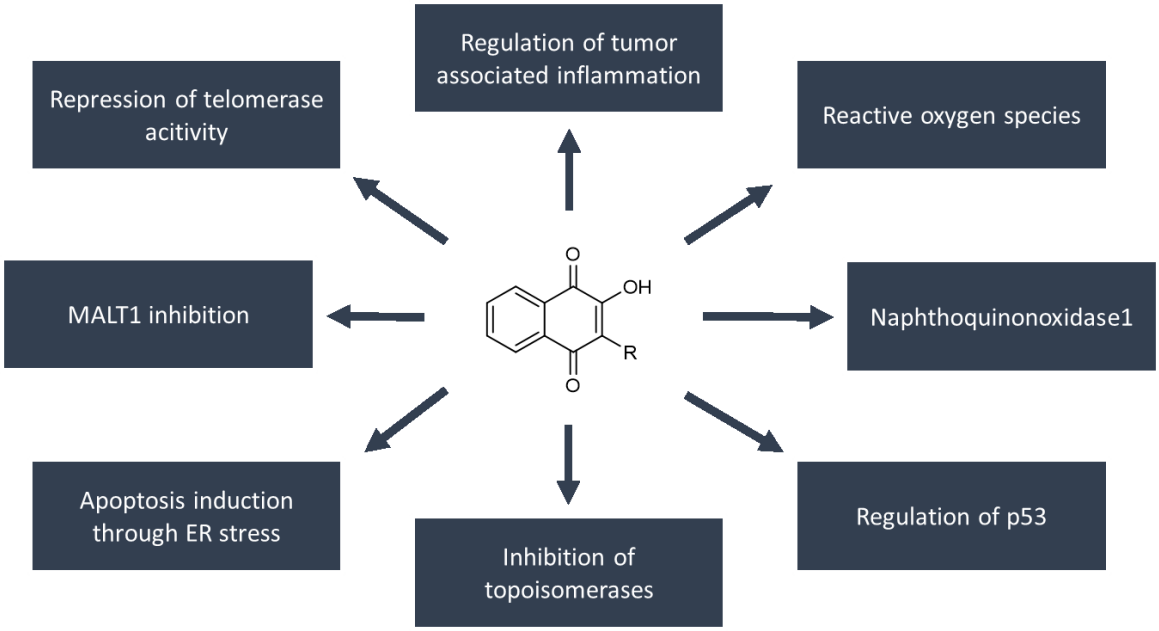

Figure 15: Mechanisms of anticancer activity of naphthoquinones. Adapted from Pereyra *et. al*.[153]

REACTIVE OXYGEN SPECIES

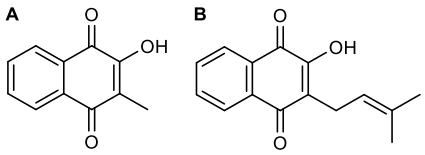

Figure 16: Phthiocol (**A**) and lapachol (**B**).

ROS production has been identified as one of the main mechanisms of naphthoquinone derivatives' cytotoxic activity.[154,155] The redox chemistry of naphthoquinones such as phthiocol and lapachol (Figure **16**) has been extensively studied.[156,157] Cyclic reduction by NAD(P)H and reoxidation from oxygen leads to intracellular release of ROS, capable of dealing damage to diverse targets.[154,155] ROS directly damage DNA and DNA repair systems, but also enzyme driven metabolic pathways are affected.[158] Cysteine proteases like cathepsin show deregulated levels in cancer. Serving for extracellular degradation, they are key feature for tumor microenvironment, progression and proliferation.[159] Cysteine based deubiquitinases (DUBs) are another example for cancer associated proteases.[160] Their role on regulating levels and localization of cellular proteins has critical impact on tumor progression.[161] Downregulation of both enzyme species by naphthoquinone derivatives has been observed, resulting from their sensitivity towards ROS.[155]

NAPTHOQUINONOXIDASE1 (NQO1)

NQO1 is a NAD(P)H utilizing enzyme, which is overexpressed in malignant cells. As a two-electron transferring biocatalyst, it usually serves for cellular detoxification and stress reduction. Being shown to reductively activate naphthoquinone derivatives for redox cycling, it is also associated to assist on ROS generation.[162,163]

TUMOR SUPPRESSOR PROTEINS (p53, p73)

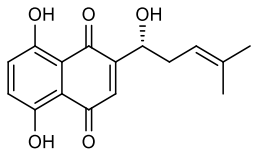

Figure 17: Shikonin.

p53 holds a decision-making role on cell survival, apoptosis, and cell cycle arrest (chapter **1.1.2**). Mutations, expression and regulative effects on the gene are therefore tightly controlled in cancer cells.[164] Naphthoquinone derivatives such as shikonin (Figure **17**) were observed to upregulate levels of the protein, to promote strong support on anti-tumor activity.[165] p73 serves an analogous role to p53 in cells. In cervix cancer cell lines, naphthoquinones induced an increase of p73 expression, to entail apoptosis.[166]

TOPOISOMERASE I/II

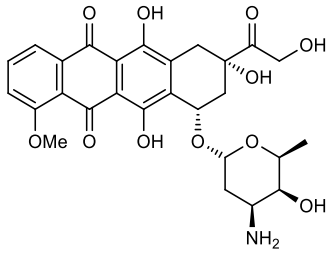

Figure 18: Doxorubicin.

Other targets of naphthoquinones are topoisomerase I and topoisomerase II. These enzymes hold a critical role in DNA processing. The ATP independent topoisomerase I relaxes supercoiled DNA *via* strand breaks, rotation and realignment.[167] The naphthoquinone derivative β-lapachone (Figure **20**) was observed to act different than other topoisomerase I inhibitors, namely *via* binding to the intermediate complex of enzyme and DNA, rather than to the individual free species.[154,168] Topoisomerase II activity is ATP dependent. The enzyme serves for rearrangement of DNA structures, featuring control of embroiled DNA loops. Intermediate cleavage of the phosphodiester bond is key mechanistic feature of this isomerase.[169] Topoisomerase II inhibitors can have different modes of action. So called “poisons” such as doxorubicin (Figure **18**) induce DNA alteration *via* strand breaks and bond formation to biomolecules. Topoisomerase II binds to these species, leading to stable complex formation and termination of enzyme activity. Other modes of action directly aim for inhibition at certain intermediate states of substrate conversion. These also involve anthracycline drugs like aclarubicin.[170–172]

ENDOPLASMIC RETICULUM STRESS

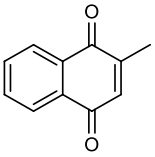

Figure 19: Plumbagin.

Further anticancer activity of naphthoquinones is based on ER stress. Plumbagin (Figure **19**) was observed to induce apoptosis partially *via* stress induction on the ER. The mode of action for plumbagin is associated with ROS induced stress.[173] But also other modes of stress induction on the ER have been reported.[153] It holds an important role in protein modification after ribosomal synthesis. Post translational modifications and protein folding are handled and controlled for their correctness. Misfolded proteins are subsequently delivered to the proteasome.[174] Shikonin was observed to inhibit proteasomal degradation in hepatoma and prostate cancer cells leading to cell death. The mode of action is assumed to involve electrophilic interaction of shikonin’s keto groups towards nucleophilic amino acids in the catalytic center of the proteases.[153,175]

Inhibition of proteasomal activity results in aggregation of misfolded proteins and therefore elevates stress on the ER.[153]

MUCOSA-ASSOCIATED LYMPHOID TISSUE LYMPHOMA TRANSLOCATION PROTEIN 1 (MALT1)

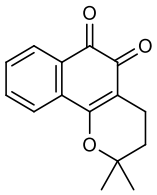

Figure 20: β-Lapachone

MALT1 is a protease with tumor promoting activity in diffuse large B cell lymphoma (DLBCL). The enzyme has a similar function to caspases (paracaspase), but cleaves with specificity for arginine.[176] Featuring a cysteine and histidine catalytic center, its proteolytic activity is associated with suppression of NF-κB downregulating factors.[177] In cancer cells, NF-κB is linked to promotion of tumor growth *via* oncogenic signaling, maintenance of inflammation and avoidance of apoptosis. Moreover, acquired resistance to chemo- and radiotherapy (*e.g.* cisplatin resistance) has been observed to be driven by the NF-κB pathway.[178–180] Suppression of NF-κB promotion by MALT1 inhibition has been examined in medical chemistry. Due to its stand-alone role in terms of mechanistic activity, targeted treatment of MALT1 is a common suggestion for avoidance of adverse effects.[181] Naphthoquinone derivatives have been investigated as MALT1 binding inhibitors and β-lapachone derivatives have shown inhibition of MALT1, to result in cytotoxic impact on DLBCL.[182]

REPRESSION OF TELOMERASE ACTIVITY

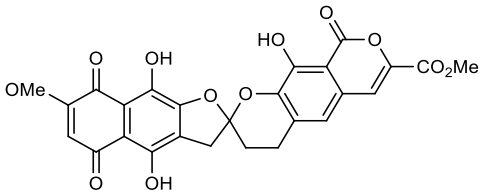

Figure 21: γ-Rubromycin

Telomerase activity plays an important role for sustaining replicative immortality in cancer (chapter **1.1.2**). Being overexpressed in malignant cells, it serves as an interesting target for cancer therapy. Telomerase inhibition has been observed for some specific quinone and naphthoquinone species. A series of spiroketal naphthoquinone derivatives (*e.g. γ*-rubromycin, Figure **21**), but also the 1,4-benzoquinone species thymoquinone have been observed to inhibit telomerase.[183–186] Plumbagin was also shown to inhibit its enzyme activity in brain cancer cells, showing higher influence on malignant cells with increased telomerase activity.[187,188] Furthermore, other quinone based derivatives (*e.g. s*hikonin, Figure **17**) are suspected to

interact with the enzyme.[189] However, modes of action for most of these observations are still not fully elucidated and must be examined for further predictions.

Regulation of tumor associated inflammation

Constant inflammation of tumor sites plays a critical role for cancer progression (chapter **1.1.2**). STAT proteins (signal transducer and activator of transcription) have impact on a broad variety of cellular pathways. Amongst its manifold tumor promoting mechanisms, STAT3 controls key mediators of inflammation such as the NF-κB pathway, or expression of certain cytokines.[180,190,191] Plumbagin (Figure **19**) was found to exert antitumor activity against esophageal cancer *via* direct binding to DNA interaction domains of STAT3, which adds up to the modes of anticancer activity of naphthoquinones.[192]

1.2.6 Ruthenium(II) complexes featuring a naphthoquinone based *N,O,O*-tridentate ligand motif

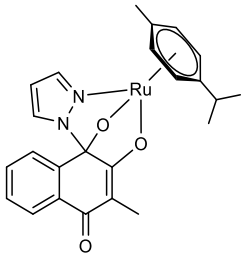

Figure 22: Phthiocol-based tridentate ruthenium(II) *p*-cymene complex.[203]

CHEMICAL PROPERTIES AND *IN VITRO* CYTOTOXICITY

Ligand variation experiments on KP2048 (Figure **13**) have brought up a novel class of piano stool complexes. Hydroxy-1,4-naphthoquinone, 1,2-diazole and ruthenium(II) arene dimer undergo *in situ* formation of a stable *N,O,O*-tridentate ligand motif (Figure **22**), initiated *via* treatment with excess of a base. This novel ligand architecture permits variation towards different naphthoquinone derivatives, 1,2-Diazole variation, arene substitution or even the choice of osmium(II) as a metal center. *In vitro* assays have shown impressive cytotoxic activities in non-small cell lung carcinoma (IC_{50}/µM = 1.2 ± 0.2; A549 cell line) and colon carcinoma cells (IC_{50}/µM = 0.094 ± 0.031; SW480 cell line). In contrast, the cisplatin sensitive ovarian teratocarcinoma cells (IC_{50}/µM > 50; CH1/PA-1 cell line) exhibited minor response to treatment.

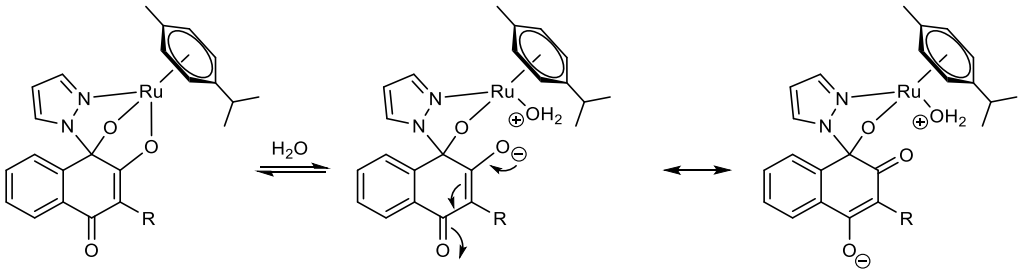

Figure 23: Aquative activation and mesomeric stabilization (R = stability determining functional group).

The complex showed high stability in aqueous medium, even after incubation for 24 hours.[203] Due to entropic effects, tridentate chelators are generally known to form complexes of higher stability than mono- or bidentates.[193] A broader study on substituent variation on the 2-hydroxy-1,4-naphthoquinone ligands' position 3 has provided further insight into the tridentate motif's chemical properties. Electron withdrawing groups (chlorine, bromine) were observed to activate the complex towards aquation in biological media (Figure **23**). In contrast, functional groups with inductive effect (methyl, ethyl substituents) stabilize the tridentate architecture. Of all coordinating atoms, the ligand's oxygen on position 2 shows the weakest bond to the metal center. Inductive effects on the naphthoquinone π system increase electron density on this coordinating position, strengthening the connection towards the ruthenium(II) core, and therefore complex stability. Robustness in aqueous solution was shown to result in higher *in vitro* toxicity, as observed for alkylated derivatives. A complex featuring an ethyl group exhibited extraordinarily high activity selectively

on non-small cell lung carcinoma (IC_{50}/μM = 0.76 ± 0.14; A549 cell line) and colon carcinoma (IC_{50}/μM = 0.046 ± 0.007; SW480 cell line), whereas no relevant impact on ovarian teratocarcinoma cells (IC_{50}/μM 62 ± 5; CH1/PA-1 cell line) was found. Notably, an increase of lipophilicity often correlates with preferred cellular uptake and therefore can be associated with the higher cytotoxic activities.[194,195,203] In comparison to *in vitro* toxicity of phthiocol based complexes, these results indicate an interplay of increased cellular uptake and intact complex delivery. Still, tremendous cytotoxic impact and selectivity towards certain cell lines remain unexpected and unresolved.[195,203]

BIOLOGICAL PROPERTIES

With regard to novelty and outstanding cytotoxic properties of the *N,O,O*-tridentate complexes, it is hard to predict modes of action for anticancer activity. Further products of the aquation process (Figure **23**) have shown loss of the naphthoquinone moiety and dimerization. Amino acid incubation studies have indicated reactivity towards cysteine containing amino acids, yielding trithiolato-bridged dimers. High affinity to thiols is important for interaction with glutathione.[196] However, these processes have yet to be examined in more detail. Further investigations on possible mechanisms have been carried out, partially orienting on commonly observed targets for naphthoquinones derivatives, as they are depicted in chapter **1.2.5**. Plasmid assays have shown no strong interaction with DNA, whereas ROS formation was not observed to be responsible for cytotoxic activity. Reactive oxygen species are central mode of anticancer activity for naphthoquinone derivatives. Exclusion as a possible mechanism is an important step towards target identification. However, the typical targets ER stress and NQO1 were shown to be at least partially involved with naphthoquinone induced ROS activity (chapter **1.2.5**). Clearly, further research on the biological behavior of *N,O,O*-tridentate complexes is necessary for more precise predictions.[195]

2 RESULTS AND DISCUSSION

2.1 AIM AND OBJECTIVE OF THIS THESIS

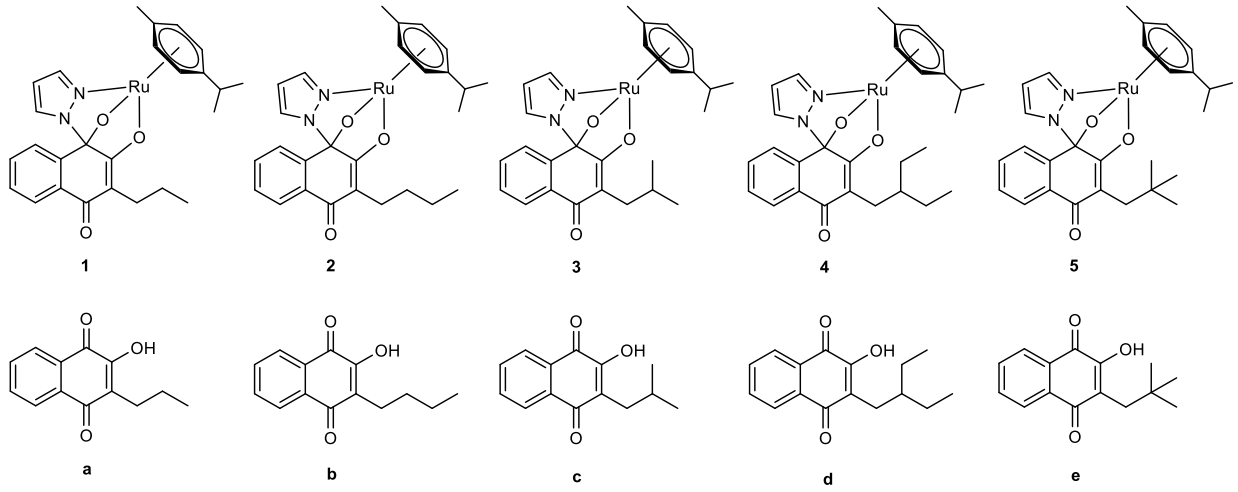

Figure 24: Complexes **1**–**5** and ligands **a**–**e**.

Main objective of this thesis was the synthesis and characterization of a series of *N,O,O*-tridentate ruthenium(II) complexes, featuring different alkyl groups at position 3 of the naphthoquinone scaffold. Rationale behind this approach are observations of increased complex stability in aqueous solution for methyl and ethyl substituents (chapter **1.2.6**). A broader spectrum of compounds featuring longer and branched alkyl chains should provide further insight into characteristics of this novel class of piano stool complexes (Figure **24**). Starting with ligand synthesis, 2-hydroxy-1,4-naphthoquinone derivatives **a**–**e** should be synthesized. Further complexation should lead to the desired ruthenium(II) complexes **1**–**5**. Characterization *via* NMR, elemental analysis and solubility determination for both ligands and complexes should be followed by investigation of complex stability *via* UV/Vis. Redox properties should be examined *via* cyclic voltammetry.

2.2 LIGAND SYNTHESES

2.2.1 General procedure

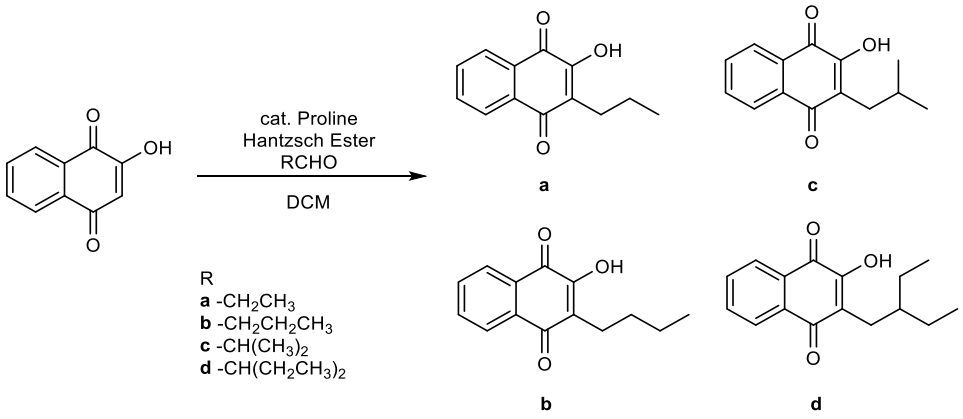

Figure 25: General procedure for ligand synthesis of ligands **a**–**e**.

Lawsone, diethyl 1,4-dihydro-2,6-dimethyl-3,5-pyridinedicarboxylate (Hantzsch ester) and the respective aldehyde RCHO were reacted to the desired ligands in moderate to good yields of 59–86%. This procedure (Figure **25**) was adapted from literature procedures, which initially had shown poor conversion and required optimization of reaction parameters.[197]

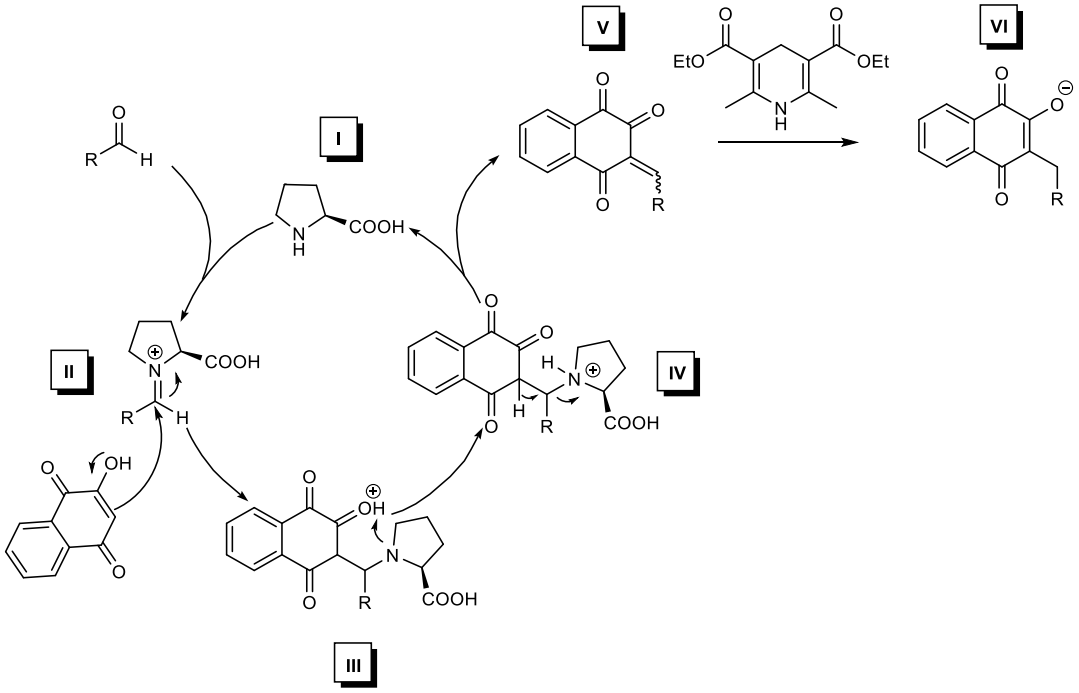

Figure 26: Proposed mechanism of the prolin catalyzed alkylation (R= alkyl chain).

Originally, a one pot reaction using lawsone, an aldehyde as alkyl donor, catalytic amounts of L-proline and Hantzsch ester in dry DCM was chosen for synthesis of desired naphthoquinone derivatives **a**–**e**. According

to literature, the reagents should be stirred at room temperature (r.t). for twelve hours to achieve the products in excellent yields.[197] As depicted in Figure **26**, the proline catalyst (**I**) is presumed to initially form an iminium ion intermediate **II** with the respective aldehyde. The electrophilic character of **II** is reason for further reaction with lawsone, to form species **III**. Protonation of the tertiary amine and subsequent release of the proline catalyst *via* elimination leads to **V**, presumably as a mixture of (*E*)- and (*Z*)-3-alkylidenenaphthalene-1,2,4(3H)-trione. Deprotonated product **VI** results from reduction by Hantzsch ester. This reaction had already been tested using acetaldehyde as an alkyl donor, and had shown good conversion. Problematically, these conditions were hardly applicable on the chosen aldehydes. Poor yields were obtained from propionaldehyde and butyraldehyde, whereas alkyl donors with a branched chain showed even lower to no conversion. This can be linked to stronger inductive effects of the alkyl chain towards the respective aldehyde carbon. Thus, it's decreased electrophilic character results in stabilization of the intermediately formed iminium ion **II** (Figure **26**). Therefore, further reaction with lawsone is hindered. Fortunately, an increase in temperature led to a higher conversion. Utilizing these considerations, reaction conditions were optimized. Temperatures were increased, whereas reaction times could be shortened *via* the use of microwave assisted heating. Thus, massive increase in yields was achieved, going up to 86%. No conversion was observed for **e**. Presumably, the iminium intermediate **II** was stabilized by the high inductive effect from the neighboring *tert*-butyl group, to show no further reaction. Therefore an alternative method was chosen (Figure **27**).

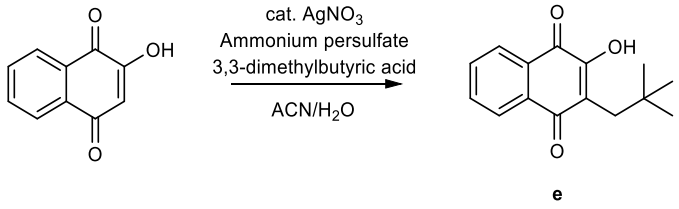

Figure 27: Synthesis of **e**.

For the synthesis of **e**, lawsone, catalytic amounts of silver nitrate and 3,3-dimethylbutanoic acid were taken up in ACN/H_2O and a solution of ammonium peroxodisulfate in water was added. Silver iron promoted decarboxylation of the acid leads to an intermediately formed carbocation *via* addition of the radical starter ammonium persulfate. Purification per column chromatography led to **e** as a yellow solid, yielding 25%. Attempts to improve yields for this reaction failed, as both variation in temperature and equivalents of reagents resulted in formation of hardly separable side products.

2.3 COMPLEX SYNTHESES

2.3.1 General procedure

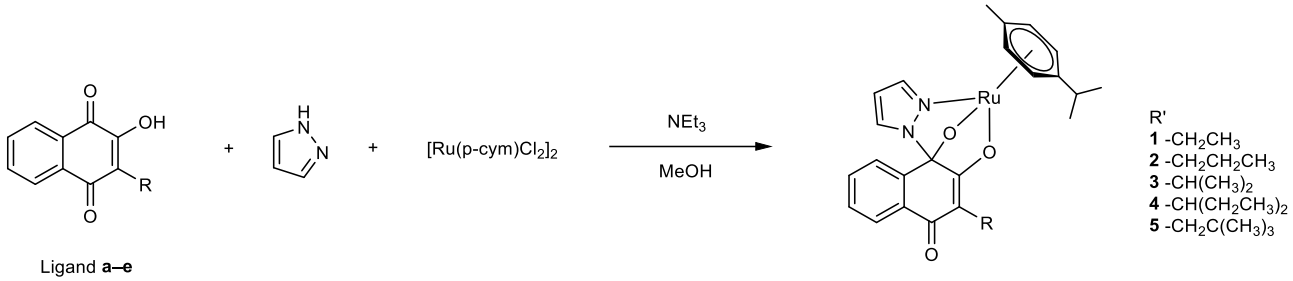

Figure 28: Complex synthesis: general procedure.

The synthesis was performed according to the first reported procedures of this compound class (Figure **28**).[195,203] The metal dimer, 1,2-diazole and the respective naphthoquinone derivative were dissolved in methanol and an excess of triethylamine was added. Stirring under microwave irradiation was followed by solvent removal under reduced pressure. The crude product was purified *via* column chromatography (silica, isocratic, 70% ethyl acetate, 5% triethylamine in *n*-hexane). The formed pale yellow to greenish solid was separated by filtration and dried. The organometallics were obtained in moderate to good yields (58 to 78%, respectively).

2.4 CHARACTERIZATION

2.4.1 NMR spectroscopy

^{1}H-NMR SPECTROSCOPY OF LIGANDS

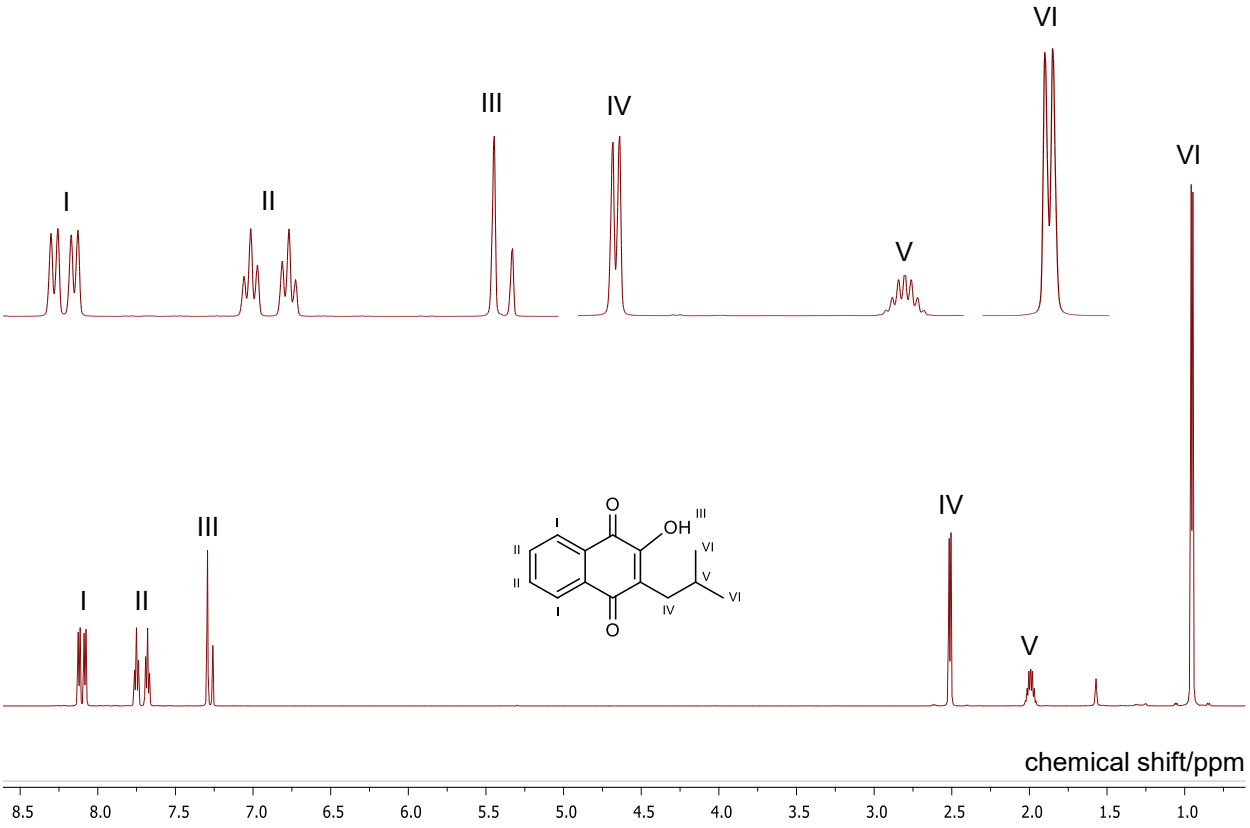

Figure 29: ^{1}H NMR spectrum of **c** in $CDCl_3$.

^{1}H NMR spectra of **a**–**e** were measured in deuterated chloroform and no impurities could be observed. As the naphthoquinone products differed in terms of alkyl substituent, the chemical shift of aromatic hydrogens showed no relevant changes. As pictured in Figure **29**, aromatic hydrogens **I** couple with both neighboring atoms **II** over four bonds, to appear as doublet of doublets (dd). The highest chemical shift results from the nearby carbonyl group. Each hydrogen **II** is capable of coupling to three atoms **I**, **I**, and **II**, to appear as a doublet of doublet of doublets (ddd). The acidic proton **III** belongs to the hydroxyl group, to be visible as a singlet. Doublet **IV** only couples to the tertiary carbon's hydrogen **V** and shows higher chemical shift due to the nearby π system. **V** appears as multiplet due to coupling with both methyl groups **VI** and methylene protons **IV**. This position shows the highest variation for different ligands **a**–**e**. Coupling to methylene **IV** is uniform, but one or two methyl groups (ligands **a** and **c)**, one or two ethyl groups (ligands **b** and **d**) or a quaternary carbon on this position result in different coupling patterns. Terminal groups show low chemical shift and splitting patterns were observed as singlets, doublets or triplets, in accordance to the neighboring group **V**.

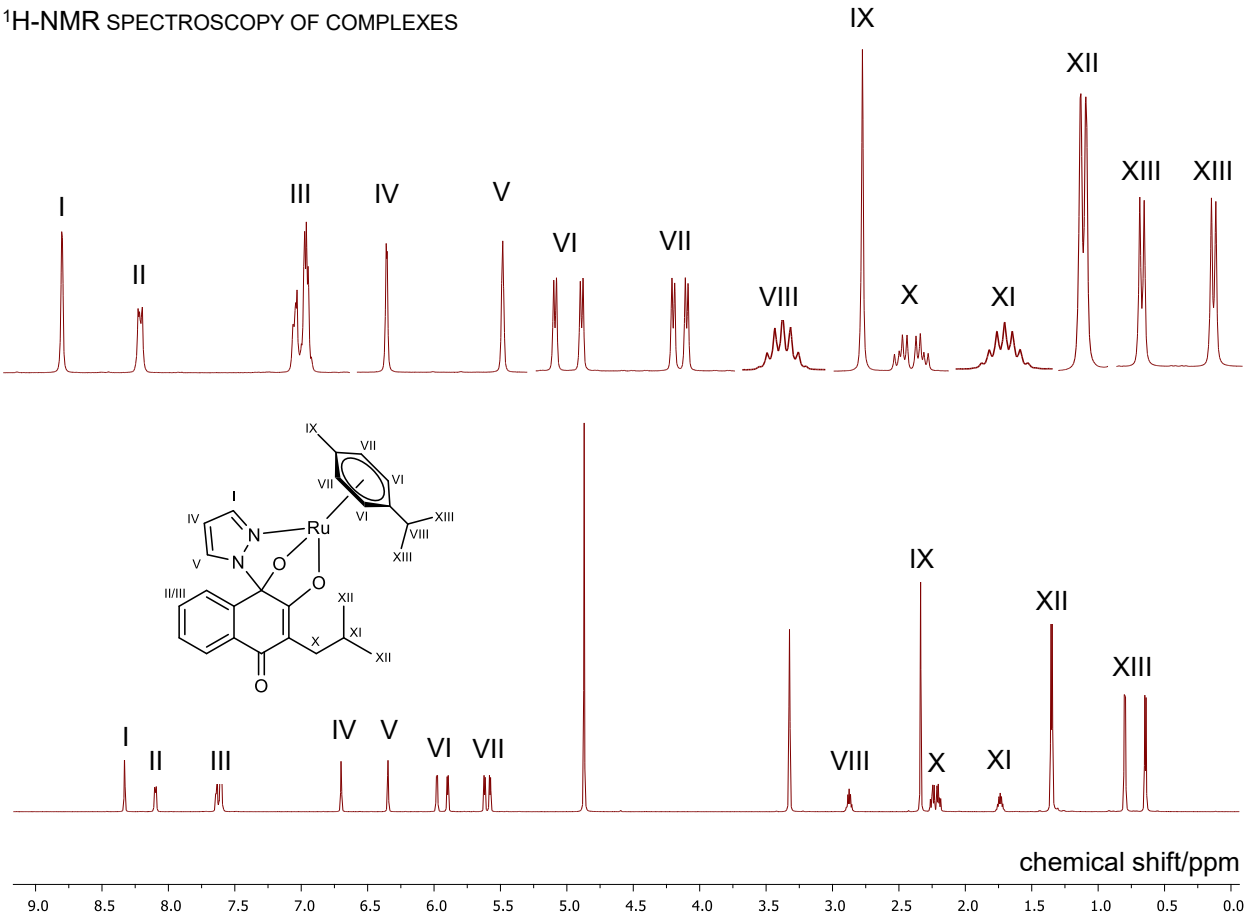

Figure 30: ^{1}H NMR Spectrum of **3** in MeOD.

^{1}H NMR spectra of **1**–**5** were measured in deuterated methanol. Consistent to the ligands' spectra, the series differed in terms of substituents in the aliphatic range, showing no variation for the eleven protons **I**–**VII**. Loss of the hydroxyl proton's signal, increased shift of pyrazole protons and four separate signals for the arene confirm the formation of the desired complex. Proton **I** showed couplings with **IV** and a high shift due to the neighboring nitrogen-ruthenium position. **II** and **III** were observed to belong to the naphthoquinone's aromatic moiety. Protons **III** are undistinguishable due to overlapping peaks, whereas **II** is presumably located nearest to the coordination positions and therefore shows increased chemical shift. **IV** and **V** both show couplings with all protons of the diazole moiety, to result in doublets of doublets. The aromatic protons of the η^6 bound arene show individual peaks and coupling with neighboring protons results in doublets of **VI** and **VII**, respectively. Highest shift of aliphatic protons was observed for the tertiary carbon's proton **VIII**, appearing as a septet due to couplings with methyl groups **XIII**. Methyl group **IX** shows a singlet with similar chemical shift to **X**. For **3** (Figure **30**), **X** does not overlap with **XI** and is perceived as ddd, to result from couplings with **XI** and long-range couplings with methyl groups **XII**. Tertiary proton **XI** both couples with **X** and **XII**, to result in a doublet of quartets, whereas **XII** overlapped and only showed couplings towards **XI**. The arene's static methyl groups **XIII** appeared as individual peaks, with couplings towards **VIII**, to be visualized as doublets.

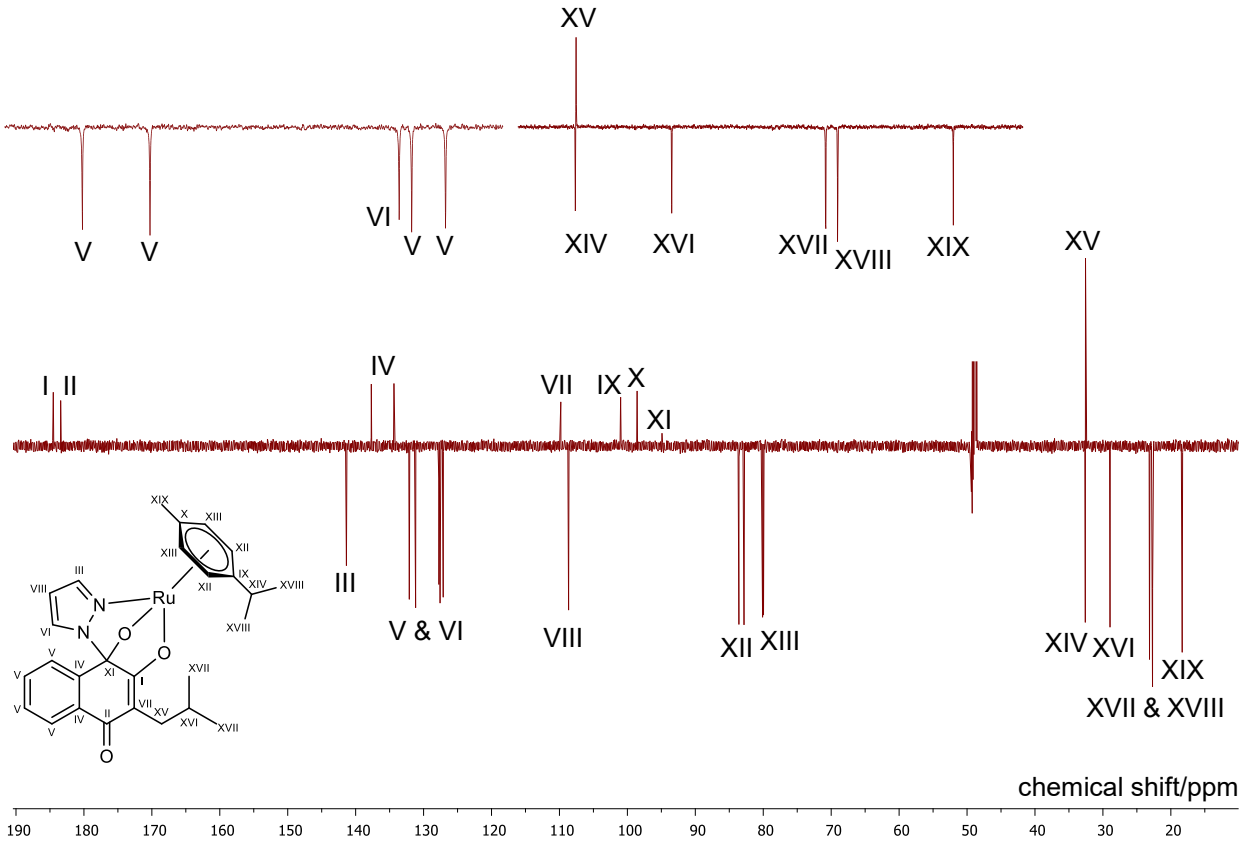

Figure 31: ^{13}C NMR Spectrum of **3** in MeOD.

^{13}C NMR spectra of **1**–**5** were measured in deuterated methanol. Quaternary peaks **I** and **II** show highest shift, both due to the nearby oxygen and their position in the naphthoquinone's π-system. Next, a range of aromatic C-H carbons **III**–**VI** and quaternary carbons **IV** are visible, with **III** showing highest shift due to the nearby ruthenium bound nitrogen. **VII** differs from the higher shift of other aromatic carbons, presumably due to the alkyl substituent. It shows similar shift to the pyrazole moiety's C-H carbon **VIII**. Characteristically, the hemiaminal carbon **XI** is depicted with very low intensity. This can be interpreted as proof of complex formation *via* tridentate ligand motif. **XII** and **XIII** show individual peaks, in correlation to ^{1}H spectrum observations. Remaining carbons are located in the aliphatic range, lower than 40 ppm. **XIV** shows almost identical shift to the secondary carbon **XV**, which are easily distinguished in phase by the DEPTq. Other carbons are the primary carbon **XVI**, and tertiary carbons **XVII**, **XVIII** and **XIX**. Both peaks for **XVII** and **XVIII** show minimal overlap of equivalent methyl groups, which indicates rotation around **XVI**, respectively **XIV**.

2.4.2 UV/Vis stability

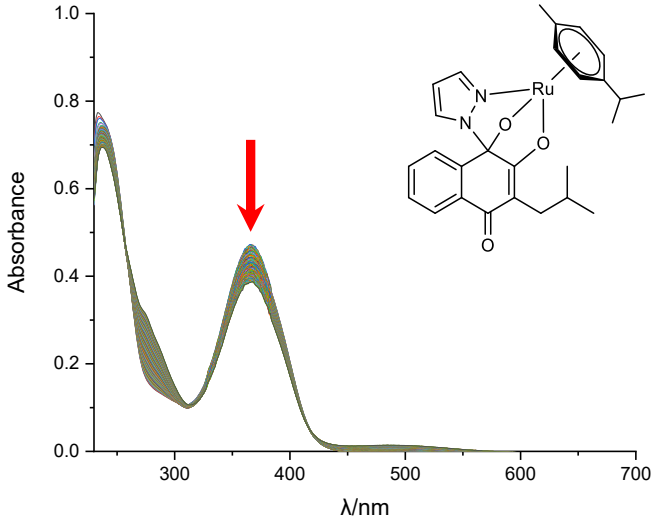

Figure 32: UV/Vis spectrum of **3** over 48 hours.

UV/Vis spectra were obtained from 40 µM solutions of compounds **1**–**5** in phosphate buffered saline (PBS) with 1% DMSO as solubilizer at 20 °C over 48 hours. As shown in Figure **32**, decreasing absorbance at the peak maximum of 366 nm was used for assessment. Data evaluation showed initial values (A_0) around 0.5 (compounds **1**–**3**) and 0.8 (compound **5**) with a decrease over time. Data was normalized ($A+(1-A_0)$) and is visualized in Figure **33**.

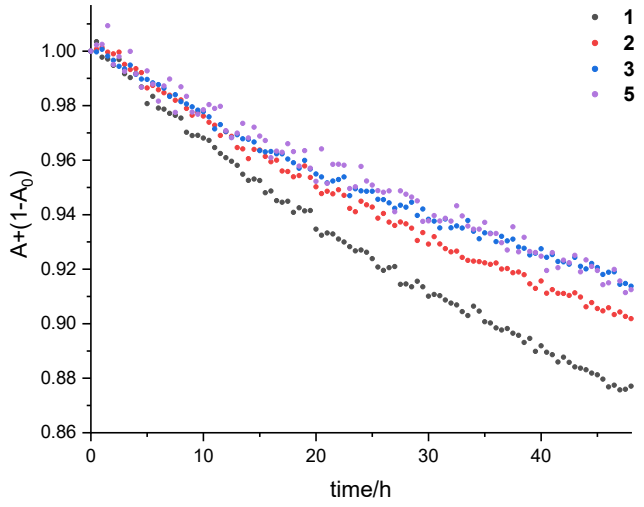

Figure 33: Decrease in Absorbance (λ= 366 nm) OVER 48 hours for **1**, **2**, **3**, **5**.

A decrease in absorbance is associated with chemical interactions of the dissolved complex towards the solvent. High differences over a short period of time can be linked to a more rapid process, whereas stable complexes' absorbance remains unchanged. Notably, UV/Vis analysis involves no identification of the aquation processes' intermediate species (Figure **23**), which can result in decreasing, but also increasing

absorbance at a given wavelength. The *n*-propyl derivative **1** shows the highest change of absorbance over time (12%), indicating a more rapid interaction towards the solvent. Second highest decrease over time was observed for the *n*-butyl derivative **2** (10%), whereas branched derivatives **3** (9%) and **5** (9%) showed equal decrease in absorbance over 48 hours. Derivative **4**, having the highest number of carbon atoms and therefore least solubility in polar medium, was observed to precipitate within the first measuring cycle. Decrease of complex concentration resulted in reduced signal intensity of A_0, with unsatisfying signal to noise ratio. Still, precipitation was observed. Insolubility in aqueous medium is a critical factor for the practical use of metallodrugs, hindering clinical application and analytical characterization. Overall these observations demonstrate the impact of alkyl substituents on complex stability. Less reactivity towards the solvent was observed for derivatives with longer alkyl chains. Derivatives **3** and **5**, which feature branched alkyl chains, showed highest stability over time.

2.4.3 Cyclic voltammetry

Cyclic voltammograms were recorded from a solution of the respective ligand **a**–**e** (2.3–3.8 mM) or complex **1**–**5** (2.01–2.44 mM) in ACN. Using a three electrode measuring setup, samples were measured at different scan rates (10–200 mV/s).

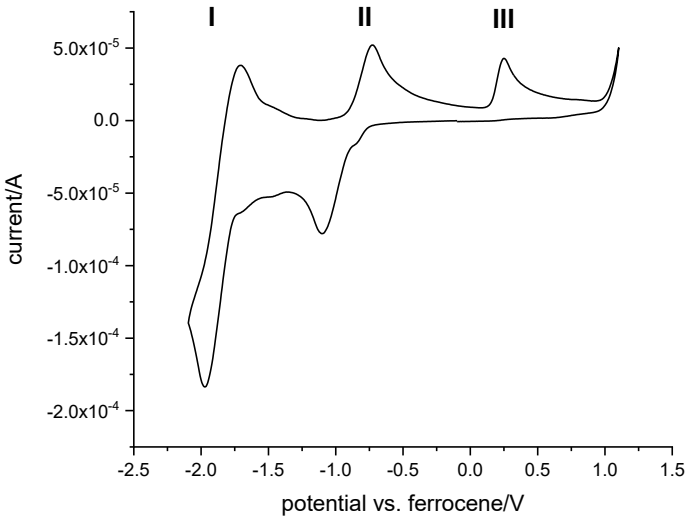

Figure 34: Cyclic voltammogram of ligand **a** (100 mV/s).

Cyclic voltammogram of ligand **a** is pictured in Figure **34**. A variety of oxidation and reduction processes occur in the range of -2 to 1.5 V. Processes **I** and **II** are irreversible, due to reduction and oxidation peak separation higher than 57 mV.[198] Redox chemistry of 2-hydroxynaphthoquinones (HQ) in aprotic media is already known to literature.[156,157] Redox processes **I** are summarized in Equation **1** and visualized in Figure 35.

Equation 1: Ligand reduction **I**.

$$(1)\ HQ + e^- \rightleftharpoons HQ^{\bullet -}$$

$$(2)\ HQ^{\bullet -} + HQ \rightarrow H_2Q^{\bullet} + Q^-$$

$$(3)\ H_2Q^{\bullet} + e^- \rightleftharpoons H_2Q^-$$

$$(4)\ H_2Q^- + HQ \rightarrow H_3Q + Q^-$$

$$3\ HQ + 2\ e^- \rightleftharpoons H_3Q + 2\ Q^-$$

Equation 2: Ligand reduction **II**.

$$Q^- + e^- \rightleftharpoons Q^{\bullet 2-}$$

With increasing negative potential, the naphthoquinones' electropositive moieties stepwise attract electrons, to form radical species. In aprotic media, the first one electron reduction occurs towards a carbonyl group, to form a negatively charged, radical species in (1). Deprotonation of another species of HQ in (2) and reduction of the second carbonyl group occurs, to form a two radical, anionic species in (3). Subsequent rearrangement to the negatively charged species and protonation from an unreacted HQ are final steps of this reductive cascade. In summary, three equivalents of ligand **a**–**e** react to 3-alkylnaphthalene-1,2,4-triol and two equivalents of deprotonated naphthoquinone, which show further reactivity in **II** (Figure **36**).

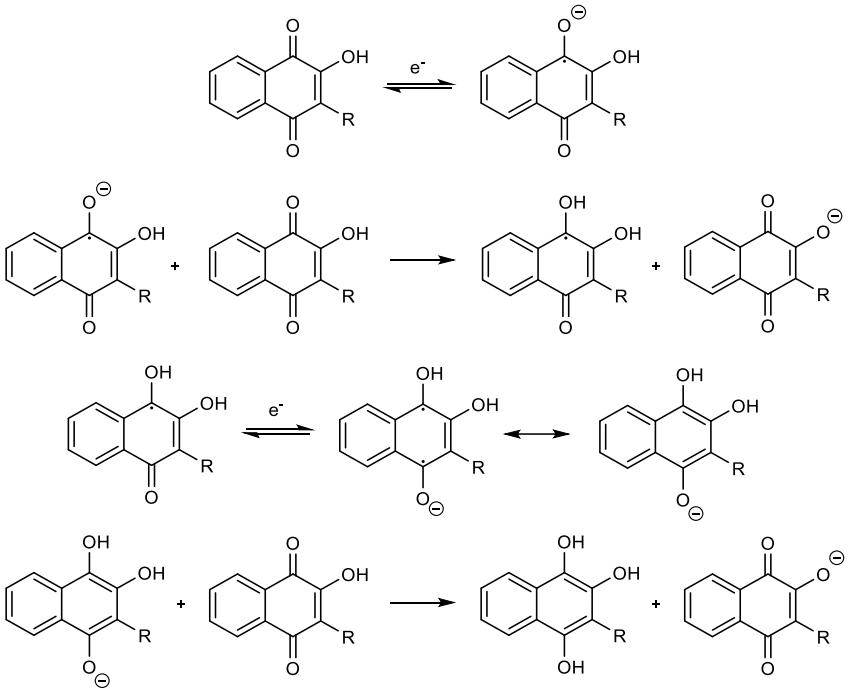

Figure 35: Proposed mechanism for the ligand reduction (Peak **I**).

Peak **II** shows an irreversible one electron transfer towards the deprotonated naphthoquinone deriving from reduction **I**. This reduction step (Equation **2**) results in a double negatively charged, radical naphthoquinone, as depicted in Figure **36**. The radical may be stabilized over mesomeric structures.

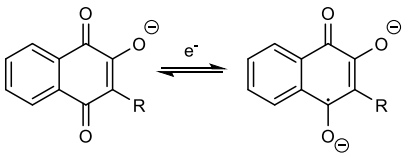

Figure 36: Ligand reduction (Peak **II**).

A third peak **III** shows an irreversible oxidation around 0.5 V, which is interpreted as a further reaction of a radical species, deriving from reductive cascades of **I**.[157]

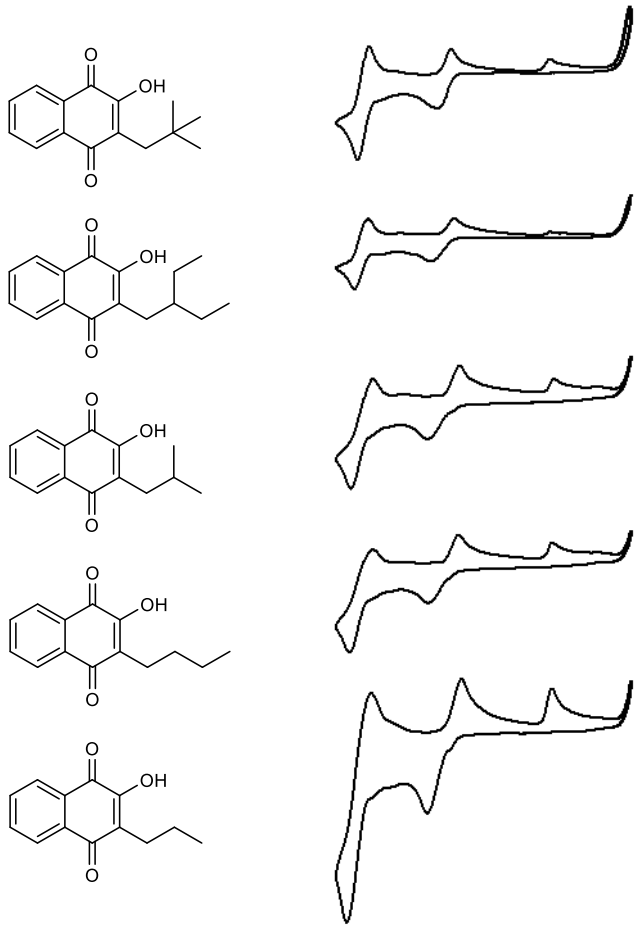

Figure 37: Cyclic voltammograms of ligands.

Figure **37** list the respective cyclic voltammograms of ligands **a**–**e**. Notably, peak heights are dependent on scan rate and sample concentration and therefore vary.[199] However, qualitative information can be obtained from the respective voltammograms. Reduction and oxidation peaks **I**–**III** are visible for all ligands, which indicates no impact of alkyl substituent variation on mechanistic behavior. These observations correlate with expectations, as redox processes depicted in Figure **35** and Figure **36** are mechanistically independent from alkyl substituents.

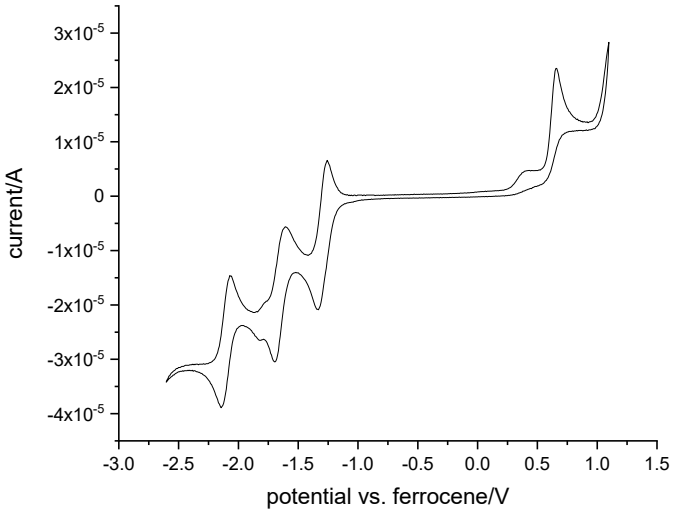

Figure 38: Cyclic voltammogram of complex **1** (10 mV/s).

Redox chemistry of the tridentate architecture is complex. High structural difference to the free ligands **a**–**e** prohibits reliable predictions based on the ligands' properties. Reductive cascades are initiated at -1 V, and are observed as three waves towards extremely negative potentials of -2.5 V. Thus being driven by harsh conditions, estimations on the mechanistic behavior would require further insight into energy states and redox characteristics. However, these processes possibly involve cleavage of the tridentate architecture and reduction of the metal center to ruthenium(I). A further possibility considers the electrophilic properties of the remaining carbonyl group of the complex. As depicted in Figure **36**, a one electron transfer leads to formation of a cationic, radical species for the ligands **a**–**e**. The same reduction could happen to the complexes' carbonyl group, as pictured in Figure **39**.

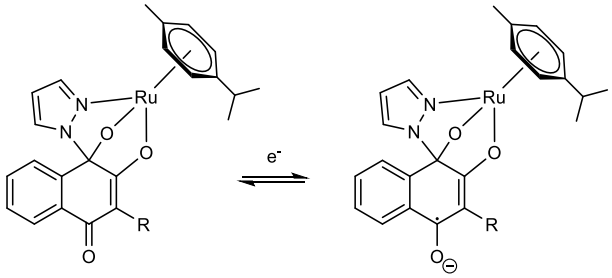

Figure 39: Proposed reduction of **1**–**5**.

Also, an irreversible oxidation takes place at positive potentials, lower than 1 V. Hypothetically, this could mean oxidation of an intermediate species of the redox processes at negative potentials, similar to the irreversible oxidation **III** of the ligands' cyclic voltammograms.

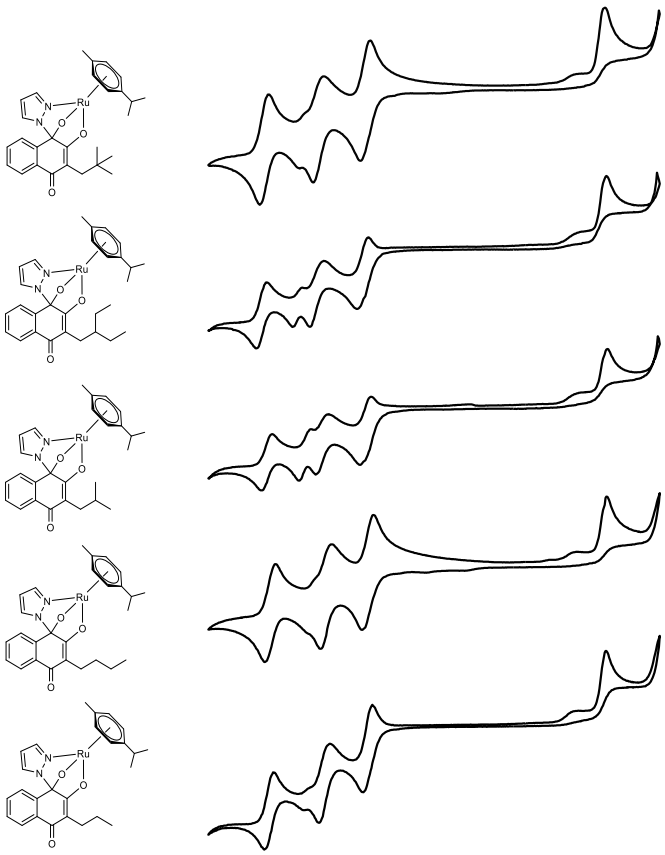

Figure 40: Cyclic voltammograms of complexes.

The opposed voltammograms of complexes **1**–**5** show the same number of reduction and oxidation processes (Figure **40**). This demonstrates that alkyl substituent variation shows no relevant impact on mechanistic behavior. Notably, in dependence on scan rates, peak height and form varies. At lower scan rate, a peak overlap visualizes in the reductive cascades, indicating further processes or chemical rearrangement of intermediate species, similar to ligands' mechanisms in **I** (Figure **35**).

BIOLOGICALLY RELEVANT REDOX PROCESSES

As known from literature, biological redox processes occur in certain ranges of electrochemical potentials. Whereas theoretical potentials of over ±1 V are possible, important cellular reduction processes (*e.g.* NAD^+/NADH, GSH/GSSG) take place at less reductive conditions than -1 V.[200,201] Harsh conditions trigger reductive cascades on complexes **1**–**5**, as depicted in Figure **38** and Figure **40**. Thus premising highly negative potentials, the compounds supposedly won't undergo equivalent mechanistic behavior under comparatively mild biological conditions. As mentioned in chapter **1.2.6**, ROS production was not identified as mode of action for this compound class of naphthoquinone-based complexes. Therefore, potential for redox cycling in the biological range would not necessarily be an expected observation. Still, as measuring setups differ from biological conditions, these results should be considered with caution, but indicate consistent redox behavior, irrespective of alkyl substituents.

3 EXPERIMENTAL PART

3.1 EQUIPMENT AND METHODS

3.1.1 Equipment

Microwave:	Biotage® Initiator+
NMR spectrometer:	700.40 MHz (AV III HD 700 Bruker BioSpin); 600.25 MHz (AV III 600 Bruker BioSpin);
Elemental analysis:	Microanalytical Laboratory of the University of Vienna, PerkinElmer *2400 Series II CHNS/O Elemental Analyzer* for CHN analyses, Eurovector *EA3000 Elemental Analyzer* for CHNS analyses;
UV/vis spectrometer:	Perkin Elmer lambda 35 photometer, PTP (Peltier Temperature Programmer), Julabo AWC 100 recirculating cooler;
Cyclic voltammetry:	Princeton Applied Research, Potentiostat/Galvanostat Model 273A;

3.1.2 Materials

Solvents were acquired from commercial suppliers and generally used without further purification. Dichloromethane was dried over anhydrous calcium chloride and stored over molecular sieve 3 Å.

Bis[dichlorido(η^6-*p*-cymene)ruthenium(II)] was synthesized in accordance to literature.[202]

Reagents were purchased from commercial suppliers: ruthenium(III) chloride hydrate (Johnson Matthey), α-Terpinene (Alfa Aesar), 2-hydroxy-1,4-naphthochinon (Acros), Hantzsch Ester (TCI), L-Prolin (Merck), propionaldehyde (TCI), butyraldehyde (TCI), isobutyraldehyde (Fluka), 2-ethylbutanal (Fluka), 3,3-dimethylbutanoic acid (Acros), ammonium peroxodisulfate (Acros-Fischer), silver nitrate (Acros), 1,2-diazole (Acros-Fischer), triethylamine (Acros-Fischer);

3.1.3 Solubility in aqueous medium

Solubility of ligands and complexes was determined in PBS with 1% DMSO. Initial dissolution of compound in pure DMSO was followed by addition of the resulting stock solution to PBS (pH 7.4, 1:100). Ligands showed immediate change of color to red, which indicates deprotonation at pH 7.4.Complexes which showed precipitation after addition to PBS were dissolved *via* doubling the amount of medium.

3.2 LIGAND SYNTHESES

3.2.1 General procedure

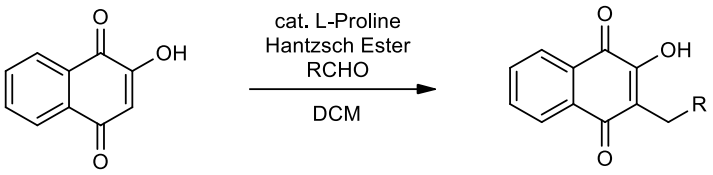

Figure 41: Ligand synthesis: general procedure.

Lawsone (1 equiv.), Hantzsch ester (1.1 equiv.) and the respective aldehyde (2 equiv.) were taken up in dry DCM (12–20 mL) and stirred for five minutes at r.t.. L-Proline (0.2 equiv.) was added and the resulting yellow suspension was stirred under microwave irradiation (85–100 °C, 25–60 minutes). The dark red solution was washed with 10% HCl and brine. The organic layer was dried over anhydrous sodium sulfate and the solvent was removed *in vacuo*, yielding the crude product as a solid or viscous oil. Pure product was obtained as a yellow solid *via* column chromatography (silica, gradient 40–80% DCM in *n*-hexane).

Yield: 59–86%

3.2.2 2-Propyl-3-hydroxynaphthalene-1,4-dione: **a**

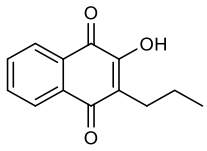

Figure 42: Ligand **a.**

The product was synthesized according to the general procedure, using lawsone (506 mg, 2.91 mmol, 1 equiv.), Hantzsch ester (800 mg, 3.16 mmol, 1.1 equiv.), propionaledehyde (412 µL, 334 mg, 5.74 mmol, 2 equiv.) and L-proline (66 mg, 0.57 mmol, 0.2 equiv.) in dry DCM (20 mL). The mixture was stirred at 85 °C for 25 min under microwave irradiation. The crude product (R_f 0.25, 50% DCM in *n*-hexane) was purified via column chromatography (silica, gradient 40–80% DCM in *n*-hexane), to yield **a** as a yellow solid (535.5 mg, 2.48 mmol, 85%).

^{1}H-NMR (700.40 MHz, $CDCl_3$): δ 8.12 (d, *J* = 7.7 Hz, *J* = 7.7 Hz, 1H, CH: arom.), 8.08 (d, *J* = 7.6 Hz, *J* = 7.6 Hz, 1H, CH: arom.), 7.75 (dd, *J* = 7.5, 7.5 Hz, 1H, CH: arom.), 7.68 (dd, *J* = 7.5, 7.5 Hzz, 1H, CH: arom.), 7.29 (s, 1H, OH), 2.59 (t, *J* = 7.6, 2H, CH_2), 1.58 (m, 2H, CH_2), 0.99 (t, *J* = 7.3, 3H, CH_3) ppm.

Elemental analysis calculated for $C_{13}H_{12}O_3$: C 72.21%, H 5.59%, O 22.20%.
Found: C 71.86%, H 5.55%, O 22.03%.

Solubility (PBS, pH 7.4, 1% DMSO): 1.71 mM.

3.2.3 2-Hydroxy-3-propylnaphthalene-1,4-dione: **b**

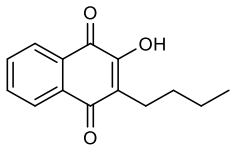

Figure 43: Ligand **b**.

The product was synthesized according to the general procedure, using lawsone (504 mg, 2.89 mmol, 1 equiv.), Hantzsch ester (810 mg, 3.20 mmol, 1.1 equiv.), butyraledehyde (517 µL, 414 mg, 5.74 mmol, 2 equiv.) and L-proline (70 mg, 0.61 mmol, 0.2 equiv.) in dry DCM (20 mL). The mixture was stirred at 85 °C for 25 min under microwave irradiation. The crude product was purified via column chromatography (silica, gradient 40–80% DCM in *n*-hexane), to yield **b** as a yellow solid (531 mg, 2.31 mmol, 80%).

^{1}H-NMR (700.40 MHz, $CDCl_3$): δ 8.12 (dd, J = 7.7, 0.5 Hz, 1H, CH: arom.), 8.07 (dd, *J* = 7.6, 0.7 Hz, 1H, CH: arom.), 7.75 (ddd, *J* = 7.6, 7.6, 1.1 Hz, 1H, CH: arom.), 7.68 (ddd, *J* = 7.5, 7.5, 1.1 Hz, 1H, CH: arom.), 7.28 (s, 1H, OH), 2.61 (m, 2H, CH_2), 1.53 (m, 2H, CH_2), 1.44 – 1.36 (m, 2H, CH_2), 0.94 (t, *J* = 7.4 Hz, 3H, CH_3) ppm.

Elemental analysis calculated for $C_{14}H_{14}O_3$: C 73.03%, H 6.13%, O 20.85%.
Found: C 72.70%, H 6.17%, O 20.65%.

Solubility (PBS, pH 7.4, 1% DMSO): 1.56 mM.

3.2.4 2-Hydroxy-3-isobutylnaphthalene-1,4-dione: **c**

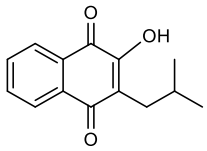

Figure 44: Ligand **c**.

The product was synthesized according to the general procedure, using lawsone (503 mg, 2.89 mmol, 1 equiv.), Hantzsch ester (817 mg, 3.22 mmol, 1.1 equiv.), isobutyraledehyde (424 µL, 414 mg, 5.74 mmol, 2 equiv.) and L-proline (72 mg, 0.62 mmol, 0.2 equiv.) in dry DCM (20 mL). The mixture was stirred at 90 °C for 45 min under microwave irradiation. The crude product was purified via column chromatography (silica, gradient 40–80% DCM in *n*-hexane), to yield **c** as a yellow solid (392 mg, 1.70 mmol, 59%).

^{1}H-NMR (700.40 MHz, $CDCl_3$): δ 8.12 (d, J = 7.7 Hz, 1H, CH: arom.), 8.08 (d, J = 7.6 Hz, 1H, CH: arom.), 7.75 (dd, *J* = 7.5, 7.5 Hz, 1H, CH: arom.), 7.68 (dd, *J* = 7.5 Hz, 1H, CH: arom.), 7.29 (s, 1H, OH), 2.51 (d, J = 7.3 Hz, 2H, CH_2), 2.06 – 1.94 (m, 1H, CH), 0.95 (d, *J* = 6.6 Hz, 6H, 2 CH_3) ppm.

Elemental analysis calculated for $C_{14}H_{14}O_3$: C 73.03%, H 6.13%, O 20.85%.
Found: C 72.93%, H 6.14%, O 20.71%.

Solubility (PBS, pH 7.4, 1% DMSO): 1.09 mM.

3.2.5 2-(2-Ethylbutyl)-3-hydroxynaphthalene-1,4-dione: **d**

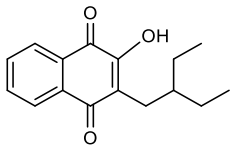

Figure 45: Ligand **d**.

The product was synthesized according to the general procedure, using lawsone (505 mg, 2.90 mmol, 1 equiv.), Hantzsch ester (813 mg, 3.21 mmol, 1.1 equiv.), 2-ethylbutanal (706 µL, 575 mg, 5.74 mmol, 2 equiv.) and L-proline (72 mg, 0.63 mmol, 0.2 equiv.) in dry DCM (20 mL). The mixture was stirred at 100 °C for 60 min under microwave irradiation. The crude product (R_f 0.59, 50% DCM in *n*-hexane) was purified via column chromatography (silica, gradient 40–80% DCM in *n*-hexane), to yield **d** as a yellow solid (273 mg, 1.05 mmol, 36%).

^{1}H-NMR (700.40 MHz, $CDCl_3$): δ 8.12 (d, *J* = 7.7 Hz, 1H, CH: arom.), 8.08 (d, *J* = 7.6 Hz, 1H, CH: arom.), 7.75 (dd, *J* = 7.5, 7.5 Hz, 1H, CH: arom.), 7.68 (dd, *J* = 7.5, 7.5 Hz, 1H, CH: arom.), 7.30 (s, 1H, OH), 2.55 (d, *J* = 7.3 Hz, 2H, CH_2), 1.68 – 1.60 (m, 1H, CH), 1.40 – 1.27 (m, 4H, 2 CH_2), 0.90 (t, *J* = 7.4 Hz, 6H, 2 CH_3) ppm.

Elemental analysis calculated for $C_{16}H_{18}O_3$: C 74.40%, H 7.02%, O 18.58%.
Found: C 74.02%, H 7.04%, O 18.62%.

Solubility (PBS, pH 7.4, 1% DMSO): 0.97 mM.

3.2.6 2-Hydroxy-3-neopentylnaphthalene-1,4-dione: **e**

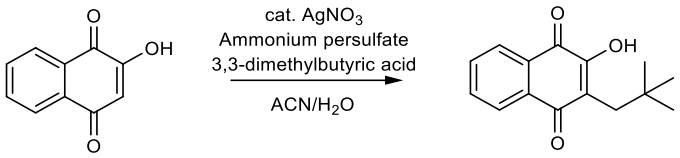

Figure 46: Ligand **e**.

2-Hydroxy-1,4-naphthochinon (1.547 g, 8.89 mmol, 1 equiv.), silver nitrate (0.296 mg, 1.74 mmol, 0.2 equiv.) and 3,3-dimethylbutanoic acid (4.39 mL, 4.003 g, 34.46 mmol, 4 equiv.) were taken up in a mixture of ACN in H_2O (50%, 40 mL) to form an orange suspension. It was heated up to 78 °C (oil bath temperature) and a solution of ammonium peroxodisulfate (3.939 g, 17.26 mmol, 2 equiv.) in water (10 mL) was added slowly, to result in precipitation of a yellow solid. After two hours, it was cooled to r.t. and 10% HCl was added. The mixture was extracted with DCM and the organic phase was washed with brine and dried over anhydrous sodium sulfate. The solvent was removed under reduced pressure to give the crude product as a solid (Rf 0.75, 50% DCM in *n*-hexane). Remains of the 3,3-dimethylbutanoic acid were removed under reduced pressure (50 mbar, 160 °C) and the crude product was purified by column chromatography (silica, gradient 40–80% DCM in n-hexane) yielding **e** as a yellow solid (0.550 g, 2.25 mmol, 25%).

^{1}H-NMR (700.40 MHz, $CDCl_3$): δ 8.13 (d, *J* = 7.7 Hz, 1H, CH: arom.), 8.09 (d, *J* = 7.6 Hz, 1H, CH: arom.), 7.76 (dd, *J* = 7.5, 7.5 Hz, 1H, CH: arom.), 7.68 (dd, *J* = 7.5, 7.5 Hz, 1H, CH: arom.), 7.36 (s, 1H, OH), 2.59 (s, 2H, CH_2), 0.96 (s, 9H, 3 CH_3) ppm.

Elemental analysis calculated for $C_{15}H_{16}O_3$: C 73.75%, H 6.60%, O 19.65%.
Found: C 73.55%, H 6.77%.

Solubility (PBS, pH 7.4, 1% DMSO): 1.05 mM

3.3 COMPLEX SYNTHESES

3.3.1 General procedure

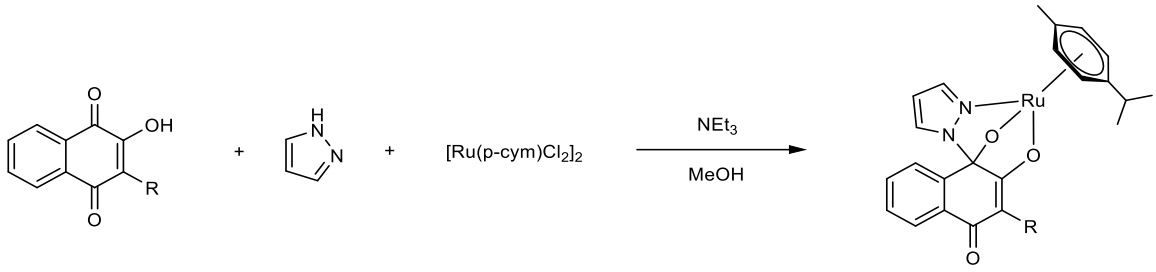

Figure 47: Complex synthesis: general procedure.

The metal dimer (1 equiv.), pyrazole (1.9 equiv.) and the respective naphthoquinone derivative (1.9 equiv.) were dissolved in methanol (12 mL) and triethylamine (6 equiv.) was added. Stirring under microwave irradiation (60 °C, 20 min) was followed by solvent removal under reduced pressure. The crude product was purified via column chromatography (silica, isocratic, 70% ethyl acetate, 5% triethylamine in *n*-hexane). The fractions where combined and the solvent was removed *in vacuo*. The residue was dissolved in a small amount of DCM, the product precipitated by the addition of *n*-hexane and stored at 4 °C overnight. The formed pale yellow to greenish solid was separated by filtration and dried at 60 °C.

Yield: 58–78%

3.3.2 [(3-Propyl-1-(1H-κ*N*2-pyrazol-1-yl)-4-oxo-1,4-dihydronaphtalene-1,2-bis(olato)-κ*O*1-κ*O*2)(η^6-*p*-cymene)ruthenium(II)]: **1**

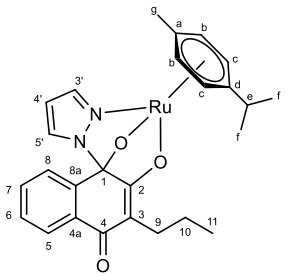

Figure 48: Complex **1**.

The product was synthesized according to the general procedure, using ruthenium(II) dimer (160 mg, 0.26 mmol, 1 equiv.), naphthoquinone derivative **a** (107 mg, 0.47 mmol, 1.9 equiv.), pyrazole (34 mg, 0.50 mmol, 1.9 equiv.) and triethylamine (217 µL, 159 mg, 1.57 mmol, 6 equiv.) in methanol (12 mL). Stirring under microwave irradiation led to the formation of a red solution. The solvent was removed under reduced pressure and the crude product was purified via column chromatography (R_f 0.24, silica, isocratic 70% ethyl acetate and 5% triethylamine in *n*-hexane). Precipitation from DCM/*n*-hexane led to the desired product **1** as a yellow powder (163 mg, 0.31 mmol, 60%).

^{1}H-NMR (600.25 MHz, MeOD): δ 8.34 (d, *J* = 2.1 Hz, 1H, CH: 3‘), 8.12 – 8.08 (m, 1H, CH: arom.), 7.64 – 7.58 (m, 3H, 3 CH arom.), 6.70 (d, *J* = 2.5 Hz, 1H, CH: 5’), 6.35 (m, 1H, CH: 4’), 5.98 (d, *J* = 5.9 Hz, 1H, CH: c), 5.89 (d, *J* = 5.9 Hz, 1H, CH: c), 5.61 (t, *J* = 6.1 Hz, 2H, 2CH: b), 2.88 (hept, *J* = 6.9 Hz, 1H, CH: e), 2.34 (s, 3H, CH_3: g), 2.39 – 2.24 (m, 2H, CH_2: 9), 1.35 (d, *J* = 6.9 Hz, 6H, 2 CH_3: f), 1.42 – 1.25 (m, 2H, CH_2: 10), 0.77 (t, *J* = 7.4 Hz, 3H, CH_3: 11) ppm.

^{13}C-NMR (700.40 MHz, MeOD): δ 184.08 (Cq: 2), 183.32 (Cq: 4), 141.40 (CH: 3’), 137.74 (Cq: arom.), 134.37 (Cq: arom.), 132.17 (CH: arom.), 131.21 (CH: arom.), 127.86 (CH: 5’), 127.66 (CH: arom.), 127.13 (CH: arom.), 110.53 (Cq: 3), 108.70 (CH: 4’), 101.22 (Cq: d), 98.52 (Cq: a), 94.89 (Cq: 1), 83.37 (CH: c), 82.82 (CH: c), 80.17 (CH: b), 80.15 (CH: b), 32.65 (CH: e), 25.60 (CH_2: 9), 23.12 (CH_3: f), 22.87 (CH_2: 10), 22.73 (CH_3: f), 18.34 (CH_3: g), 14.29 (CH_3: 11) ppm.

Elemental analysis calculated for $C_{26}H_{28}N_2O_3Ru$: C 60.33%, H 5.45%, N 5.41%, O 9.27%.
Found: C 59.95%, H 5.45%, N 5.49%, O 9.16%.

Solubility (PBS, pH 7.4, 1% DMSO): 0.50 mM

3.3.3 [(3-Butyl-1-(1H-κ*N*2-pyrazol-1-yl)-4-oxo-1,4-dihydronaphtalene-1,2-bis(olato)-κ*O*1-κ*O*2)(η^6-*p*-cymene)ruthenium(II)]: **2**

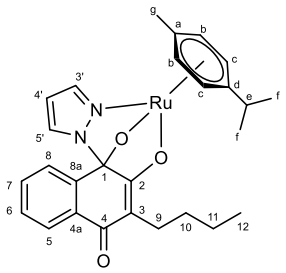

Figure 49: Complex **2**.

The product was synthesized according to the general procedure, using ruthenium(II) dimer (160 mg, 0.26 mmol, 1 equiv.), naphthoquinone derivative **b** (107 mg, 0.47 mmol, 1.9 equiv.), pyrazole (33 mg, 0.48 mmol, 1.9 equiv.) and triethylamine (204 µL, 149 mg, 1.47 mmol, 6 equiv.) in methanol (12 mL). Stirring under microwave irradiation led to the formation of a brown/blackish solution. The solvent was removed under reduced pressure and the crude product was purified via column chromatography (R_f 0.30, silica, isocratic 70% ethyl acetate and 5% triethylamine in *n*-hexane). Precipitation from DCM/*n*-hexane led to the desired product **2** as a green powder (161 mg, 0.30 mmol, 58%).

^{1}H-NMR (600.25 MHz, MeOD): δ 8.34 (d, *J* = 2.0 Hz, 1H, CH: 3'), 8.13 – 8.06 (m, 1H, CH: arom.), 7.66 – 7.57 (m, 3H, 3 CH: arom.), 6.69 (d, *J* = 2.4 Hz, 1H, CH: 5'), 6.35 (dd, J = 2.3 Hz, 2.3 Hz, 1H, 4'), 5.98 (d, J = 5.9 Hz, 1H, CH: c), 5.89 (d, J = 5.9 Hz, 1H, CH: c), 5.62 (dd, J = 6.1, 6.1 Hz, 2H, 2 CH: b), 2.88 (hept, J = 6.9 Hz, 1H, CH: e), 2.34 (s, 3H, CH_3: g), 2.42 – 2.27 (m, 2H, CH_2: 9), 1.35 (d, *J* = 6.1 Hz, 6H, 2 CH_3: f), 1.39 – 1.14 (m, 4H, 2 CH_2: 10, CH_2: 11), 0.85 (t, J = 7.3 Hz, 3H, CH_3: 12) ppm.

^{13}C-NMR (600.25 MHz, MeOD): δ 183.94 (Cq: 2), 183.27 (Cq: 4), 141.40 (CH: 3'), 137.73 (Cq: arom.), 134.38 (Cq: arom.), 132.16 (CH: arom.), 131.21 (CH: arom.), 127.85 (CH: C5'), 127.65 (CH: arom.), 127.12 (CH: arom.), 110.76 (Cq: 3), 108.69 (CH: 4'), 101.21 (Cq: d), 98.49 (Cq: a), 94.89 (Cq: 1), 83.36 (CH: c), 82.83 (CH: c), 80.16 (2 CH: b), 32.64 (CH: e), 32.06 (CH_2: 9), 23.61 (CH_2: 10), 23.27 (CH_2: 11), 23.12 (CH_3: f), 22.76 (CH_3: f), 18.36 (CH_3: g), 14.52 (CH_3: 12) ppm.

Elemental analysis calculated for $C_{27}H_{30}N_2O_3Ru \cdot 0.15\ H_2O$: C 60.69%, H 5.72%, N 5.24%, O 9.43%. Found: C 60.50%, H 5.67%, N 5.35%, O 9.15%.

Solubility (PBS, pH 7.4, 1% DMSO): 0.47 mM

3.3.4 [(3-Isobutyl-1-(1H-κ*N*2-pyrazol-1-yl)-4-oxo-1,4-dihydronaphtalene-1,2-bis(olato)-κ*O*1-κ*O*2)(η^6-*p*-cymene)ruthenium(II)]: **3**

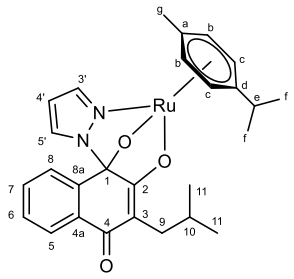

Figure 50: Complex **3**.

The product was synthesized according to the general procedure, using ruthenium(II) dimer (105 mg, 0.17 mmol, 1 equiv.), naphthoquinone derivative **c** (72 mg, 0.31 mmol, 1.9 equiv.), 1,2-diazole (21 mg, 0.31 mmol, 1.9 equiv.) and triethylamine (136 µL, 99 mg, 0.98 mmol, 6 equiv.) in methanol (12 mL). Stirring under microwave irradiation led to the formation of a brown/blackish solution. The solvent was removed under reduced pressure and the crude product was purified via column chromatography (R_f 0.30, silica, isocratic 70% ethyl acetate and 5% triethylamine in *n*-hexane). Precipitation from DCM/*n*-hexane led to the desired product **3** as a yellow powder (116.0 mg, 0.22 mmol, 64%).

^{1}H-NMR (700.40 MHz, MeOD): δ 8.33 (d, *J* = 1.4 Hz, 1H, CH: 3'), 8.13 – 8.07 (m, 1H, CH: arom.), 7.68 – 7.57 (m, 3H, 3 CH: arom.), 6.70 (d, *J* = 2.0 Hz, 1H, CH: 5'), 6.35 (m, 1H, CH: 4'), 5.98 (d, *J* = 5.8 Hz, 1H, CH: c), 5.90 (d, *J* = 5.8 Hz, 1H, CH: c), 5.62 (d, *J* = 5.8 Hz, 1H, CH: b), 5.58 (d, *J* = 5.8 Hz, 1H, CH: b), 2.87 (hept, *J* = 6.9 Hz, 1H: CH: e), 2.34 (s, 3H, CH_3: g), 2.22 (m, 2H, 10), 1.74 (m, 1H, CH: 10), 0.80 (d, *J* = 6.6 Hz, 3H, CH_3: 11), 0.64 (d, *J* = 6.6 Hz, 3H, CH_3: 11) ppm.

^{13}C-NMR (700.40 MHz, MeOD): δ 184.54 (Cq: 2), 183.45 (Cq: 4), 141.39 (CH: 3'), 137.73 (Cq: arom.), 134.40 (Cq: arom.), 132.14 (CH: arom.), 131.21 (CH: arom.), 127.78 (CH: 5'), 127.61 (CH: arom.), 127.14 (CH: arom.), 109.84 (Cq: 3), 108.69 (CH: 4'), 101.04 (Cq: d), 98.60 (Cq: a), 94.95 (Cq: 1), 83.62 (CH: c), 82.87 (CH: c), 80.14 (CH: b), 80.00 (CH: b), 32.64 (CH: e), 32.61 (CH_2: 9), 29.00 (CH: 10), 23.20 (CH_3: 11), 23.19 (CH_3: 11), 22.75 (CH_3: f), 22.74 (CH_3: f), 18.38 (CH_3: g) ppm.

Elemental analysis calculated for $C_{27}H_{30}N_2O_3Ru \cdot 0.15\ H_2O$: C 60.69%, H 5.72%, N 5.24%, O 9.43%. Found: C 60.43%, H 5.66%, N 5.44%, O 9.24%.

Solubility (PBS, pH 7.4, 1% DMSO): 0.17 mM

3.3.5 [(3-(2-Ethylbutyl)-1-(1H-κ*N*2-pyrazol-1-yl)-4-oxo-1,4-dihydronaphtalene-1,2-bis(olato)-κ*O*1-κ*O*2)(η^6-*p*-cymene)ruthenium(II)]: **4.**

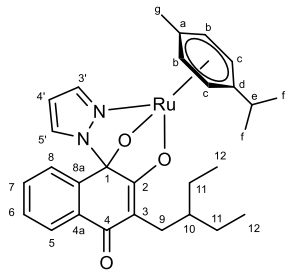

Figure 51: Complex **4**.

The product was synthesized according to the general procedure, using ruthenium(II) dimer (113 mg, 0.18 mmol, 1 equiv.), naphthoquinone derivative **d** (88 mg, 0.34 mmol, 1.9 equiv.), pyrazole (24 mg, 0.35 mmol, 1.9 equiv.) and triethylamine (149 µL, 109 mg, 1.08 mmol, 6 equiv.) in methanol (12 mL). Stirring under microwave irradiation led to the formation of a black solution. The solvent was removed under reduced pressure and the crude product was purified via column chromatography (R_f 0.32, silica, isocratic 70% ethyl acetate and 5% triethylamine in *n*-hexane). Precipitation from DCM/*n*-hexane led to the desire product **4** as a yellow powder (107 mg, 0.19 mmol, 52%).

^{1}H-NMR (600.25 MHz, MeOD): δ 8.35 (d, 1H, CH: C3'), 8.14 – 8.08 (m, 1H, CH: arom.), 7.71 – 7.58 (m, 3H, 3 CH: arom.), 6.70 (d, *J* = 1.8 Hz, 1H, C5'), 6.36 (d, *J* = 1.8 Hz, 1H, CH: C4'), 5.99 (d, *J* = 5.8 Hz, 1H, CH: c), 5.92 (d, *J* = 5.8 Hz, 1H, CH: c), 5.64 (d, *J* = 5.7 Hz, 1H, CH: b), 5.59 (d, *J* = 5.7 Hz, 1H, CH: b), 2.89 (hept, *J* = 6.7 Hz, 1H, CH: e), 2.36 (s, 3H, CH_3: g), 2.35 – 2.24 (m, 2H, CH_2: 9), 1.43 (1H, CH: 10), 1.37 (d, *J* = 6.6 Hz, 6H, 2 CH_3: f), 1.21 (m, 2H, CH_2: 11), 1.07 (m, 2H, CH_2: 11), 0.82 (t, *J* = 7.2 Hz, 3H, CH_3: 12), 0.77 (t, *J* = 7.2 Hz, 3H, CH_3: 12) ppm.

^{13}C-NMR (600.25 MHz, MeOD): δ 184.39 (Cq: 2), 183.50 (Cq: 4), 141.38 (CH: 3'), 137.72 (Cq: arom.), 134.45 (Cq: arom.), 132.09 (CH: arom.), 131.20 (CH: arom.), 127.75 C (CH: 5'), 127.58 (CH: arom.), 127.13 (CH: arom.), 109.99 (Cq: 3), 108.65 (CH: 4'), 100.92 (Cq: d), 98.66 (Cq: a), 95.00 (Cq: 1), 83.66 (CH: c), 82.98 (CH: c), 80.10 (CH: b), 79.97 (CH: b) 41.21 (CH: 10), 32.62 (CH: e), 27.80 (CH_2: 9), 26.71 (CH_2: 11), 26.28 (CH_2: 11), 23.18 (CH_3: f), 22.81 (CH_3: f), 18.44 (CH_3: g), 11.64 (CH_3: 12), 11.27 (CH_3: 12) ppm.

Elemental analysis calculated for $C_{29}H_{34}N_2O_3Ru \cdot 0.15\ H_2O$: C 61.94%, H 6.15%, N 4.98%, O 8.96%. Found: C 61.63%, H 6.21%, N 5.01%, O 8.71%.

Solubility (PBS, pH 7.4, 1% DMSO): 0.10 mM

3.3.6 [(3-Neopentyl-1-(1H-κ*N*2-pyrazol-1-yl)-4-oxo-1,4-dihydronaphtalene-1,2-bis(olato)-κ*O*1-κ*O*2)(η^6-p-cymene)ruthenium(II)]: **5**

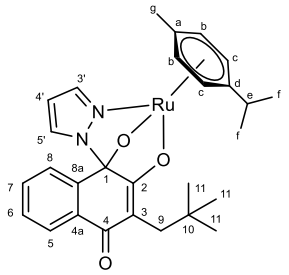

Figure 52: Complex **5**.

The product was synthesized according to the general procedure, using ruthenium(II) dimer (110 mg, 0.18 mmol, 1 equiv.), naphthoquinone derivative **e** (84 mg, 0.34 mmol, 1.9 equiv.), pyrazole (23 mg, 0.34 mmol, 1.9 equiv.) and triethylamine (149 µL, 109 mg, 1.08 mmol, 6 equiv.) in methanol (12 mL). Stirring under microwave irradiation led to formation of a brown/blackish solution. The solvent was removed under reduced pressure and the crude product was purified via column chromatography (R_f 0.35, silica, isocratic 70% ethyl acetate and 5% triethylamine in *n*-hexane). Precipitation with DCM/*n*-hexane led to the product **5** as a yellow powder (153 mg, 0.28 mmol, 78%).

^{1}H-NMR (600.25 MHz, MeOD): δ 8.34 (d, 1H, CH: 3'), 8.15 – 8.08 (m, 1H, CH: arom.), 7.71 – 7.59 (m, 3H, 3 CH: arom.), 6.74 (d, *J* = 2.2 Hz, 1H, CH: 5'), 6.37 (d, *J* = 2.0 Hz, 1H, CH: C4'), 5.98 (d, *J* = 5.8 Hz, 1H, CH: c), 5.93 (d, *J* = 5.7 Hz, 1H, CH: c), 5.65 (d, *J* = 5.7 Hz, 1H, CH: b), 5.55 (d, *J* = 5.8 Hz, 1H, CH: b), 2.89 (hept, *J* = 6.8 Hz, 1H, CH: e), 2.36 (s, 3H, CH_3: g), 2.32 (q, 2H, CH_2: 9), 1.37 (d, 6H, 2 CH_3: f), 0.72 (s, 9H, 3 CH_3: 11) ppm.

^{13}C-NMR (600.25 MHz, MeOD): δ 185.14 (Cq: 2), 183.62 (Cq: 4), 141.38 (CH: 3'), 137.61 (Cq: arom.), 134.51 (Cq: arom.), 132.08 (CH: arom.), 131.17 (CH: arom.), 127.70 (CH 5'), 127.55 (CH: arom.), 127.28 (CH: arom.), 108.70 (CH: 4'), 108.64 (Cq: 3), 100.76 (Cq: d), 98.72 (Cq: a), 95.12 (Cq: 1), 83.80 (CH: c), 83.06 (CH: c), 80.07 (CH: b), 79.93 (CH: b), 36.07 (CH_2: 9), 34.29 (Cq: 10), 32.63 (CH: e), 30.54 (3 CH_3: 11), 23.18 (CH_3: f), 22.84 (CH_3: f), 18.48 (CH_3: g) ppm.

Elemental analysis calculated for $C_{28}H_{32}N_2O_3Ru \cdot 0.15\ H_2O$: C 61.33%, H 5.94%, N 5.11%, O 9.19%. Found: C 61.10%, H 5.93%, N 5.25%, O 8.88%.

Solubility (PBS, pH 7.4, 1% DMSO): 0.32 mM

3.4 UV/VIS STABILITY

Complexes **1**–**5** were dissolved in PBS with 1% DMSO in cuvettes. Concentrations of 40 µmol/L led to initial absorbances (A_0) from 0.45 to 0.8. The samples and a blank of PBS with 1% DMSO were measured at 20 °C over 97 measuring cycles of 30 minutes each at 200–700 nm. Absolute values of the peak maximum at 366 nm were normalized by Equation **3**. Those are pictured in Figure **53**, whereas normalized data is depicted in Figure **33**.

Equation 3: Normalization of UV/Vis data.

$$A_{normalized} = A + (1 - A_0)$$

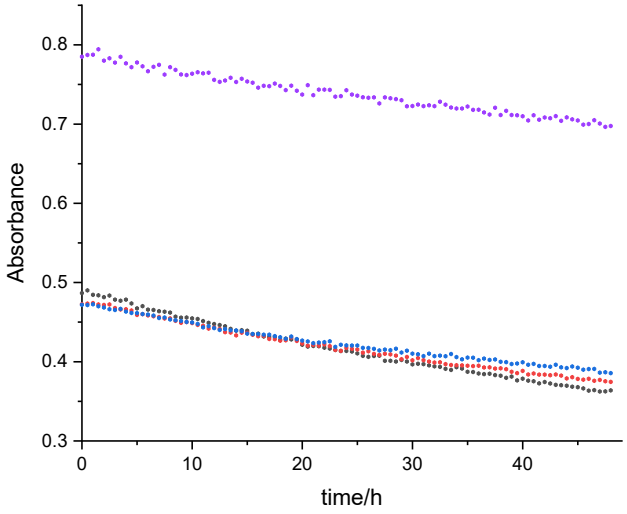

Figure 53: Raw data of UV/Vis spectroscopy.

3.5 CYCLIC VOLTAMMETRY

Dissolution of ligand in degassed measuring medium (2.3–3.8 mM ligand **a**–**e** and 2.01–2.44 mM complex **1**–**5**, 3 mL 0.1 M tetrabutylammonium tetrafluoroborate in ACN) was followed by cyclic voltammetry measurements over potentials from -2.5–1.5 V with variation in scan rate (10–200 mV/second). Subsequent addition of ferrocene as a standard was measured at 100 mV/second, in order to normalize data. Subtraction of ferrocenes' half level potentials led to the final spectra, as depicted in chapter **2.4.3**.

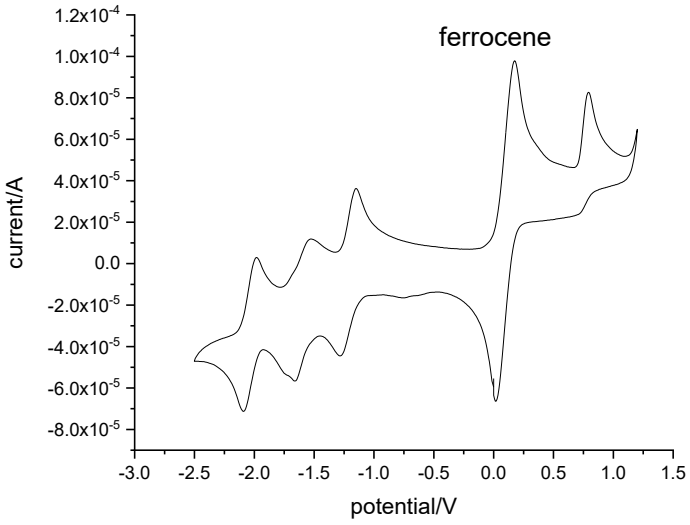

Figure 54: Ferrocene standard with complex **5**.

4 CONCLUSIONS AND OUTLOOK

A novel compound class of *N,O,O*-tridentate ruthenium(II) arene complexes has been investigated. Based on promising attributes of cytotoxicity and selectivity towards cancer cell lines, an investigation on stability enhancing functional groups was conducted. Therefore, a series of 3-alkylated 2-hydroxy-1,4-naphthoquinone ligands was synthesized and used for complexation. All purified compounds were characterized *via* NMR and elemental analysis. The obtained ruthenium(II) arene complexes were examined by standard analytical methods and investigated for their aqueous stability and redox properties. Solubility of the complexes was determined in PBS with 1% DMSO and were found below 1 mM for all complexes. This issue turned out as a problem for analysis of complex **4**, which precipitated already during the UV/Vis measurements. For other complexes, UV/Vis stability measurements showed increasing stability in aqueous medium, in correlation to longer and branched alkyl chains. A study on the impact of substituent variation on redox processes was conducted *via* cyclic voltammetry, to show no influence on mechanistic behavior. Complex reduction cascades were observed at harsh conditions, which are supposedly out of range of biological redox processes. Overall, these observations can serve as starting point of further investigations. Higher stability of complexes with branched alkyl substituents indicates *iso*-propyl and *tert*-butyl featuring derivatives to be interesting candidates for upcoming syntheses and examinations. Furthermore, complexation works properly with osmium(II) as a metal center.[203] However, determination of *in vitro* cytotoxicity of synthesized derivatives will be the most important next step. Thus, anticancer potencies can be put into relation with previous works. A trend towards lower IC_{50} values in correlation to higher complex stability and lipophilic character is expected (chapter **1.2.6**). In addition to *in vitro* studies, research on biological behavior will be necessary. Mechanisms of antitumor activity include activation chemistry and interaction with certain molecular targets. Elucidation of molecular successions is an important step for further examinations. As DNA interaction and ROS production have been excluded as modes of action (chapter **1.2.6**), antitumor activity might be based on other naphthoquinone typical targets like topoisomerase I/II, NQO1 or telomerase (chapter **1.2.5**). Binding behavior towards these enzymes can be examined *via* certain essays, whereas affinity towards amino acids or small peptides can be elucidated from liquid chromatography coupled mass spectrometry after incubation. Not only impressive cytotoxic impact, but also unexpected selectivity for certain cell lines *in vitro* may be further object of investigation. Broader insight on these central characteristics may give option to fine tune ligand design, diminish adverse effects or raise anticancer potencies and selectivity. Ultimately, *in vivo* studies on most promising candidates are a critical step towards significant conclusions on drug design, selectivity and applicability as anticancer agents. Overall, the compound class of novel tridentate naphthoquinone based metallodrugs has shown outstanding attributes, although various central characteristics remain unknown. Thus being of great interest for further examination and medical application, intense research on given uncertainties is critical.

5 REFERENCES

(1) The Biology of Cancer by Robert A. Weinberg, Robert A Weinberg (z-Lib.Org).Pdf.

(2) Omran, A. R. The Epidemiologic Transition. A Theory of the Epidemiology of Population Change. 1971. *Bull World Health Organ* **2001**, *79* (2), 161–170.

(3) CP, W.; E, W.; BW, S. *World Cancer Report: Cancer Research for Cancer Prevention*.

(4) Cancer today http://gco.iarc.fr/today/home (accessed 2021 -05 -06).

(5) Sung, H.; Ferlay, J.; Siegel, R. L.; Laversanne, M.; Soerjomataram, I.; Jemal, A.; Bray, F. Global Cancer Statistics 2020: GLOBOCAN Estimates of Incidence and Mortality Worldwide for 36 Cancers in 185 Countries. *CA: A Cancer Journal for Clinicians n/a* (n/a). https://doi.org/10.3322/caac.21660.

(6) Commar, A.; Prasad, V. K.; Tursan d'Espaignet, E.; Wolfenden, L.; Weltgesundheitsorganisation. *WHO Global Report on Trends in Prevalence of Tobacco Smoking 2000-2025*; 2018.

(7) *Gender, Women and the Tobacco Epidemic*; Samet, J. M., Yoon, S.-Y., World Health Organization, Eds.; World Health Organization: Geneva, 2010.

(8) Barta, J. A.; Powell, C. A.; Wisnivesky, J. P. Global Epidemiology of Lung Cancer. *Annals of Global Health* **2019**, *85* (1), 8. https://doi.org/10.5334/aogh.2419.

(9) Rawla, P. Epidemiology of Prostate Cancer. *World J Oncol* **2019**, *10* (2), 63–89. https://doi.org/10.14740/wjon1191.

(10) Parsonnet, J.; Friedman, G. D.; Vandersteen, D. P.; Chang, Y.; Vogelman, J. H.; Orentreich, N.; Sibley, R. K. Helicobacter Pylori Infection and the Risk of Gastric Carcinoma. *New England Journal of Medicine* **1991**, *325* (16), 1127–1131. https://doi.org/10.1056/NEJM199110173251603.

(11) Sangro, B.; Sarobe, P.; Hervás-Stubbs, S.; Melero, I. Advances in Immunotherapy for Hepatocellular Carcinoma. *Nat Rev Gastroenterol Hepatol* **2021**. https://doi.org/10.1038/s41575-021-00438-0.

(12) Llovet, J. M.; Zucman-Rossi, J.; Pikarsky, E.; Sangro, B.; Schwartz, M.; Sherman, M.; Gores, G. Hepatocellular Carcinoma. *Nat Rev Dis Primers* **2016**, *2*, 16018. https://doi.org/10.1038/nrdp.2016.18.

(13) WHO | Key statistics https://www.who.int/cancer/resources/keyfacts/en/ (accessed 2021 -06 -08).

(14) Chin, L.; Gray, J. W. Translating Insights from the Cancer Genome into Clinical Practice. *Nature* **2008**, *452* (7187), 553–563. https://doi.org/10.1038/nature06914.

(15) Dang, C. V. MYC on the Path to Cancer. *Cell* **2012**, *149* (1), 22–35. https://doi.org/10.1016/j.cell.2012.03.003.

(16) Fernández-Medarde, A.; Santos, E. Ras in Cancer and Developmental Diseases. *Genes & Cancer* **2011**, *2* (3), 344–358. https://doi.org/10.1177/1947601911411084.

(17) Anderson M W; Reynolds S H; You M; Maronpot R M. Role of Proto-Oncogene Activation in Carcinogenesis. *Environmental Health Perspectives* **1992**, *98*, 13–24. https://doi.org/10.1289/ehp.929813.

(18) Mitelman, F. Recurrent Chromosome Aberrations in Cancer. *Mutation Research/Reviews in Mutation Research* **2000**, *462* (2), 247–253. https://doi.org/10.1016/S1383-5742(00)00006-5.

(19) Hanahan, D.; Weinberg, R. A. Hallmarks of Cancer: The Next Generation. *Cell* **2011**, *144* (5), 646–674. https://doi.org/10.1016/j.cell.2011.02.013.

(20) Hanahan, D.; Weinberg, R. A. The Hallmarks of Cancer. *Cell* **2000**, *100* (1), 57–70. https://doi.org/10.1016/S0092-8674(00)81683-9.

(21) Ingley, E. Src Family Kinases: Regulation of Their Activities, Levels and Identification of New Pathways. *Biochimica et Biophysica Acta (BBA) - Proteins and Proteomics* **2008**, *1784* (1), 56–65. https://doi.org/10.1016/j.bbapap.2007.08.012.

(22) Denhardt, D. T. Signal-Transducing Protein Phosphorylation Cascades Mediated by Ras/Rho Proteins in the Mammalian Cell: The Potential for Multiplex Signalling. *Biochem J* **1996**, *318* (Pt 3), 729–747.

(23) Belli, S.; Esposito, D.; Servetto, A.; Pesapane, A.; Formisano, L.; Bianco, R. C-Src and EGFR Inhibition in Molecular Cancer Therapy: What Else Can We Improve? *Cancers (Basel)* **2020**, *12* (6). https://doi.org/10.3390/cancers12061489.

(24) Src and Ras are involved in separate pathways in epithelial cell scattering https://www.embopress.org/doi/epdf/10.1093/emboj/16.19.5904 (accessed 2021 -06 -09). https://doi.org/10.1093/emboj/16.19.5904.

(25) Weiss, R. A. A Perspective on the Early Days of RAS Research. *Cancer Metastasis Rev* **2020**, *39* (4), 1023–1028. https://doi.org/10.1007/s10555-020-09919-1.

(26) Sever, R.; Brugge, J. S. Signal Transduction in Cancer. *Cold Spring Harb Perspect Med* **2015**, *5* (4). https://doi.org/10.1101/cshperspect.a006098.

(27) Blagosklonny, M. V. Cell Cycle Arrest Is Not Senescence. *Aging (Albany NY)* **2011**, *3* (2), 94–101.

(28) Giacinti, C.; Giordano, A. RB and Cell Cycle Progression. *Oncogene* **2006**, *25* (38), 5220–5227. https://doi.org/10.1038/sj.onc.1209615.

(29) Takeda, D. Y.; Dutta, A. DNA Replication and Progression through S Phase. *Oncogene* **2005**, *24* (17), 2827–2843. https://doi.org/10.1038/sj.onc.1208616.

(30) Fischer, M.; Dang, C. V.; DeCaprio, J. A. Chapter 17 - Control of Cell Division. In *Hematology (Seventh Edition)*; Hoffman, R., Benz, E. J., Silberstein, L. E., Heslop, H. E., Weitz, J. I., Anastasi, J., Salama, M. E., Abutalib, S. A., Eds.; Elsevier, 2018; pp 176–185. https://doi.org/10.1016/B978-0-323-35762-3.00017-2.

(31) Ryan, K. M.; Phillips, A. C.; Vousden, K. H. Regulation and Function of the P53 Tumor Suppressor Protein. *Current Opinion in Cell Biology* **2001**, *13* (3), 332–337. https://doi.org/10.1016/S0955-0674(00)00216-7.

(32) Olsson, A.; Manzl, C.; Strasser, A.; Villunger, A. How Important Are Post-Translational Modifications in P53 for Selectivity in Target-Gene Transcription and Tumour Suppression? *Cell Death Differ* **2007**, *14* (9), 1561–1575. https://doi.org/10.1038/sj.cdd.4402196.

(33) Di Micco, R.; Krizhanovsky, V.; Baker, D.; d'Adda di Fagagna, F. Cellular Senescence in Ageing: From Mechanisms to Therapeutic Opportunities. *Nat Rev Mol Cell Biol* **2021**, *22* (2), 75–95. https://doi.org/10.1038/s41580-020-00314-w.

(34) Kruse, J.-P.; Gu, W. SnapShot: P53 Posttranslational Modifications. *Cell* **2008**, *133* (5), 930-30.e1. https://doi.org/10.1016/j.cell.2008.05.020.

(35) Vaughan, C. A.; Singh, S.; Subler, M. A.; Windle, J. J.; Inoue, K.; Fry, E. A.; Pillappa, R.; Grossman, S. R.; Windle, B.; Andrew Yeudall, W.; Deb, S. P.; Deb, S. The Oncogenicity of Tumor-Derived Mutant P53 Is Enhanced by the Recruitment of PLK3. *Nature Communications* **2021**, *12* (1), 704. https://doi.org/10.1038/s41467-021-20928-8.

(36) Friedl, P.; Locker, J.; Sahai, E.; Segall, J. E. Classifying Collective Cancer Cell Invasion. *Nature Cell Biology* **2012**, *14* (8), 777–783. https://doi.org/10.1038/ncb2548.

(37) Jung, A. R.; Jung, C.-H.; Noh, J. K.; Lee, Y. C.; Eun, Y.-G. Epithelial-Mesenchymal Transition Gene Signature Is Associated with Prognosis and Tumor Microenvironment in Head and Neck Squamous Cell Carcinoma. *Sci Rep* **2020**, *10*. https://doi.org/10.1038/s41598-020-60707-x.

(38) Elia, I.; Doglioni, G.; Fendt, S.-M. Metabolic Hallmarks of Metastasis Formation. *Trends in Cell Biology* **2018**, *28* (8), 673–684. https://doi.org/10.1016/j.tcb.2018.04.002.

(39) Henke, E.; Nandigama, R.; Ergün, S. Extracellular Matrix in the Tumor Microenvironment and Its Impact on Cancer Therapy. *Front. Mol. Biosci.* **2020**, *6*. https://doi.org/10.3389/fmolb.2019.00160.

(40) Valastyan, S.; Weinberg, R. A. Tumor Metastasis: Molecular Insights and Evolving Paradigms. *Cell* **2011**, *147* (2), 275–292. https://doi.org/10.1016/j.cell.2011.09.024.

(41) Fares, J.; Fares, M. Y.; Khachfe, H. H.; Salhab, H. A.; Fares, Y. Molecular Principles of Metastasis: A Hallmark of Cancer Revisited. *Sig Transduct Target Ther* **2020**, *5* (1), 28. https://doi.org/10.1038/s41392-020-0134-x.

(42) Shay, J. W. Role of Telomeres and Telomerase in Aging and Cancer. *Cancer Discov* **2016**, *6* (6), 584–593. https://doi.org/10.1158/2159-8290.CD-16-0062.

(43) Okamoto, K.; Seimiya, H. Revisiting Telomere Shortening in Cancer. *Cells* **2019**, *8* (2). https://doi.org/10.3390/cells8020107.

(44) Maciejowski, J.; de Lange, T. Telomeres in Cancer: Tumour Suppression and Genome Instability. *Nat Rev Mol Cell Biol* **2017**, *18* (3), 175–186. https://doi.org/10.1038/nrm.2016.171.

(45) Saman, H.; Raza, S. S.; Uddin, S.; Rasul, K. Inducing Angiogenesis, a Key Step in Cancer Vascularization, and Treatment Approaches. *Cancers (Basel)* **2020**, *12* (5). https://doi.org/10.3390/cancers12051172.

(46) Nishida, N.; Yano, H.; Nishida, T.; Kamura, T.; Kojiro, M. Angiogenesis in Cancer. *Vasc Health Risk Manag* **2006**, *2* (3), 213–219.

(47) Ribatti, D.; Crivellato, E. Immune Cells and Angiogenesis. *J Cell Mol Med* **2009**, *13* (9a), 2822–2833. https://doi.org/10.1111/j.1582-4934.2009.00810.x.

(48) Bruno, A.; Pagani, A.; Pulze, L.; Albini, A.; Dallaglio, K.; Noonan, D. M.; Mortara, L. Orchestration of Angiogenesis by Immune Cells. *Front Oncol* **2014**, *4*. https://doi.org/10.3389/fonc.2014.00131.

(49) Aguilar-Cazares, D.; Chavez-Dominguez, R.; Carlos-Reyes, A.; Lopez-Camarillo, C.; Hernadez de la Cruz, O. N.; Lopez-Gonzalez, J. S. Contribution of Angiogenesis to Inflammation and Cancer. *Front Oncol* **2019**, *9*. https://doi.org/10.3389/fonc.2019.01399.

(50) Lugano, R.; Ramachandran, M.; Dimberg, A. Tumor Angiogenesis: Causes, Consequences, Challenges and Opportunities. *Cell. Mol. Life Sci.* **2020**, *77* (9), 1745–1770. https://doi.org/10.1007/s00018-019-03351-7.

(51) Elmore, S. Apoptosis: A Review of Programmed Cell Death. *Toxicol Pathol* **2007**, *35* (4), 495–516. https://doi.org/10.1080/01926230701320337.

(52) Igney, F. H.; Krammer, P. H. Death and Anti-Death: Tumour Resistance to Apoptosis. *Nat Rev Cancer* **2002**, *2* (4), 277–288. https://doi.org/10.1038/nrc776.

(53) Pistritto, G.; Trisciuoglio, D.; Ceci, C.; Garufi, A.; D'Orazi, G. Apoptosis as Anticancer Mechanism: Function and Dysfunction of Its Modulators and Targeted Therapeutic Strategies. *Aging* **2016**, *8* (4), 603–619. https://doi.org/10.18632/aging.100934.

(54) Wong, R. S. Apoptosis in Cancer: From Pathogenesis to Treatment. *J Exp Clin Cancer Res* **2011**, *30* (1), 87. https://doi.org/10.1186/1756-9966-30-87.

(55) Falzone, L.; Salomone, S.; Libra, M. Evolution of Cancer Pharmacological Treatments at the Turn of the Third Millennium. *Front. Pharmacol.* **2018**, *9*. https://doi.org/10.3389/fphar.2018.01300.

(56) Weinstein, I. B.; Case, K. The History of Cancer Research: Introducing an AACR Centennial Series. *Cancer Res* **2008**, *68* (17), 6861–6862. https://doi.org/10.1158/0008-5472.CAN-08-2827.

(57) Gianfaldoni, S.; Gianfaldoni, R.; Wollina, U.; Lotti, J.; Tchernev, G.; Lotti, T. An Overview on Radiotherapy: From Its History to Its Current Applications in Dermatology. *Open Access Maced J Med Sci* **2017**, *5* (4), 521–525. https://doi.org/10.3889/oamjms.2017.122.

(58) Röntgen, W. C. On a New Kind of Rays. *Science* **1896**, *3* (59), 227–231. https://doi.org/10.1126/science.3.59.227.

(59) Radiation Therapy for Cancer - National Cancer Institute https://www.cancer.gov/about-cancer/treatment/types/radiation-therapy (accessed 2021 -05 -31).

(60) Müller, C.; van der Meulen, N. P.; Benešová, M.; Schibli, R. Therapeutic Radiometals Beyond ^{177}Lu and ^{90}Y: Production and Application of Promising α-Particle, β^--Particle, and Auger Electron Emitters. *J Nucl Med* **2017**, *58* (Supplement 2), 91S-96S. https://doi.org/10.2967/jnumed.116.186825.

(61) Baskar, R.; Lee, K. A.; Yeo, R.; Yeoh, K.-W. Cancer and Radiation Therapy: Current Advances and Future Directions. *Int J Med Sci* **2012**, *9* (3), 193–199. https://doi.org/10.7150/ijms.3635.

(62) Kennedy, L. B.; Salama, A. K. S. A Review of Cancer Immunotherapy Toxicity. *CA: A Cancer Journal for Clinicians* **2020**, *70* (2), 86–104. https://doi.org/10.3322/caac.21596.

(63) Waldman, A. D.; Fritz, J. M.; Lenardo, M. J. A Guide to Cancer Immunotherapy: From T Cell Basic Science to Clinical Practice. *Nat Rev Immunol* **2020**, *20* (11), 651–668. https://doi.org/10.1038/s41577-020-0306-5.

(64) Targeted Therapy for Cancer - National Cancer Institute https://www.cancer.gov/about-cancer/treatment/types/targeted-therapies (accessed 2021 -06 -07).

(65) Targeted Cancer Therapies Fact Sheet - National Cancer Institute https://www.cancer.gov/about-cancer/treatment/types/targeted-therapies/targeted-therapies-fact-sheet (accessed 2021 -06 -07).

(66) Xie, Y.-H.; Chen, Y.-X.; Fang, J.-Y. Comprehensive Review of Targeted Therapy for Colorectal Cancer. *Sig Transduct Target Ther* **2020**, *5* (1), 22. https://doi.org/10.1038/s41392-020-0116-z.

(67) How Chemotherapy Drugs Work https://www.cancer.org/treatment/treatments-and-side-effects/treatment-types/chemotherapy/how-chemotherapy-drugs-work.html (accessed 2021 -06 -09).

(68) Shewach, D. S.; Kuchta, R. D. Introduction to Cancer Chemotherapeutics. *Chem. Rev.* **2009**, *109* (7), 2859–2861. https://doi.org/10.1021/cr900208x.

(69) Vasan, N.; Baselga, J.; Hyman, D. M. A View on Drug Resistance in Cancer. *Nature* **2019**, *575* (7782), 299–309. https://doi.org/10.1038/s41586-019-1730-1.

(70) Kummar, S.; Gutierrez, M.; Doroshow, J. H.; Murgo, A. J. Drug Development in Oncology: Classical Cytotoxics and Molecularly Targeted Agents. *Br J Clin Pharmacol* **2006**, *62* (1), 15–26. https://doi.org/10.1111/j.1365-2125.2006.02713.x.

(71) Huang, C.-Y.; Ju, D.-T.; Chang, C.-F.; Reddy, P. M.; Velmurugan, B. K. A Review on the Effects of Current Chemotherapy Drugs and Natural Agents in Treating Non–Small Cell Lung Cancer. *BioMedicine* **2017**, *7* (4), 23. https://doi.org/10.1051/bmdcn/2017070423.

(72) Basu, A.; Krishnamurthy, S. Cellular Responses to Cisplatin-Induced DNA Damage. *Journal of Nucleic Acids* **2010**, *2010*, e201367. https://doi.org/10.4061/2010/201367.

(73) Jamieson, E. R.; Lippard, S. J. Structure, Recognition, and Processing of Cisplatin−DNA Adducts. *Chem. Rev.* **1999**, *99* (9), 2467–2498. https://doi.org/10.1021/cr980421n.

(74) Onoa, G. B.; Cervantes, G.; Moreno, V.; Prieto, M. J. Study of the Interaction of DNA with Cisplatin and Other Pd(II) and Pt(II) Complexes by Atomic Force Microscopy. *Nucleic Acids Research* **1998**, *26* (6), 1473–1480. https://doi.org/10.1093/nar/26.6.1473.

(75) Alberts, D. S. Carboplatin versus Cisplatin in Ovarian Cancer. *Semin Oncol* **1995**, *22* (5 Suppl 12), 88–90.

(76) Knox, R. J.; Friedlos, F.; Lydall, D. A.; Roberts, J. J. Mechanism of Cytotoxicity of Anticancer Platinum Drugs: Evidence That Cis-Diamminedichloroplatinum(II) and Cis-Diammine-(1,1-Cyclobutanedicarboxylato)Platinum(II) Differ Only in the Kinetics of Their Interaction with DNA. *Cancer Res* **1986**, *46* (4 Part 2), 1972–1979.

(77) Oun, R.; Moussa, Y. E.; Wheate, N. J. The Side Effects of Platinum-Based Chemotherapy Drugs: A Review for Chemists. *Dalton Trans.* **2018**, *47* (19), 6645–6653. https://doi.org/10.1039/C8DT00838H.

(78) Culy, C. R.; Clemett, D.; Wiseman, L. R. Oxaliplatin. *Drugs* **2000**, *60* (4), 895–924. https://doi.org/10.2165/00003495-200060040-00005.

(79) Amable, L. Cisplatin Resistance and Opportunities for Precision Medicine. *Pharmacological Research* **2016**, *106*, 27–36. https://doi.org/10.1016/j.phrs.2016.01.001.

(80) Konkankit, C. C.; Marker, S. C.; Knopf, K. M.; Wilson, J. J. Anticancer Activity of Complexes of the Third Row Transition Metals, Rhenium, Osmium, and Iridium. *Dalton Trans.* **2018**, *47* (30), 9934–9974. https://doi.org/10.1039/C8DT01858H.

(81) Fischer, B.; Dubler, E.; Meienberger, M.; Hegetschweiler, K. Molybdenum Complexes of the Anticancer Drug 6-Mercaptopurine. *Inorganica Chimica Acta* **1998**, *279* (2), 136–143. https://doi.org/10.1016/S0020-1693(98)00108-X.

(82) Ndagi, U.; Mhlongo, N.; Soliman, M. E. Metal Complexes in Cancer Therapy – an Update from Drug Design Perspective. *Drug Des Devel Ther* **2017**, *11*, 599–616. https://doi.org/10.2147/DDDT.S119488.

(83) Frezza, M.; Hindo, S.; Chen, D.; Davenport, A.; Schmitt, S.; Tomco, D.; Dou, Q. P. Novel Metals and Metal Complexes as Platforms for Cancer Therapy. *Curr Pharm Des* **2010**, *16* (16), 1813–1825.

(84) Valiahdi, S. M.; Heffeter, P.; Jakupec, M. A.; Marculescu, R.; Berger, W.; Rappersberger, K.; Keppler, B. K. The Gallium Complex KP46 Exerts Strong Activity against Primary Explanted Melanoma Cells and Induces Apoptosis in Melanoma Cell Lines. *Melanoma Res* **2009**, *19* (5), 283–293. https://doi.org/10.1097/CMR.0b013e32832b272d.

(85) Kircheva, N.; Dudev, T. Novel Insights into Gallium's Mechanism of Therapeutic Action: A DFT/PCM Study of the Interaction between Ga3+ and Ribonucleotide Reductase Substrates. *J. Phys. Chem. B* **2019**, *123* (26), 5444–5451. https://doi.org/10.1021/acs.jpcb.9b03145.

(86) Aye, Y.; Li, M.; Long, M. J. C.; Weiss, R. S. Ribonucleotide Reductase and Cancer: Biological Mechanisms and Targeted Therapies. *Oncogene* **2015**, *34* (16), 2011–2021. https://doi.org/10.1038/onc.2014.155.

(87) Chitambar, C. R.; Antholine, W. E. Iron-Targeting Antitumor Activity of Gallium Compounds and Novel Insights Into Triapine®-Metal Complexes. *Antioxid Redox Signal* **2013**, *18* (8), 956–972. https://doi.org/10.1089/ars.2012.4880.

(88) Chamberlain, S.; Cole, H. D.; Roque, J.; Bellnier, D.; McFarland, S. A.; Shafirstein, G. TLD1433-Mediated Photodynamic Therapy with an Optical Surface Applicator in the Treatment of Lung Cancer Cells In Vitro. *Pharmaceuticals (Basel)* **2020**, *13* (7). https://doi.org/10.3390/ph13070137.

(89) Theralase Inc. *A Phase II Clinical Study of Intravesical Photodynamic Therapy in Patients With BCG-Unresponsive Non-Muscle Invasive Bladder Cancer ("NMIBC") Or Patients Who Are Intolerant to BCG Therapy ("Study").*; Clinical trial registration NCT03945162; clinicaltrials.gov, 2021.

(90) Monro, S.; Colón, K. L.; Yin, H.; Roque, J.; Konda, P.; Gujar, S.; Thummel, R. P.; Lilge, L.; Cameron, C. G.; McFarland, S. A. Transition Metal Complexes and Photodynamic Therapy from a Tumor-Centered Approach: Challenges, Opportunities, and Highlights from the Development of TLD1433. *Chem Rev* **2019**, *119* (2), 797–828. https://doi.org/10.1021/acs.chemrev.8b00211.

(91) Lilge, L. D.; Kulkani, G.; Mandel, A.; Perlis, N.; Nesbitt, M.; White, R.; Embree, W.; Jewett, M. TLD-1433 Photodynamic Therapy for BCG-Unresponsive NMIBC: A Phase IB Clinical Study (Conference Presentation). In *17th International Photodynamic Association World Congress*; International Society for Optics and Photonics, 2019; Vol. 11070, p 1107025. https://doi.org/10.1117/12.2526187.

(92) Steba Biotech S.A. *Multicenter Phase 3 Pivotal Study to Evaluate the Safety and Efficacy of TOOKAD (Padeliporfin) Vascular Targeted Photodynamic Therapy in the Treatment of Low Grade Upper Tract Urothelial Cancer*; Clinical trial registration NCT04620239; clinicaltrials.gov, 2021.

(93) Steba Biotech S.A. *Study of the Efficacy, Safety and Quality of Life After TOOKAD® Soluble Vascular Targeted Photodynamic Therapy (VTP) for Minimally Invasive Treatment of Localized Intermediate Risk Prostate Cancer.*; Clinical trial registration NCT03315754; clinicaltrials.gov, 2021.

(94) K. Stultz, L.; Hunsucker, A.; Middleton, S.; Grovenstein, E.; O'Leary, J.; Blatt, E.; Miller, M.; Mobley, J.; K. Hanson, P. Proteomic Analysis of the S. Cerevisiae Response to the Anticancer Ruthenium Complex KP1019. *Metallomics* **2020**, *12* (6), 876–890. https://doi.org/10.1039/D0MT00008F.

(95) Hartinger, C. G.; Jakupec, M. A.; Zorbas-Seifried, S.; Groessl, M.; Egger, A.; Berger, W.; Zorbas, H.; Dyson, P. J.; Keppler, B. K. KP1019, A New Redox-Active Anticancer Agent – Preclinical Development and Results of a Clinical Phase I Study in Tumor Patients. *Chemistry & Biodiversity* **2008**, *5* (10), 2140–2155. https://doi.org/10.1002/cbdv.200890195.

(96) Trondl, R.; Heffeter, P.; Kowol, C. R.; Jakupec, M. A.; Berger, W.; Keppler, B. K. NKP-1339, the First Ruthenium-Based Anticancer Drug on the Edge to Clinical Application. *Chem. Sci.* **2014**, *5* (8), 2925–2932. https://doi.org/10.1039/C3SC53243G.

(97) Stultz, L. K.; Hunsucker, A.; Middleton, S.; Grovenstein, E.; O'Leary, J.; Blatt, E.; Miller, M.; Mobley, J.; Hanson, P. K. Proteomic Analysis of the S. Cerevisiae Response to the Anticancer Ruthenium Complex KP1019. *Metallomics* **2020**, *12* (6), 876–890. https://doi.org/10.1039/d0mt00008f.

(98) Safety and activity of IT-139, a ruthenium-based compound, in patients with advanced solid tumours: a first-in-human, open-label, dose-escalation phase I study with expansion cohort | Elsevier Enhanced Reader https://reader.elsevier.com/reader/sd/pii/S2059702920325060?token=9EA08B4CF59B534315F5179A09B88A9EE0E509B4EC8360875FDD60BA643BC24B9A7F02A054CB39C44C4659C78000B74F&originRegion=eu-west-1&originCreation=20210511145711 (accessed 2021 -05 -11). https://doi.org/10.1136/esmoopen-2016-000154.

(99) Neuditschko, B.; Legin, A. A.; Baier, D.; Schintlmeister, A.; Reipert, S.; Wagner, M.; Keppler, B. K.; Berger, W.; Meier-Menches, S. M.; Gerner, C. Interaction with Ribosomal Proteins Accompanies Stress Induction of the Anticancer Metallodrug BOLD-100/KP1339 in the Endoplasmic Reticulum. *Angewandte Chemie International Edition* **2021**, *60* (10), 5063–5068. https://doi.org/10.1002/anie.202015962.

(100) Yan, Y. K.; Melchart, M.; Habtemariam, A.; Sadler, P. J. Organometallic Chemistry, Biology and Medicine: Ruthenium Arene Anticancer Complexes. *Chem. Commun.* **2005**, No. 38, 4764. https://doi.org/10.1039/b508531b.

(101) Wang, M.; Wey, S.; Zhang, Y.; Ye, R.; Lee, A. S. Role of the Unfolded Protein Response Regulator GRP78/BiP in Development, Cancer, and Neurological Disorders. *Antioxid Redox Signal* **2009**, *11* (9), 2307–2316. https://doi.org/10.1089/ars.2009.2485.

(102) Inc, B. T. FDA Grants Bold Therapeutics' BOLD-100 an Orphan Drug Designation (ODD) in the Treatment of Gastric Cancer https://www.prnewswire.com/news-releases/fda-grants-bold-therapeutics-bold-100-an-orphan-drug-designation-odd-in-the-treatment-of-gastric-cancer-301288416.html (accessed 2021 -05 -31).

(103) Leijen, S.; Burgers, S. A.; Baas, P.; Pluim, D.; Tibben, M.; van Werkhoven, E.; Alessio, E.; Sava, G.; Beijnen, J. H.; Schellens, J. H.; M. Phase I/II Study with Ruthenium Compound NAMI-A and Gemcitabine in Patients with Non-Small Cell Lung Cancer after First Line Therapy. *Investigational New Drugs* **2015**, *33* (1), 201–214. http://dx-doi-org.uaccess.univie.ac.at/10.1007/s10637-014-0179-1.

(104) Groessl, M.; Reisner, E.; Hartinger, C. G.; Eichinger, R.; Semenova, O.; Timerbaev, A. R.; Jakupec, M. A.; Arion, V. B.; Keppler, B. K. Structure−Activity Relationships for NAMI-A-Type Complexes (HL)[Trans-RuCl4L(S-Dmso)Ruthenate(III)] (L = Imidazole, Indazole, 1,2,4-Triazole, 4-Amino-1,2,4-Triazole, and 1-Methyl-1,2,4-Triazole): Aquation, Redox Properties, Protein Binding, and Antiproliferative Activity. *J. Med. Chem.* **2007**, *50* (9), 2185–2193. https://doi.org/10.1021/jm061081y.

(105) Bacac, M.; Hotze, A. C. G.; Schilden, K. van der; Haasnoot, J. G.; Pacor, S.; Alessio, E.; Sava, G.; Reedijk, J. The Hydrolysis of the Anti-Cancer Ruthenium Complex NAMI-A Affects Its DNA Binding and Antimetastatic Activity: An NMR Evaluation. *Journal of Inorganic Biochemistry* **2004**, *98* (2), 402–412. https://doi.org/10.1016/j.jinorgbio.2003.12.003.

(106) Webb, M. I.; Walsby, C. J. Control of Ligand-Exchange Processes and the Oxidation State of the Antimetastatic Ru(III) Complex NAMI-A by Interactions with Human Serum Albumin. *Dalton Trans.* **2011**, *40* (6), 1322–1331. https://doi.org/10.1039/C0DT01168A.

(107) Bergamo, A.; Masi, A.; Jakupec, M. A.; Keppler, B. K.; Sava, G. Inhibitory Effects of the Ruthenium Complex KP1019 in Models of Mammary Cancer Cell Migration and Invasion. *Metal-Based Drugs* **2009**, *2009*, e681270. https://doi.org/10.1155/2009/681270.

(108) Webb, M. I.; Walsby, C. J. Control of Ligand-Exchange Processes and the Oxidation State of the Antimetastatic Ru(Iii) Complex NAMI-A by Interactions with Human Serum Albumin. *Dalton Trans.* **2011**, *40* (6), 1322. https://doi.org/10.1039/c0dt01168a.

(109) Thirty Years of the Drug Candidate NAMI-A and the Myths in the Field of Ruthenium Anticancer Compounds: A Personal Perspective https://chemistry-europe-onlinelibrary-wiley-com.uaccess.univie.ac.at/doi/epdf/10.1002/ejic.201600986 (accessed 2021 -05 -12). https://doi.org/10.1002/ejic.201600986.

(110) Gasser, G.; Ott, I.; Metzler-Nolte, N. Organometallic Anticancer Compounds. *J. Med. Chem.* **2011**, *54* (1), 3–25. https://doi.org/10.1021/jm100020w.

(111) Harringer, S.; Matzinger, M.; Gajic, N.; Hejl, M.; Jakupec, M. A.; Kandioller, W.; Keppler, B. K. First Insights into the Novel Class of Organometallic Compounds Bearing a Bidentate Selenopyridone Coordination Motif: Synthesis, Characterization, Stability and Biological Investigations. *Inorganica Chimica Acta* **2020**, *513*, 119919. https://doi.org/10.1016/j.ica.2020.119919.

(112) Controlling platinum, ruthenium, and osmium reactivity for anticancer drug design | Elsevier Enhanced Reader https://reader.elsevier.com/reader/sd/pii/S0898883809002013?token=417B121684348B9A0049FE1C158F71B2CCFAF645C1101D5270D6A67E325054CB45C2A00889B6FEA4F31E17ABB468F40F&originRegion=eu-west-1&originCreation=20210603152155 (accessed 2021 -06 -03). https://doi.org/10.1016/S0898-8838(09)00201-3.

(113) Liu, H.-K.; Sadler, P. J. Metal Complexes as DNA Intercalators https://pubs.acs.org/doi/pdf/10.1021/ar100140e (accessed 2021 -06 -07). https://doi.org/10.1021/ar100140e.

(114) Scolaro, C.; Hartinger, C. G.; Allardyce, C. S.; Keppler, B. K.; Dyson, P. J. Hydrolysis Study of the Bifunctional Antitumour Compound RAPTA-C, [Ru(H6-p-Cymene)Cl2(Pta)]. *Journal of Inorganic Biochemistry* **2008**, *102* (9), 1743–1748. https://doi.org/10.1016/j.jinorgbio.2008.05.004.

(115) Rausch, M.; Dyson, P. J.; Nowak-Sliwinska, P. Recent Considerations in the Application of RAPTA-C for Cancer Treatment and Perspectives for Its Combination with Immunotherapies. *Advanced Therapeutics* **2019**, *2* (9), 1900042. https://doi.org/10.1002/adtp.201900042.

(116) Murray, B. S.; Babak, M. V.; Hartinger, C. G.; Dyson, P. J. The Development of RAPTA Compounds for the Treatment of Tumors. *Coordination Chemistry Reviews* **2016**, *306*, 86–114. https://doi.org/10.1016/j.ccr.2015.06.014.

(117) Babak, M. V.; Meier, S. M.; Huber, K. V. M.; Reynisson, J.; Legin, A. A.; Jakupec, M. A.; Roller, A.; Stukalov, A.; Gridling, M.; Bennett, K. L.; Colinge, J.; Berger, W.; Dyson, P. J.; Superti-Furga, G.; Keppler, B. K.; Hartinger, C. G. Target Profiling of an Antimetastatic RAPTA Agent by Chemical Proteomics: Relevance to the Mode of Action. *Chem. Sci.* **2015**, *6* (4), 2449–2456. https://doi.org/10.1039/C4SC03905J.

(118) Groessl, M.; Terenghi, M.; Casini, A.; Elviri, L.; Lobinski, R.; Dyson, P. J. Reactivity of Anticancer Metallodrugs with Serum Proteins: New Insights from Size Exclusion Chromatography-ICP-MS and ESI-MS. *J. Anal. At. Spectrom.* **2010**, *25* (3), 305–313. https://doi.org/10.1039/B922701F.

(119) Meier-Menches, S. M.; Gerner, C.; Berger, W.; Hartinger, C. G.; Keppler, B. K. Structure–Activity Relationships for Ruthenium and Osmium Anticancer Agents – towards Clinical Development. *Chem. Soc. Rev.* **2018**, *47* (3), 909–928. https://doi.org/10.1039/C7CS00332C.

(120) Antonarakis, E. S.; Emadi, A. Ruthenium-Based Chemotherapeutics: Are They Ready for Prime Time? *Cancer Chemother Pharmacol* **2010**, *66* (1), 1–9. https://doi.org/10.1007/s00280-010-1293-1.

(121) Weiss, A.; H. Berndsen, R.; Dubois, M.; Müller, C.; Schibli, R.; W. Griffioen, A.; J. Dyson, P.; Nowak-Sliwinska, P. In Vivo Anti-Tumor Activity of the Organometallic Ruthenium(Ii)-Arene Complex [Ru(η 6 - p -Cymene)Cl 2 (Pta)] (RAPTA-C) in Human Ovarian and Colorectal Carcinomas. *Chemical Science* **2014**, *5* (12), 4742–4748. https://doi.org/10.1039/C4SC01255K.

(122) Wang, F.; Xu, J.; Wu, K.; Weidt, S. K.; Mackay, C. L.; Langridge-Smith, P. R. R.; Sadler, P. J. Competition between Glutathione and DNA Oligonucleotides for Ruthenium(II) Arene Anticancer Complexes. *Dalton Trans.* **2013**, *42* (9), 3188–3195. https://doi.org/10.1039/C2DT32091F.

(123) Lin, Y.; Wang, J.; Zheng, W.; Luo, Q.; Wu, K.; Du, J.; Zhao, Y.; Wang, F. Organometallic Ruthenium Anticancer Complexes Inhibit Human Peroxiredoxin I Activity by Binding to and Inducing Oxidation

of Its Catalytic Cysteine Residue. *Metallomics* **2019**, *11* (3), 546–555. https://doi.org/10.1039/C8MT00352A.

(124) Hayward, R. L.; Schornagel, Q. C.; Tente, R.; Macpherson, J. S.; Aird, R. E.; Guichard, S.; Habtemariam, A.; Sadler, P.; Jodrell, D. I. Investigation of the Role of Bax, P21/Waf1 and P53 as Determinants of Cellular Responses in HCT116 Colorectal Cancer Cells Exposed to the Novel Cytotoxic Ruthenium(II) Organometallic Agent, RM175. *Cancer Chemother Pharmacol* **2005**, *55* (6), 577–583. https://doi.org/10.1007/s00280-004-0932-9.

(125) Renfrew, A. K. Transition Metal Complexes with Bioactive Ligands: Mechanisms for Selective Ligand Release and Applications for Drug Delivery. *Metallomics* **2014**, *6* (8), 1324–1335. https://doi.org/10.1039/C4MT00069B.

(126) Talevi, A. Multi-Target Pharmacology: Possibilities and Limitations of the “Skeleton Key Approach” from a Medicinal Chemist Perspective. *Front. Pharmacol.* **2015**, *6*. https://doi.org/10.3389/fphar.2015.00205.

(127) Fernández, A.; Sanguino, A.; Peng, Z.; Crespo, A.; Ozturk, E.; Zhang, X.; Wang, S.; Bornmann, W.; Lopez-Berestein, G. Rational Drug Redesign to Overcome Drug Resistance in Cancer Therapy: Imatinib Moving Target. *Cancer Res* **2007**, *67* (9), 4028–4033. https://doi.org/10.1158/0008-5472.CAN-07-0345.

(128) Vock, C. A.; Ang, W. H.; Scolaro, C.; Phillips, A. D.; Lagopoulos, L.; Juillerat-Jeanneret, L.; Sava, G.; Scopelliti, R.; Dyson, P. J. Development of Ruthenium Antitumor Drugs That Overcome Multidrug Resistance Mechanisms. *J. Med. Chem.* **2007**, *50* (9), 2166–2175. https://doi.org/10.1021/jm070039f.

(129) Patra, M.; Gasser, G. The Medicinal Chemistry of Ferrocene and Its Derivatives. *Nature Reviews Chemistry* **2017**, *1* (9), 1–12. https://doi.org/10.1038/s41570-017-0066.

(130) Zhang, P.; Sadler, P. J. Advances in the Design of Organometallic Anticancer Complexes. *Journal of Organometallic Chemistry* **2017**, *839*, 5–14. https://doi.org/10.1016/j.jorganchem.2017.03.038.

(131) Ornelas, C. Application of Ferrocene and Its Derivatives in Cancer Research. *New J. Chem.* **2011**, *35* (10), 1973–1985. https://doi.org/10.1039/C1NJ20172G.

(132) Wang, R.; Chen, H.; Yan, W.; Zheng, M.; Zhang, T.; Zhang, Y. Ferrocene-Containing Hybrids as Potential Anticancer Agents: Current Developments, Mechanisms of Action and Structure-Activity Relationships. *European Journal of Medicinal Chemistry* **2020**, *190*, 112109. https://doi.org/10.1016/j.ejmech.2020.112109.

(133) Spoerlein-Guettler, C.; Mahal, K.; Schobert, R.; Biersack, B. Ferrocene and (Arene)Ruthenium(II) Complexes of the Natural Anticancer Naphthoquinone Plumbagin with Enhanced Efficacy against

Resistant Cancer Cells and a Genuine Mode of Action. *Journal of Inorganic Biochemistry* **2014**, *138*, 64–72. https://doi.org/10.1016/j.jinorgbio.2014.04.020.

(134) Singh, A.; Lumb, I.; Mehra, V.; Kumar, V. Ferrocene-Appended Pharmacophores: An Exciting Approach for Modulating the Biological Potential of Organic Scaffolds. *Dalton Trans.* **2019**, *48* (9), 2840–2860. https://doi.org/10.1039/C8DT03440K.

(135) Golbaghi, G.; Pitard, I.; Lucas, M.; Haghdoost, M. M.; de los Santos, Y. L.; Doucet, N.; Patten, S. A.; Sanderson, J. T.; Castonguay, A. Synthesis and Biological Assessment of a Ruthenium(II) Cyclopentadienyl Complex in Breast Cancer Cells and on the Development of Zebrafish Embryos. *European Journal of Medicinal Chemistry* **2020**, *188*, 112030. https://doi.org/10.1016/j.ejmech.2019.112030.

(136) Castonguay, A.; Doucet, C.; Juhas, M.; Maysinger, D. New Ruthenium(II)–Letrozole Complexes as Anticancer Therapeutics. *J. Med. Chem.* **2012**, *55* (20), 8799–8806. https://doi.org/10.1021/jm301103y.

(137) Simpson, E. R.; Clyne, C.; Rubin, G.; Boon, W. C.; Robertson, K.; Britt, K.; Speed, C.; Jones, M. Aromatase—A Brief Overview. *Annu. Rev. Physiol.* **2002**, *64* (1), 93–127. https://doi.org/10.1146/annurev.physiol.64.081601.142703.

(138) Geisler, J. Differences between the Non-Steroidal Aromatase Inhibitors Anastrozole and Letrozole – of Clinical Importance? *Br J Cancer* **2011**, *104* (7), 1059–1066. https://doi.org/10.1038/bjc.2011.58.

(139) Fabian, C. J. The What, Why and How of Aromatase Inhibitors: Hormonal Agents for Treatment and Prevention of Breast Cancer. *International Journal of Clinical Practice* **2007**, *61* (12), 2051–2063. https://doi.org/10.1111/j.1742-1241.2007.01587.x.

(140) Wiseman, L. R.; Adkins, J. C. Anastrozole. *Drugs & Aging* **1998**, *13* (4), 321–332. https://doi.org/10.2165/00002512-199813040-00008.

(141) Golbaghi, G.; Haghdoost, M. M.; Yancu, D.; Santos, Y. L. de los; Doucet, N.; Patten, S. A.; Sanderson, J. T.; Castonguay, A. Organoruthenium(II) Complexes Bearing an Aromatase Inhibitor: Synthesis, Characterization, in Vitro Biological Activity and in Vivo Toxicity in Zebrafish Embryos. *Organometallics* **2019**. https://doi.org/10.1021/acs.organomet.8b00897.

(142) Petrelli, A.; Giordano, S. From Single- to Multi-Target Drugs in Cancer Therapy: When Aspecificity Becomes an Advantage. *Current medicinal chemistry* **2008**, *15*, 422–432. https://doi.org/10.2174/092986708783503212.

(143) Sharom, F. J. The P-Glycoprotein Efflux Pump: How Does It Transport Drugs? *J. Membrane Biol.* **1997**, *160* (3), 161–175. https://doi.org/10.1007/s002329900305.

(144) Sharom, F. J. Complex Interplay between the P-Glycoprotein Multidrug Efflux Pump and the Membrane: Its Role in Modulating Protein Function. *Front. Oncol.* **2014**, *4*. https://doi.org/10.3389/fonc.2014.00041.

(145) Mitra, K.; Shettar, A.; Kondaiah, P.; Chakravarty, A. R. Biotinylated Platinum(II) Ferrocenylterpyridine Complexes for Targeted Photoinduced Cytotoxicity. *Inorg. Chem.* **2016**, *55* (11), 5612–5622. https://doi.org/10.1021/acs.inorgchem.6b00680.

(146) Unprecedented Inhibition of P-Gp Activity by a Novel Ruthenium-Cyclopentadienyl Compound Bearing a Bipyridine-Biotin Ligand. *European Journal of Medicinal Chemistry* **2019**, *163*, 853–863. https://doi.org/10.1016/j.ejmech.2018.12.022.

(147) Legina, M. S.; Nogueira, J. J.; Kandioller, W.; Jakupec, M. A.; González, L.; Keppler, B. K. Biological Evaluation of Novel Thiomaltol-Based Organometallic Complexes as Topoisomerase IIα Inhibitors. *J Biol Inorg Chem* **2020**, *25* (3), 451–465. https://doi.org/10.1007/s00775-020-01775-2.

(148) Hackl, C. M.; Schoenhacker-Alte, B.; Klose, M. H. M.; Henke, H.; Legina, M. S.; Jakupec, M. A.; Berger, W.; Keppler, B. K.; Brüggemann, O.; Teasdale, I.; Heffeter, P.; Kandioller, W. Synthesis and in Vivo Anticancer Evaluation of Poly(Organo)Phosphazene-Based Metallodrug Conjugates. *Dalton Trans.* **2017**, *46* (36), 12114–12124. https://doi.org/10.1039/C7DT01767G.

(149) Harringer, S.; Happl, B.; Ozenil, M.; Kast, C.; Hejl, M.; Wernitznig, D.; Legin, A. A.; Schweikert, A.; Gajic, N.; Roller, A.; Koellensperger, G.; Jakupec, M. A.; Kandioller, W.; Keppler, B. K. Synthesis, Modification, and Biological Evaluation of a Library of Novel Water-Soluble Thiopyridone-Based Organometallic Complexes and Their Unexpected (Biological) Behavior. *Chemistry – A European Journal* **2020**, *26* (24), 5419–5433. https://doi.org/10.1002/chem.201905546.

(150) Saibu, M.; Sagar, S.; Green, I.; Ameer, F.; Meyer, M. Evaluating the Cytotoxic Effects of Novel Quinone Compounds. *Anticancer Research* **2014**, *34* (8), 4077–4086.

(151) Lien, J.-C.; Huang, L.-J.; Teng, C.-M.; Wang, J.-P.; Kuo, S.-C. Synthesis of 2-Alkoxy 1,4-Naphthoquinone Derivatives as Antiplatelet, Antiinflammatory, and Antiallergic Agents. *Chem. Pharm. Bull.* **2002**, *50* (5), 672–674. https://doi.org/10.1248/cpb.50.672.

(152) Widhalm, J. R.; Rhodes, D. Biosynthesis and Molecular Actions of Specialized 1,4-Naphthoquinone Natural Products Produced by Horticultural Plants. *Hortic Res* **2016**, *3* (1), 1–17. https://doi.org/10.1038/hortres.2016.46.

(153) Pereyra, C. E.; Dantas, R. F.; Ferreira, S. B.; Gomes, L. P.; Silva-Jr, F. P. The Diverse Mechanisms and Anticancer Potential of Naphthoquinones. *Cancer Cell Int* **2019**, *19* (1), 207. https://doi.org/10.1186/s12935-019-0925-8.

(154) Gong, Q.; Hu, J.; Wang, P.; Li, X.; Zhang, X. A Comprehensive Review on β-Lapachone: Mechanisms, Structural Modifications, and Therapeutic Potentials. *European Journal of Medicinal Chemistry* **2021**, *210*, 112962. https://doi.org/10.1016/j.ejmech.2020.112962.

(155) Gopinath, P.; Mahammed, A.; Ohayon, S.; Gross, Z.; Brik, A. Understanding and Predicting the Potency of ROS-Based Enzyme Inhibitors, Exemplified by Naphthoquinones and Ubiquitin Specific Protease-2. *Chem. Sci.* **2016**, *7* (12), 7079–7086. https://doi.org/10.1039/C6SC02758J.

(156) González, F. J. Cyclic Voltammetry of Two Analogue K-Group Vitamin Compounds in Dimethylsulfoxide. *Electroanalysis* **1998**, *10* (9), 638–642. https://doi.org/10.1002/(SICI)1521-4109(199807)10:9<638::AID-ELAN638>3.0.CO;2-R.

(157) Guin, P. S.; Das, S.; Mandal, P. C. Electrochemical Reduction of Quinones in Different Media: A Review. *International Journal of Electrochemistry* **2011**, *2011*, 1–22. https://doi.org/10.4061/2011/816202.

(158) ROS and the DNA damage response in cancer | Elsevier Enhanced Reader https://reader.elsevier.com/reader/sd/pii/S2213231718309017?token=3CCAA2D3D104A32F88E3330C5C165FD1786E677670C1ED81AB429919E1928C52952FC90BF4459F0C3A9F2D7A53EDAEAB&originRegion=eu-west-1&originCreation=20210609180221 (accessed 2021 -06 -09). https://doi.org/10.1016/j.redox.2018.101084.

(159) Olson, O. C.; Joyce, J. A. Cysteine Cathepsin Proteases: Regulators of Cancer Progression and Therapeutic Response. *Nat Rev Cancer* **2015**, *15* (12), 712–729. https://doi.org/10.1038/nrc4027.

(160) Cotto-Rios, X. M.; Békés, M.; Chapman, J.; Ueberheide, B.; Huang, T. T. Deubiquitinases as a Signaling Target of Oxidative Stress. *Cell Reports* **2012**, *2* (6), 1475–1484. https://doi.org/10.1016/j.celrep.2012.11.011.

(161) Fraile, J. M.; Quesada, V.; Rodríguez, D.; Freije, J. M. P.; López-Otín, C. Deubiquitinases in Cancer: New Functions and Therapeutic Options. *Oncogene* **2012**, *31* (19), 2373–2388. https://doi.org/10.1038/onc.2011.443.

(162) Ross, D.; Siegel, D. Functions of NQO1 in Cellular Protection and CoQ10 Metabolism and Its Potential Role as a Redox Sensitive Molecular Switch. *Front Physiol* **2017**, *8*. https://doi.org/10.3389/fphys.2017.00595.

(163) Pink, J. J.; Planchon, S. M.; Tagliarino, C.; Varnes, M. E.; Siegel, D.; Boothman, D. A. NAD(P)H:Quinone Oxidoreductase Activity Is the Principal Determinant of β-Lapachone Cytotoxicity. *Journal of Biological Chemistry* **2000**, *275* (8), 5416–5424. https://doi.org/10.1074/jbc.275.8.5416.

(164) Alvarado-Ortiz, E.; de la Cruz-López, K. G.; Becerril-Rico, J.; Sarabia-Sánchez, M. A.; Ortiz-Sánchez, E.; García-Carrancá, A. Mutant P53 Gain-of-Function: Role in Cancer Development, Progression, and Therapeutic Approaches. *Front. Cell Dev. Biol.* **2021**, *8*. https://doi.org/10.3389/fcell.2020.607670.

(165) Wu, Z.; Wu, L.; Li, L.; Tashiro, S.; Onodera, S.; Ikejima, T. P53-Mediated Cell Cycle Arrest and Apoptosis Induced by Shikonin via a Caspase-9-Dependent Mechanism in Human Malignant Melanoma A375-S2 Cells. *Journal of Pharmacological Sciences* **2004**, *94* (2), 166–176. https://doi.org/10.1254/jphs.94.166.

(166) Kang, K.-H.; Lee, J.-H.; Kim, K.-C.; Ham, S.-W.; Kim, M.-Y.; Choi, K. H. Induction of P73β by a Naphthoquinone Analog Is Mediated by E2F-1 and Triggers Apoptosis in HeLa Cells. *FEBS Letters* **2002**, *522* (1–3), 161–167. https://doi.org/10.1016/S0014-5793(02)02921-6.

(167) Pommier, Y. Topoisomerase I Inhibitors: Camptothecins and Beyond. *Nat Rev Cancer* **2006**, *6* (10), 789–802. https://doi.org/10.1038/nrc1977.

(168) Li, C. J.; Averboukh, L.; Pardee, A. B. Beta-Lapachone, a Novel DNA Topoisomerase I Inhibitor with a Mode of Action Different from Camptothecin. *Journal of Biological Chemistry* **1993**, *268* (30), 22463–22468. https://doi.org/10.1016/S0021-9258(18)41552-9.

(169) Pommier, Y.; Sun, Y.; Huang, S. N.; Nitiss, J. L. Roles of Eukaryotic Topoisomerases in Transcription, Replication and Genomic Stability. *Nat Rev Mol Cell Biol* **2016**, *17* (11), 703–721. https://doi.org/10.1038/nrm.2016.111.

(170) Krishnan, P.; Bastow, K. F. Novel Mechanisms of DNA Topoisomerase II Inhibition by Pyranonaphthoquinone Derivatives—Eleutherin, α Lapachone, and β Lapachone∗. *Biochemical Pharmacology* **2000**, *60* (9), 1367–1379. https://doi.org/10.1016/S0006-2952(00)00437-8.

(171) Krishnan, P.; Bastow, K. F. Novel Mechanism of Cellular DNA Topoisomerase II Inhibition by the Pyranonaphthoquinone Derivatives α-Lapachone and β-Lapachone. *Cancer Chemother Pharmacol* **2001**, *47* (3), 187–198. https://doi.org/10.1007/s002800000221.

(172) Nitiss, J. L. Targeting DNA Topoisomerase II in Cancer Chemotherapy. *Nat Rev Cancer* **2009**, *9* (5), 338–350. https://doi.org/10.1038/nrc2607.

(173) Huang, H.; Xie, H.; Pan, Y.; Zheng, K.; Xia, Y.; Chen, W. Plumbagin Triggers ER Stress-Mediated Apoptosis in Prostate Cancer Cells via Induction of ROS. *CPB* **2018**, *45* (1), 267–280. https://doi.org/10.1159/000486773.

(174) Lord, J. M. Protein Degradation: Go Outside and See the Proteasome. *Current Biology* **1996**, *6* (9), 1067–1069. https://doi.org/10.1016/S0960-9822(02)70666-0.

(175) Yang, H.; Zhou, P.; Huang, H.; Chen, D.; Ma, N.; Cui, Q. C.; Shen, S.; Dong, W.; Zhang, X.; Lian, W.; Wang, X.; Dou, Q. P.; Liu, J. Shikonin Exerts Antitumor Activity via Proteasome Inhibition and Cell Death Induction in Vitro and in Vivo. *International Journal of Cancer* **2009**, *124* (10), 2450–2459. https://doi.org/10.1002/ijc.24195.

(176) Young, R. M.; Staudt, L. M. A New "Brew" of MALT1 Inhibitors. *Cancer Cell* **2012**, *22* (6), 706–707. https://doi.org/10.1016/j.ccr.2012.11.011.

(177) Jaworski, M.; Thome, M. The Paracaspase MALT1: Biological Function and Potential for Therapeutic Inhibition. *Cell. Mol. Life Sci.* **2016**, *73* (3), 459–473. https://doi.org/10.1007/s00018-015-2059-z.

(178) Tabruyn, S. P.; Griffioen, A. W. NF-KB: A New Player in Angiostatic Therapy. *Angiogenesis* **2008**, *11* (1), 101–106. https://doi.org/10.1007/s10456-008-9094-4.

(179) Godwin, P.; Baird, A.-M.; Heavey, S.; Barr, M.; O'Byrne, K.; Gately, K. A. Targeting Nuclear Factor-Kappa B to Overcome Resistance to Chemotherapy. *Front. Oncol.* **2013**, *3*. https://doi.org/10.3389/fonc.2013.00120.

(180) Yu, H.; Pardoll, D.; Jove, R. STATs in Cancer Inflammation and Immunity: A Leading Role for STAT3. *Nat Rev Cancer* **2009**, *9* (11), 798–809. https://doi.org/10.1038/nrc2734.

(181) Fontan, L.; Yang, C.; Kabaleeswaran, V.; Volpon, L.; Osborne, M. J.; Beltran, E.; Garcia, M.; Cerchietti, L.; Shaknovich, R.; Yang, S. N.; Fang, F.; Gascoyne, R. D.; Martinez-Climent, J. A.; Glickman, J. F.; Borden, K.; Wu, H.; Melnick, A. MALT1 Small Molecule Inhibitors Specifically Suppress ABC-DLBCL In Vitro and In Vivo. *Cancer Cell* **2012**, *22* (6), 812–824. https://doi.org/10.1016/j.ccr.2012.11.003.

(182) Lim, S. M.; Jeong, Y.; Lee, S.; Im, H.; Tae, H. S.; Kim, B. G.; Park, H. D.; Park, J.; Hong, S. Identification of β-Lapachone Analogs as Novel MALT1 Inhibitors To Treat an Aggressive Subtype of Diffuse Large B-Cell Lymphoma. *J. Med. Chem.* **2015**, *58* (21), 8491–8502. https://doi.org/10.1021/acs.jmedchem.5b01415.

(183) Brasholz, M.; Sörgel, S.; Azap, C.; Reißig, H.-U. Rubromycins: Structurally Intriguing, Biologically Valuable, Synthetically Challenging Antitumour Antibiotics. *European Journal of Organic Chemistry* **2007**, *2007* (23), 3801–3814. https://doi.org/10.1002/ejoc.200601054.

(184) Rathwell, D. C. K.; Yang, S.-H.; Tsang, K. Y.; Brimble, M. A. An Efficient Formal Synthesis of the Human Telomerase Inhibitor (±)-γ-Rubromycin. *Angewandte Chemie* **2009**, *121* (43), 8140–8144. https://doi.org/10.1002/ange.200903316.

(185) Ueno, T.; Takahashi, H.; Oda, M.; Mizunuma, M.; Yokoyama, A.; Goto, Y.; Mizushina, Y.; Sakaguchi, K.; Hayashi, H. Inhibition of Human Telomerase by Rubromycins: Implication of

Spiroketal System of the Compounds as an Active Moiety. *Biochemistry* **2000**, *39* (20), 5995–6002. https://doi.org/10.1021/bi992661i.

(186) Gurung, R. L.; Lim, S. N.; Khaw, A. K.; Soon, J. F. F.; Shenoy, K.; Ali, S. M.; Jayapal, M.; Sethu, S.; Baskar, R.; Hande, M. P. Thymoquinone Induces Telomere Shortening, DNA Damage and Apoptosis in Human Glioblastoma Cells. *PLOS ONE* **2010**, *5* (8), e12124. https://doi.org/10.1371/journal.pone.0012124.

(187) Sameni, S.; Hande, M. P. Plumbagin Triggers DNA Damage Response, Telomere Dysfunction and Genome Instability of Human Breast Cancer Cells. *Biomedicine & Pharmacotherapy* **2016**, *82*, 256–268. https://doi.org/10.1016/j.biopha.2016.05.007.

(188) Khaw, A. K.; Sameni, S.; Venkatesan, S.; Kalthur, G.; Hande, M. P. Plumbagin Alters Telomere Dynamics, Induces DNA Damage and Cell Death in Human Brain Tumour Cells. *Mutation Research/Genetic Toxicology and Environmental Mutagenesis* **2015**, *793*, 86–95. https://doi.org/10.1016/j.mrgentox.2015.06.004.

(189) Lu, Q.; Liu, W.; Ding, J.; Cai, J.; Duan, W. Shikonin Derivatives: Synthesis and Inhibition of Human Telomerase. *Bioorganic & Medicinal Chemistry Letters* **2002**, *12* (10), 1375–1378. https://doi.org/10.1016/S0960-894X(02)00158-0.

(190) STAT3 signaling in immunity | Elsevier Enhanced Reader https://reader.elsevier.com/reader/sd/pii/S1359610116300612?token=B5436AB3A32C23C6E1B6878C9FD296AFEB359AD20E09482951015962A0F903D6DC6B32FA800A98275ED747072EE54998&originRegion=eu-west-1&originCreation=20210611105252 (accessed 2021 -06 -11). https://doi.org/10.1016/j.cytogfr.2016.05.001.

(191) La Sala, G.; Michiels, C.; Kükenshöner, T.; Brandstoetter, T.; Maurer, B.; Koide, A.; Lau, K.; Pojer, F.; Koide, S.; Sexl, V.; Dumoutier, L.; Hantschel, O. Selective Inhibition of STAT3 Signaling Using Monobodies Targeting the Coiled-Coil and N-Terminal Domains. *Nat Commun* **2020**, *11* (1), 4115. https://doi.org/10.1038/s41467-020-17920-z.

(192) Cao, Y.-Y.; Yu, J.; Liu, T.-T.; Yang, K.-X.; Yang, L.-Y.; Chen, Q.; Shi, F.; Hao, J.-J.; Cai, Y.; Wang, M.-R.; Lu, W.-H.; Zhang, Y. Plumbagin Inhibits the Proliferation and Survival of Esophageal Cancer Cells by Blocking STAT3-PLK1-AKT Signaling. *Cell Death Dis* **2018**, *9* (2), 17. https://doi.org/10.1038/s41419-017-0068-6.

(193) Chelate | chemistry https://www.britannica.com/science/chelate (accessed 2021 -06 -10).

(194) Jakupec, M. A.; Kandioller, W.; Schoenhacker-Alte, B.; Trondl, R.; Berger, W.; Keppler, B. K. Trends and Perspectives of Ruthenium Anticancer Compounds (Non-PDT). In *Ruthenium*

Complexes; John Wiley & Sons, Ltd, 2018; pp 271–291. https://doi.org/10.1002/9783527695225.ch14.

(195) Geisler, H.; Westermayr, J.; Cseh, K.; Wenisch, D.; Fuchs, V.; Harringer, S.; Plutzar, S.; Gajic, N.; Hejl, M.; Jakupec, M. A.; Marquetand, P.; Kandioller, W. Tridentate 3-Substituted Naphthoquinone Ruthenium Arene Complexes: Synthesis, Characterization, Aqueous Behavior, and Theoretical and Biological Studies. *Inorg. Chem.* **2021**, acs.inorgchem.1c01083. https://doi.org/10.1021/acs.inorgchem.1c01083.

(196) Fuyi Wang; Jingjing Xu; Abraha Habtemariam; Juraj Bella, and; Sadler*, P. J. Competition between Glutathione and Guanine for a Ruthenium(II) Arene Anticancer Complex: Detection of a Sulfenato Intermediate https://pubs.acs.org/doi/pdf/10.1021/ja053387k (accessed 2021 -06 -17). https://doi.org/10.1021/ja053387k.

(197) Ramachary, D. B.; Anif Pasha, M.; Thirupathi, G. Organocatalytic Asymmetric Formal [3+2] Cycloaddition as a Versatile Platform to Access Methanobenzo[7]Annulenes. *Angewandte Chemie International Edition* **2017**, *56* (42), 12930–12934. https://doi.org/10.1002/anie.201706557.

(198) Elgrishi, N.; Rountree, K. J.; McCarthy, B. D.; Rountree, E. S.; Eisenhart, T. T.; Dempsey, J. L. A Practical Beginner's Guide to Cyclic Voltammetry. *J. Chem. Educ.* **2018**, *95* (2), 197–206. https://doi.org/10.1021/acs.jchemed.7b00361.

(199) Mabbott, G. A. An introduction to cyclic voltammetry https://pubs.acs.org/doi/pdf/10.1021/ed060p697 (accessed 2021 -06 -21). https://doi.org/10.1021/ed060p697.

(200) Schafer, F.; Buettner, G. Redox State and Redox Environment in Biology; 2004; pp 1–14. https://doi.org/10.1007/0-306-48412-9_1.

(201) Mallikarjun, V.; Clarke, D. J.; Campbell, C. J. Cellular Redox Potential and the Biomolecular Electrochemical Series: A Systems Hypothesis. *Free Radical Biology and Medicine* **2012**, *53* (2), 280–288. https://doi.org/10.1016/j.freeradbiomed.2012.04.034.

(202) Tönnemann, J.; Risse, J.; Grote, Z.; Scopelliti, R.; Severin, K. Efficient and Rapid Synthesis of Chlorido-Bridged Half-Sandwich Complexes of Ruthenium, Rhodium, and Iridium by Microwave Heating. *European Journal of Inorganic Chemistry* **2013**, *2013* (26), 4558–4562. https://doi.org/10.1002/ejic.201300600.

(203) Geisler, H.; Wernitznig, D.; Hejl, M.; Gajic, N.; Jakupec, M. A.; Kandioller, W.; Keppler, B. K. Novel Phthiocol-Based Organometallics with Tridentate Coordination Motif and Their Unexpected Cytotoxic Behaviour. *Dalton Trans.* **2020**, *49* (5), 1393–1397. https://doi.org/10.1039/C9DT04462K.

6 ABBREVIATIONS

%	percent
°C	degree centigrade
µL	microliter
µM	micromolar
µmol/L	micromole per liter
A	absorbance
Å	angstrom
A_0	initial absorbance
ACN	acetonitrile
AI	aromatase inhibitor
arom.	aromatic
ATP	adenosine triphosphate
cat.	catalytical
$CDCl_3$	deuterated chloroform
CH	tertiary carbon
CH_2	secondary carbon
CH_3	primary carbon
Cq	quarternary carbon
d	doublet
DCM	methylene chloride
dd	doublet of doublets
ddd	doublet of doublet of doublets
DEPTq	distorsionless enhancement by polarization transfer including the detection of quaternary nuclei
DLBCL	diffuse large B cell lymphoma

DMSO	dimethyl sulfoxide
DNA	deoxyribonucleic acid
dq	doublet of quartets
DUB	deubiquitinase
e.g.	exempli gratia
EGFR	external growth factor receptor
EMT	epithelial-mesenchymal transition (gene)
equiv.	equivalent
ER	endoplasmic reticulum
FDA	food and drug administration
GRP78	binding immunoglobulin protein
GSH	glutathione
h	hours
HCl	hydrochloric acid
hept	heptet
HQ	2-hydroxynaphthoquinone
HSA	human serum albumin
Hz	hertz
IC_{50}	half maximal inhibitory concentration
M	molarity (mol/L)
m	multiplet
MALT1	mucosa-associated lymphoid tissue lymphoma translocation protein 1
MeOD	deuterated methanol
MeOH	methanol
mg	milligram
MHz	megahertz

min	minutes
mL	milliliter
mM	millimolar
mmol	millimol
mRNA	messenger ribonucleic acid
mV	millivolt
mV/s	millivolt per second
$NAD(P)^+$	oxidized nicotinamide adenine dinucleotide (phosphate)
NAD(P)H	nicotinamide adenine dinucleotide (phosphate)
NEt_3	triethylamine
NF-κB	nuclear factor kappa-light-chain-enhancer of activated B-cells
nm	nanometer
NMR	nuclear magnetic resonance
NQO1	naphthoquinonoxidase1
PBS	phosphate buffered saline
PGP	plasma membrane glycoprotein
pH	potential of hydrogen
ppm	parts per million
PTA	1,3,5-triaza-7-phosphaadamantane
r.t.	room temperature
RAS	rat sarcoma
Rb	retinoplastome
RCHO	aldehyde
R_f	retardation factor
RNR	ribonucleotide reductase
ROS	reactive oxygen species

s	singlet
STAT	signal transducer and activator of transcription
t	triplet
tert	tertiary
UV/Vis	ultraviolet/visible (spectroscopy)
V	volt
VEGF	vascular endothelial growth factor
WHO	world health organization